IDŐJÁRÁS

QUARTERLY JOURNAL
OF THE HUNGARIAN METEOROLOGICAL SERVICE

CONTENTS

VOL. 127 * NO. 3 * JULY – SEPTEMBER 2023

DOI:10.28974/idojaras.2023.3.1

IDŐJÁRÁS

Quarterly Journal of the Hungarian Meteorological Service
Vol. 127, No. 3, July – September, 2023, pp. 267–283

Investigation and analysis of the Iranian autumn rainfall thickness pattern

Hossein Jahantigh

Natural Resources Faculty
Saravan Higher Education Complex, Iran.

Author E–mail: hjahantigh5@gmail.com

(Manuscript received in final form December 5, 2022)

Abstract— The purpose of this study was to investigate and analyze the trend of autumn precipitation thickness pattern in Iran. For this purpose, two environmental and atmospheric databases have been used. Environmental data is prepared and networked in two stages, in the first stage with the help of 1434 stations and in the second stage with the help of 1061 stations. Atmospheric data includes geopotential height data obtained from the National Center for Environmental Prediction and the National Center for Atmospheric Research (NCEP / NCAR). The spatial resolution of this data is 2.5 × 2.5 degrees. The thickness of the atmosphere, which is usually between 500 and 1000 hectopascals, is shown. This thickness is considered as the thickness of the whole atmosphere. The results of the autumn precipitation trend showed that although autumn precipitation on monthly and annual scales has experienced an increasing trend in most regions, in less than 5% of Iran, the upward trend has been significant. The most intense upward trend is observed in the form of spots in the central and northern parts of the Zagros Mountain, while the greatest decreasing trend has been observed in the form of cores along the Caspian coastal cities. The results of the autumn precipitation thickness pattern showed that the autumn precipitation thickness pattern is affected by deflection and instability due to high latitude cold and humid weather and low latitude hot and humid weather occurred in North Africa, in such a way that the Black Sea and the Mediterranean Sea provide the required moisture in high latitudes and the Red Sea and the Persian Gulf in low latitudes.

Key-words: precipitation, trend, atmospheric thickness, synoptic patterns, Iran

1. Introduction

Precipitation is the most vital climatic element that affects almost all aspects of life on Earth and is directly or indirectly evident and felt in various human activities. Precipitation as a random variable has many temporal and spatial variations. The climatic situation of Iran is such that in terms of latitude and penetration of subtropical high-pressure systems, in addition to low precipitation, its precipitation regime, especially spring precipitation, fluctuates sharply (*Jalali et al.,* 2019). Climate change can be studied by tracking characteristics such as the quantity, spatiotemporal pattern, and circulation patterns of climatic elements, especially temperature and precipitation. For example, precipitation as one of the basic elements of the climate, especially during the twentieth century, has increased by about 0.1% in the middle and upper latitudes of the northern hemisphere, while no change in southern hemisphere precipitation is observed (*Ventura et al*., 2002).

Due to its proximity to the abundant moisture resources of the Mediterranean Sea in the west, the Persian Gulf the Oman Sea, and the sea surface temperature moisture regions in the south, the Caspian Sea in the north, the Black Sea and the Indian Ocean in the east, our country has a relatively high impact. Therefore, the study of these effects on the amount of precipitation in the country has a key role in recognizing precipitation fluctuations and predicting precipitation (*Rezaei Banafsheh et al*., 2010). One of the climatic characteristics of each region is the amount of precipitation. This climatic characteristic is one of the most unstable climatic variables that affect the water resources of an area (*Rezaei* and *Abed*, 2010; *Mirzayi et al*., 2020). Since the temporal and spatial distribution of precipitation in Iran is affected by the distribution of global circulation systems, the slightest change in its pattern is followed by severe climatic anomalies. Therefore, spatial and temporal anomalies of precipitation, severe changes in precipitation intensity, and differences in the type of precipitation are the main features of precipitation in Iran (*Babaei* and *Farajzadeh*, 2002; *Mafakheri et al*., 2019). Local and regional climates are influenced by large-scale patterns of atmospheric circulation (*Kidson*, 2000). These patterns, along with fronts, cyclone and anticyclone systems, control different climatic elements and phenomena in mid-altitudes (*Zappa et al*., 2020). Iran's precipitation over time and in different places is affected by different patterns, systems, and climatic characteristics leading to a huge difference in Iran's annual precipitation in terms of time and place (*Farajzadeh et al*., 2002). In contrast to the Caspian coasts, Zagros and Alborz Mountains, which have very high precipitation, the central regions have much less precipitation (*Asgari* and *Rahimzadeh*, 2006). However, very low precipitation, in addition to heterogeneous spatial distribution, also has severe

time fluctuations. Therefore, this heterogeneous temporal and spatial distribution in Iran is affected by the distribution of global circulation systems, and the slightest change in its pattern leads to severe climatic anomalies (*Frišmantas* and *Stankūnavičius*, 2020).

Due to its large size, Iran always benefits from different circulation systems, so that this situation has caused the mechanism of precipitation patterns in Iran to be different. For example, precipitation and the resulting processes in the southwest are mostly influenced by the strengthening and intensification of the Sudanese low pressure system and the Red Sea convergence region and their transformation into dynamic systems (*Lashkari*, 2005). This is why Sabziparvar considers the presence of deep troughs at a high level in addition to the above (so that the axis of the trough extends to the south to the south of the Red Sea) (*Sabziparvar*, 1991). However, circulation patterns in northwestern Iran are mostly influenced by the Siberian high pressure system, the mountain effects on atmospheric phenomena, the European high pressure systems, and the monsoon low pressure system (*Ashjaei*, 2000). On the other hand, the rains in the north of the countryare the result of the existence of a high pressure system, and the negative rotation dependent on the effect of the high pressure ridge located on the Caspian coast. It should be noted that in the high pressure and hybrid models, the most important mechanism of precipitation is the presence of cyclones in the region (*Mofidi et al.*, 2007), while some researchers have considered the occurrence of precipitation on the southern Caspian coast due to convection (*Alijani*, 2002). However, towards the lower latitudes, especially in the southeast part of the country, the mechanisms are more diverse and obvious. Limited studies have been performed on the synoptic pattern of autumn precipitation. For example, *Qian* and *Xu* (2020) examined the forecast of autumn precipitation in the Yangtze River Basin based on climatic indicators. The results showed that the spatial pattern of autumn precipitation changes is almost uniform throughout the region.

Any object that expands with increasing temperature decreases its density, and any object that contracts, increases its density. Therefore, with the fall of cold air, the density of air is compressed (increased), and consequently, the thickness of the atmosphere is reduced. Conversely, with the fall of hot air, the density of the air mass expands (decreases) and the molecules tend to diverge, which increases the thickness of the atmosphere following the divergence of the air molecules (*Rousta et al.*, 2016). Therefore, it can be said that every object that expands with increasing temperature decreases its density, and every object that contracts, increases its density. Since autumn is a transitional season between cold and hot seasons, the type of atmospheric thickness pattern is of great importance for the occurrence of precipitation in this season. As it has been observed, most of the analyses that have been done on autumn precipitation in Iran were done only regionally or as a transition of the effects, the changes of agricultural products, and its relationship with autumn

precipitation (*Sohrabi et al*., 2020). Therefore, in this study, while examining and statistically analyzing the autumn precipitation in Iran, the atmospheric thickness pattern of the autumn precipitation has been studied and analyzed.

2. Data and methodology

The purpose of this study is a statistical-synoptic analysis of autumn precipitation in Iran with an emphasis on the atmospheric thickness. In this regard, two databases have been used.

1. Environmental data: This group of data (the so-called Al-Isfizari database) is obtained by the interpolation of stationary values of daily precipitation for the statistical period 1961 to 2003. This database has a spatial resolution of 15 × 15 km produced in the form of Lambert Conformal Conic Projection image system, and arranged in the form of a matrix of 15992 × 7187 with S arrangement (time in rows and space in columns). According to the time frame of this study (autumn season) with scripting in MATLAB software environment, data related to the autumn season (3848 days) has been extracted from the entire Al-Isfizari database and arranged in a matrix with dimensions of 3848 × 7187. In order to complete the 50-year statistical period and increase the accuracy of the research results, another set of relevant data from 2004 to 2010 using daily precipitation data of 1061 synoptic, climatic, and hydrometric stations, received from the World Meteorological Organization, was arranged and interpolated. The distribution of the stations used in both stages is shown in *Fig. 1 a* and *b*.

2. Atmospheric data: This part of the data that is used to calculate the thickness of the atmosphere includes geopotential height data in hPa unit, which is received from the database of the National Center for Environmental Prediction and the National Center for Atmospheric Research (NCEP / NCAR). The spatial resolution of this data is 2.5 × 2.5 degrees. One of the maps used in synoptic climatology is the thickness maps. These maps show the thickness of the atmosphere, which is usually between 500 and 1000 hPa. This thickness is considered as the thickness of the whole atmosphere. In fact, by examining the thickness between these two layers (thickness between the level of 500 and 1000 hPa), the condition of the whole layer is examined. According to *Rousta et al*. (2019), the thickness of the atmosphere has been calculated (*Fig. 1*. *c* and *d*).

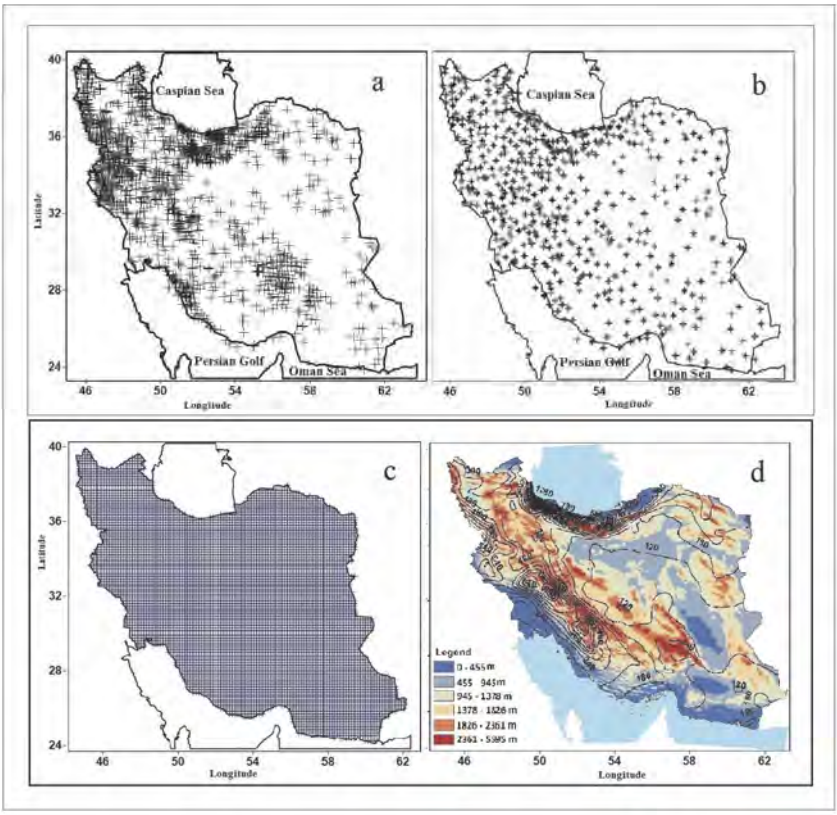

Fig. 1. Distribution of Al-Isfizari database (a), and distribution of supplementary stations (b), spatial resolution of NCEP/NCAR geopotential height data (c), and the calculated atmospheric thickness (d).

2.1. Methodology

In the present study, an attempt has been made to identify and analyze the thickness patterns effective in creating inclusive autumn precipitation in the country, using the environmental approach to the circulatory approach. After extracting the thickness of the atmosphere, cluster analysis was used to identify the thickness patterns of the inclusive autumn precipitation in Iran. In the next step, with the aim of classifying the atmospheric thickness data and identifying the representative days, a cluster analysis was performed on this data. The cluster analysis is a method in which variables are classified into specific groups based on the wanted characteristics. The purpose of cluster analysis is to find the actual categories of subjects and reduce the amount of data. In other words, the goal is to identify a smaller number of groups, so that data that are more similar

to each other are grouped together in a way that the intragroup diffraction is minimal and the intergroup diffraction is maximal. In this method, data is grouped based on the distance or similarity between them. There are various methods for measuring the distance between data, one of the most widely used methods is the Euclidean distance method. In order to select the representative days of the groups obtained from the classification of data related to the atmospheric thickness, the Lund correlation method was used. In this way, to select the representative day, the day that has the most similarity with the maximum number of group of days is selected. The correlation coefficient represents the degree of similarity of the patterns of the two maps with each other. To do this, a certain threshold of the correlation coefficient must be accepted. The value of the correlation coefficient in such cases typically varies between 0.5 to 0.7 (*Yarnal*, 2011). Representative days were extracted based on a threshold of 0.5. Thus, the day that has a correlation coefficient of 0.5 with more days was selected as the representative day.

3. Results and discussion

3.1. Descriptive characteristics

Fig. 2 shows the spatial distribution of the monthly mean and the coefficient of the variation of autumn precipitation. The spatial distribution of average precipitation in October shows that the highest amount of average precipitation is related to the coastal shores of the Caspian Sea. The average precipitation in this part of the country reaches over 30 mm, while the southern and eastern parts of the country experience their minimum precipitation in October. Although the Iranian precipitation masses enter Iran from the west of the country in autumn, it is observed that due to local mechanisms, especially the huge source of Caspian Sea moisture, most of the precipitation is related to the Caspian shore (*Sari Sarraf et al.*, 2010). After the Caspian Sea coast, the Zagros Mountains, especially the Middle Zagros (western regions of the country) had the highest average precipitation in October.

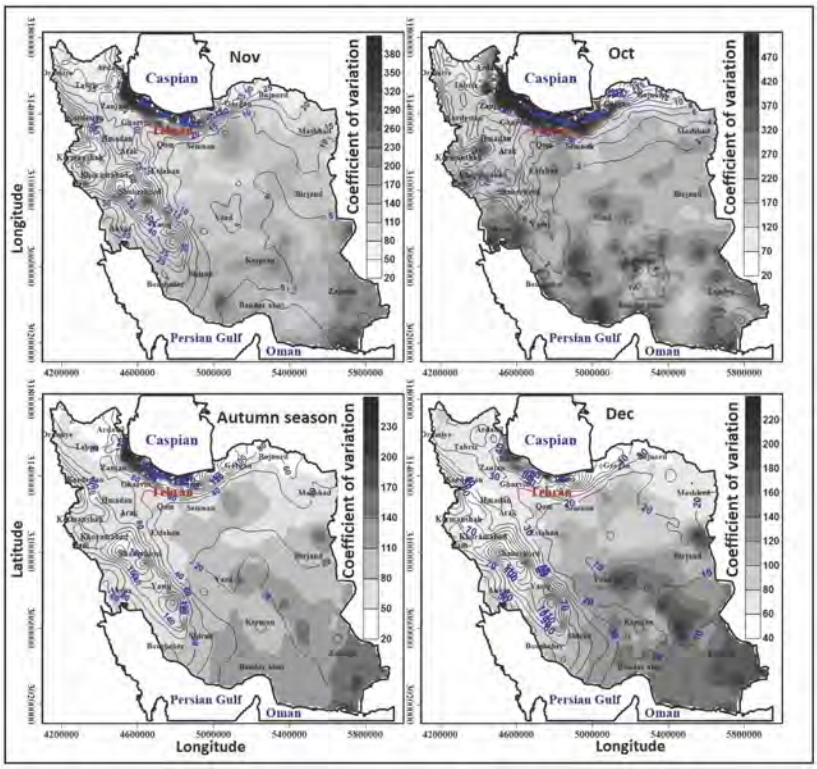

Fig. 2. Spatial distribution of the monthly mean and the coefficient of the variation of autumn precipitation in Iran.

Considering that autumn is a transient season between the departure of the subtropical high pressure from Iran and the beginning of the arrival of western winds in Iran, the spatial coefficient of variation of Iranian precipitation in autumn is extremely high, so that 90.8% of the country has experienced a coefficient of precipitation change above 100%. Therefore, the highest coefficient of variation in the form of more nuclei is scattered in the southern and eastern regions of the country. However, in this month, 91.8% of the area of Iran had less than 20 mm of precipitation (*Table 1*). In November, due to the fact that the western winds have entered Iran almost completely, the spatial distribution of precipitation throughout Iran has increased significantly. For example, the average precipitation compared to October in northwestern Iran has increased by about 15 mm and in the northeast by about 10 mm (see the November pattern of *Fig. 2*). However, in the southern half of the country, due to the fact that subtropical high-pressure systems have not yet completely left Iran, and on the other hand, western precipitation systems have less covered the

southern regions of the country, the average precipitation in this month (November) has not increased significantly compared to October. However, the intensity of the spatial coefficient of variation of precipitation has decreased in this month, still many parts of the country have experienced a coefficient of variation is close to 100%. In this month, areas with precipitation between 20 and 40 mm reach 19.1%, while in October it was 5.2%. However, in this month, about 66% of the country has an average precipitation of less than 20 mm (*Table 1*).

Table 1. Mean classes and the coefficient of variation of autumn precipitation in Iran

		Average classification			
	class	**precent**		**class**	**precent**
Oct	20<	91.8	**Nov**	20<	66.3
	20 to 40	5.2		20 to 40	19.1
	40 to 60	1		40 to 60	9.3
Dec	60>	1.9	**Autumn season**	60>	5.3
	20<	42.8		20<	20.1
	20 to 40	31.8		20 to 40	35.6
		Classification			
	class	**precent**		**class**	**precent**
Oct	40<	0	**Nov**	40<	0
	40 to 70	4		40 to 70	6.2
	70 to 100	5.2		70 to 100	24.7
Dec	100>	90.8	**Autumn season**	100>	69.1
	40<	0		40<	3.5
	40 to 70	20.3		40 to 70	33.3

With the complete domination of western precipitation systems over Iran in December, the spatial distribution of Iran's average precipitation has increased significantly. In addition, with the stability of these precipitation systems in Iran, the spatial coefficient of variation of precipitation in Iran in December compared to October and November has decreased significantly. For example, in this month, 31.8% of the country has an average precipitation of between 20 and 40 mm, and 15.6% of the area of Iran, which covers most of the northern half of the country, has an average precipitation of more than 60 mm. The highest spatial coefficient of variation of precipitation of this month is observed in the southern half, especially in the southeast part of the country. As it was mentioned, the highest average precipitation in every three months is observed

on the Caspian coast, because the local mechanism of the Caspian Sea plays an important role in precipitation in this region. The three types of Siberian systems, the high-pressure systems, low-pressure systems, and migratory cyclones are effective in precipitation on the southern shores of the Caspian Sea, among which, precipitation of Siberian high-pressure origin is more frequent. The required moisture of the precipitation caused by the Siberian high-pressure is due to the evaporation from the Caspian Sea. Whenever a short high-pressure ridge is established on the ground on the southern shore of the Caspian Sea, due to the spread of cold air in the region and there is a trough in the middle and upper levels of the atmosphere, the necessary conditions for heavy precipitation in the region are provided. It is necessary to explain that this cold air, when crossing the Caspian Sea, due to the season and the high sea water, becomes hot and humid from below, and as a result, it becomes unstable (*Moradi*, 2004). Therefore, the existence of the Caspian Sea as the main source of moisture, the presence of Alborz Mountains in the south of the coast and the dominance of north and northwest winds in the region cause the formation of suitable climatic conditions in terms of precipitation in this part of the country. With these conditions, generally, in autumn, the most precipitation has occurred along the Zagros Mountains and the coast of the Caspian Sea, which indicates the effect of altitude and distance to the sea in the spatial distribution of precipitation. For example, distance to the Caspian Sea and the altitude are the most important local factors influencing precipitation in the Talesh region (*Sari Sarraf et al*., 2010).

In order to study and analyze Iran autumn precipitation in more detail, the monthly precipitation trend of autumn season is presented in *Fig. 3*, where the points seen on the map indicate the significance of the trend. The spatial distribution of the autumn precipitation trend indicates that in this season (except for October), in most parts of Iran, the precipitation has increased. In the distribution of precipitation in October in the northern half of the country, especially in the northwest, precipitation has decreased by an average of about -1 to -2 mm (*Fig. 3*). However, this declining trend was significant only on the Caspian coast at the 95% confidence level. In this month, although precipitation has increased in 40% of the area of Iran, it is observed that it has not been statistically significant (*Table 2*). In November the situation is almost the opposite, i.e., 40% of the area of Iran has a decreasing trend and the rest has an increasing trend (*Table 2*). In this month, the heights of Zagros in November has experienced a significant upward trend in contrast to October. In this month, despite the fact that precipitation has decreased in 40% of the country, less than 1% of it has been significant at the 95% confidence level (*Table 2*). In December, the trend of precipitation changes is completely different than that of October and November, so that in this month, precipitation has increased in almost 87% of the country. This increasing trend has occurred in the coastal shores of the Persian Gulf, along the Zagros Mountains and the southeast part of

the country, especially the coastal areas of the Oman Sea (*Fig. 3*). Only 11% of these uptrends were significant at the 95% confidence level. In general, the distribution of autumn precipitation trend indicates that in most areas of Iran (above 80%), the autumn precipitation has been increasing. This upward trend along the Zagros Mountains reaches over 5 mm. However, significant trends are scattered throughout Iran. Still, the western parts of the Caspian Sea coast have experienced a downward trend of about -3.5 mm.

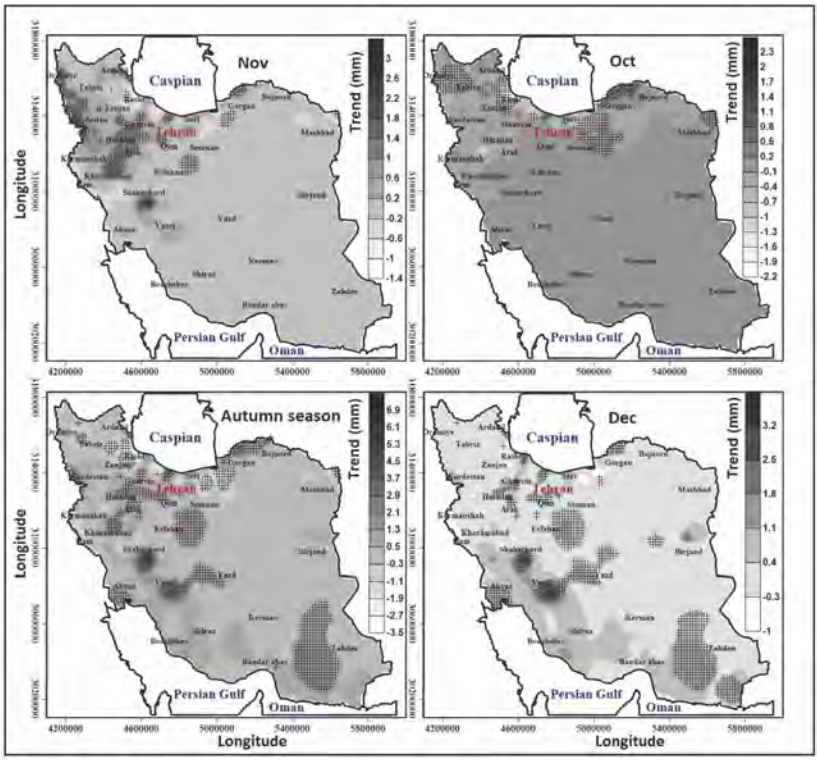

Fig. 3. Spatial distribution of the monthly trend of autumn precipitation in Iran.

Table 2. Type and percentage covered by the trend of autumn precipitation in Iran

Month	trend type	Percentage covered	The significance level	Percentage covered	Month	trend type	Percentage covered	The significance level	Percentage covered
Oct	decreasing	59.2	sig	4.9	Nov	decreasing	41	sig	0.47
			non sig	54.2				non sig	40.5
	increasing	40.7	sig	0.58		increasing	58.9	sig	4.4
			non sig	40.1				non sig	54.2
Dec	decreasing	12.8	sig	0.11	Autumn season	decreasing	19.9	sig	1.8
			non sig	12.7				non sig	18.1
	increasing	87.1	sig	11.5		increasing	80.1	sig	11.1
			non sig	75.5				non sig	68.9

3.2. Synoptic analysis of the autumn precipitation thickness

Fig. 4 shows the dendrogram of the cluster analysis on the atmosphere thickness of the Iranian autumn precipitation. According to *Fig. 4*, atmospheric thickness maps were drawn for the representative days of different groups (2 to 7 groups) at the correlation level of 0.5, then, by comparing the maps of the representative days of the members of each group and through the trial and error method, the appropriate place to cut the chart and the appropriate grouping number to extract the patterns were determined. According to the studies, the division into four groups was found appropriate, and the representative days of each group have been determined. According to *Fig. 5*, the highest frequency of the autumn precipitation patterns is the fourth pattern.

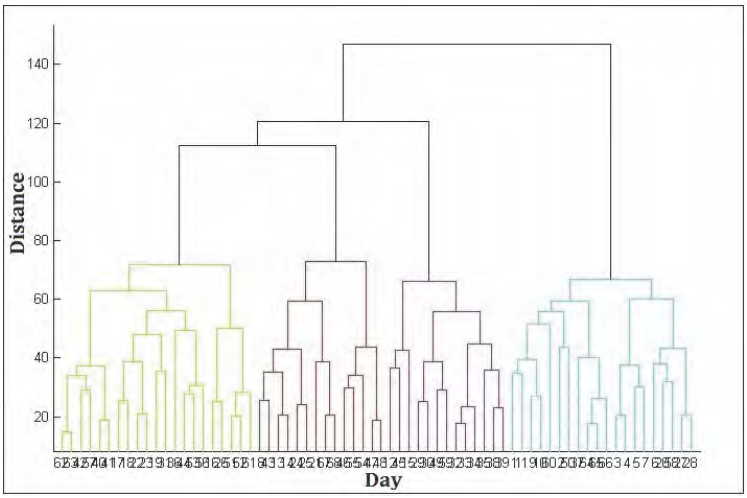

Fig. 4. Dendrogram from cluster analysis on the atmospheric thickness of inclusive autumn precipitation.

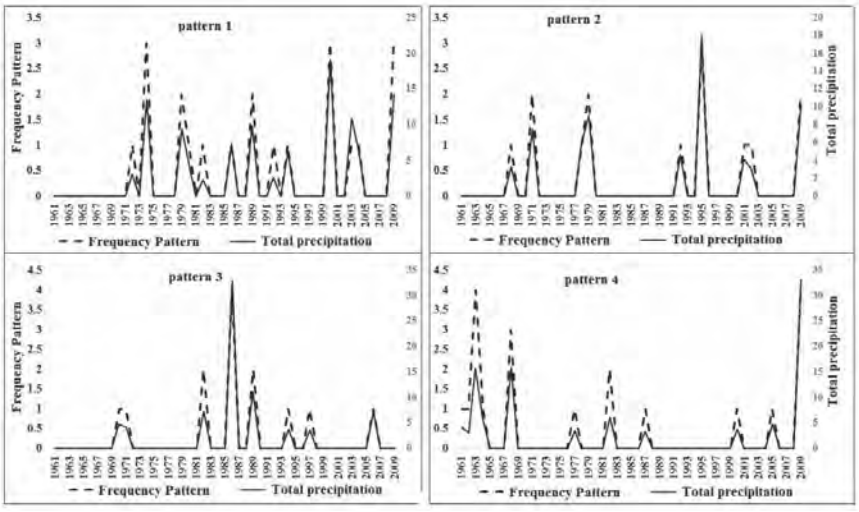

Fig. 5. Frequency and total autumn precipitation for different patterns during the study period.

Fig. 6 shows the patterns of atmospheric thickness of autumn precipitation in Iran. *Fig. 6a* shows that a deep ridge extends from the western part of the Mediterranean to North Africa and over Algeria. Although this ridge has a great depth, its wavelength is not very wide and has not affected a large range (*Fig. 6a*). Since the western part of the ridge is accompanied by a negative

vorticity (*Lashkari*, 2005), it has caused the cold and humid air to advect from the Mediterranean Sea to the northern regions of the Middle East, but in the central regions of the Middle East, it has caused ridges and has led to the advection of hot air (*Fig. 6a*). On the other hand, a low-altitude system with a cold core is located in the central regions of Iran, so that the minimum thickness of the atmospheric layer in the Middle East region fully corresponds to this low-altitude system, and its descending arm has caused the transfer of cold air from higher latitudes to lower latitudes, affecting Iraq, Saudi Arabia, southwestern Iran, and the Persian Gulf basin. Given this, it can be said that the cold air flow that has descended from the western half of ridge on Iraq, the western parts of Iran, the northern parts of Saudi Arabia, and the Persian Gulf basin, in response to the warm weather that has spread from Northeast Africa and Saudi Arabia, has created an allobaric zone on the study area, and has provided conditions for atmospheric instability (*Rezaei Banafsheh et al*., 2015). Since the thickness of the atmosphere is different due to the type of prevailing air (*Fig. 6a*), the highest thickness of the atmosphere is in the southern regions of the Middle East, especially in the southern parts of Saudi Arabia, the Arab Sea, and the Persian Gulf, because in autumn the high latitude atmospheric systems are not strong enough to advance to the low latitudes of the study area, and the lowest thickness of the atmosphere is located in the central regions of Iran, which is completely consistent with the dynamic low-altitude system (*Masoudian*, 2005). The spatiotemporal distribution of the autumn precipitation pattern of the thick layer of the Middle East atmosphere indicates that a wide low-altitude system with average pressure (5390 geopotential meters) was formed in Northern Europe and crossed the Black Sea into the northern parts of the Middle East (*Fig. 6b*). This low-altitude system has transferred cold air from high latitudes to lower latitudes, and since it has crossed the Black Sea and the eastern parts of the Mediterranean, it has transferred moisture to the northern regions of the study area. During the rule of this model, the flows drawn on the central and southern regions of the Middle East, due to the low latitude, have transferred cold air to the study area, and this has caused high pressure gradients and instability in the northern regions of the Middle East. However, due to the fact that the low altitude system of Northern Europe extends over the Black Sea and the Mediterranean, it can bring a lot of moisture to the study area (*Fig.6b*). At the same time, the warm air mass has penetrated from North Africa to the central and southern regions of the Middle East, so that the southern regions of the Middle East have the highest thickness of the atmosphere (5650 to 5750 meters) and the northern regions have less atmospheric thickness. The spatiotemporal distribution of the third pattern (*Fig. 6c*) of autumn precipitation for the thick layer of the atmosphere in the Middle East shows that two low-altitude cores are located in the Mediterranean Sea and southwestern Europe, directing eastward flows to North Africa. On the other hand, a deep ridge is located in the northern regions of the Middle East, and in the western part of the

ridge, cold air has fallen in the northern regions of Europe towards the northern regions of the Middle East, in such a way that in the central regions of Turkey it has led to the phenomenon of blocking and a wide range of cold air advection into the Middle East. On the other hand, since the central regions of the Middle East are under the influence of the hot weather of North Africa, there is a high pressure gradient in the northern and central regions of the Middle East, as it is clear from the compaction of the same height lines (*Fig. 6c*).

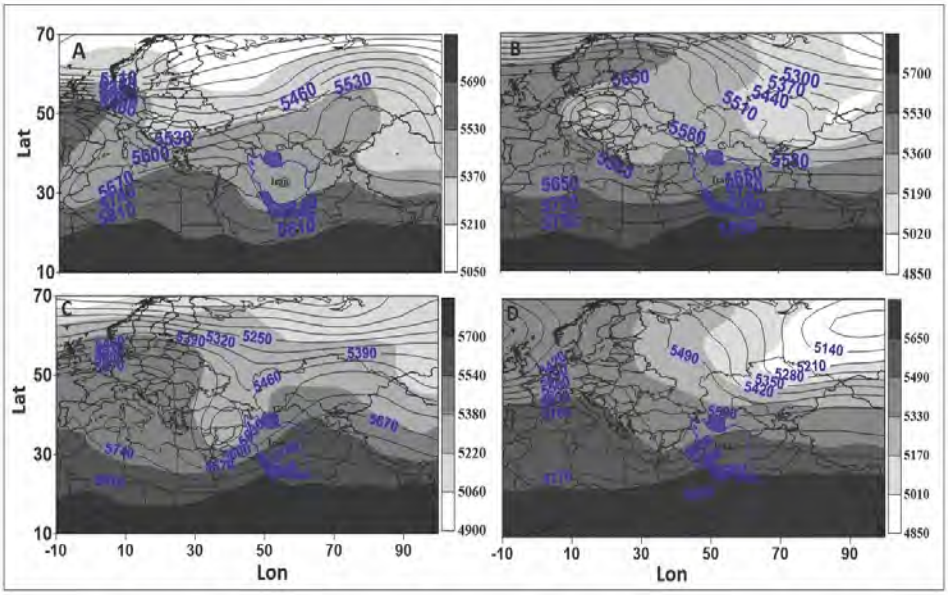

Fig. 6. Patterns of atmospheric thickness and height of atmospheric geopotential for autumn precipitation in Iran.

It is also observed that the passage of cold flows of high latitudes through the northern regions of the Middle East has caused compaction of the thick layer of the atmosphere and reduced the thickness of the atmosphere. So that the minimum amount of atmosphere thickness (5000 meters) is completely consistent with the blocking located in Turkey and the maximum amount of atmosphere thickness (5700 meters) is in the southern regions of Saudi Arabia, because it is completely under the influence of the hot weather of North Africa. The large difference in atmospheric thickness in the southern and northern regions of the Middle East region indicates the large temperature difference in the thick layer of the atmosphere (*Fig. 6c*). During the reign of this model, the

cold air of Europe falls through this deep trough and the penetration of hot and humid tropical air from the Red Sea, which is characterized by the establishment of ridges in the eastern and northeastern pats of Iran. Baroclinic conditions are established in the Middle East and cause widespread precipitation in the northeastern regions, especially in the western regions of Iran (*Masoudian* and *Karsaz*, 2013). The spatiotemporal distribution of the fourth autumn precipitation pattern shows that the establishment of the trough on Europe and its eastern part location in the Eastern Europe has caused cold air to fall to the lower latitudes and the northern regions of the Middle East. As a result, the thickness of the atmosphere in the northern regions of the Middle East has reached a minimum (5350 meters) in the northern regions of the Middle East (*Fig. 6d*). At the same time, a weak low-altitude system with a cold core has been deployed in North Africa, preventing cold and humid Mediterranean air from flowing into North Africa in its cyclonic motion. On the other hand, the orbital flows of North Africa and their passage through the southern regions of the Middle East indicate the advection of hot air in the study area, which together with the cold European air fall by deep European trough leads to a baroclinic atmosphere, fronts and finally instability in the northern regions of the Middle East. However, the peak of baroclinic instability is in the northern regions of Saudi Arabia, Iraq, and western Iran, which, due to the transport of moisture from the Mediterranean, the Black Sea, and the Red Sea, can cause widespread precipitation in the study area (*Fig. 6d*).

4. Results

The results of the analysis of the autumn precipitation trend indicate that although the precipitation has increased in most areas, except for limited areas including the Zagros Mountains, other areas have not experienced a significant upward trend. Also, a decreasing trend has been observed in the form of spots along the coastline in the Caspian Sea. The results of the analysis of the thickness pattern of autumn precipitation showed that since low-altitude systems, troughs, and air fronts provide conditions for atmospheric instability, the establishment of low-altitude systems on Iran and the transfer of cold air and moisture from the Mediterranean Sea by the Mediterranean trough to the western regions of the Middle East have caused precipitation in the region. Therefore, the expansion of the European low-altitude system and its crossing over the Mediterranean and Black Seas, along with the transfer of Red Sea moisture to the central regions of the Middle East and the creation of an allobaric atmosphere in the northern regions of the study area, have provided instability and precipitation in the Middle East. Also, the passage of northern flows over the Black Sea and induction of blocking phenomenon in the central regions of Turkey have caused severe instability and possibly widespread

precipitation, but the location of the eastern part of the trough on Iran, which is accompanied by positive vorticity, maximum ascent, and instability can cause widespread precipitation by transferring moisture from the Black Sea, the Persian Gulf and the Red Sea. According to the precipitation patterns of autumn, it can be said that the rains in the Middle East region occur due to baroclinic instability due to cold and humid air of high altitudes and hot and humid air of low latitudes in North Africa, in such a way that the Black Sea and the Mediterranean Sea provide the required moisture in the high latitudes and the Red Sea and the Persian Gulf provide the required moisture in the low latitudes. The thickness of the atmosphere in the Middle East in autumn has the most fluctuations and changes, because the temperature difference in autumn in the Middle East is very large due to the infiltration of westerly winds to the north and the prevailing warm weather in the southern regions of the Middle East.

References

Alijani, B., 2002: Synoptic study of 500 hPa surface patterns in the Middle East, Nivar, consecutive issue, 44–45.

Asgari, A. and *Rahimzadeh, F.*, 2006: Study of precipitation variability in recent decades in Iran. *Geograph. Res. 58*, 67–.80

Ashjaei, M., 2000: Study and presentation of synoptic models of heavy precipitation in northwestern Iran. Master Thesis, Supervisor, Mohammad Kheirandish, Tarbiat Modares University.

Babaei Feini, O. and *Farajzadeh, M.*, 2002: Patterns of spatial and temporal variations in rainfall in Iran. *J.Spatial Plan. 6*(4), 51–76.

Farajzadeh, Manouchehr, Babaei Fini, Um al-Salame 2002: Patterns of spatial and temporal changes in precipitation in Iran. *Winter 2002, Vol. 6*(4).

Frišmantas, D. and *Stankūnavičius, G.*, 2020: Spatial Features of Heavy Precipitation Pattern in Lithuania. Vilnius University Proceedings 10, 53–53. https://doi.org/10.15388/Klimatokaita.2020.45

Jalali, M., Doostkamian, M., Shiri Karim Vandi, A., 2019: The studying and synoptic analysis of mechanical in mechanism of widespread winter precipitation of Iran. *Res. Geograp. Sci.* 19(55), 37–55. https://doi.org/10.29252/jgs.19.55.37

Kidson, J.W., 2000: An Analysis of New Zeealand Synoptic Types and their use in defining Weather Regimes. *Int. J. Climatol. 20*, 299–316. https://doi.org/10.1002/(SICI)1097-0088(20000315)20:3<299::AID-JOC474>3.0.CO;2-B

Lashkari, H., 2005: Synoptic Analysis of Two Samples of Winter Precipitation Patterns in South-East of Iran. *J Spat. Plan. 9*, 169-196.

Mafakheri, O., Saligheh, M., and *Kermani, A.*, 2019: Changes in Effective Components of Peak Rainfalls in Iran. *Phys. Geograp. Res. Quart. 51*(1), 87–103. 10.22059/jphgr.2019.254175.1007192

Masoudian, S.A., 2005: Study of Circulation Patterns Causing Large Floods in Karun. *J. Geogr. Develop. 5*,161–182.

Mirzayi, A., Abghari, H., and *Erfanian, M.*, 2020: Rainfall trend analysis and precipitation concentration index in synoptic stations of Urmia Lake Basin. *Geograp. Develop. Iranian J. 18*(59), 21–40. https://doi.org/10.22111/gdij.2020.5458

Mofidi, Abbas, Zarrin, Azar, Janbaz Ghobadi, Gholamreza, 2007: Determining the synoptic pattern of heavy and partial autumn precipitation on the southern shores of the Caspian Sea. *J. Earth Space Phys. 33*, 131–154.

Moradi, H.R. 2004: The role of the Caspian Sea in the rainy conditions of the northern coasts of the country. *J. Marine Sci. Technol 2*,. 77–87.

Qian, H. and *Xu, S.B.*, 2020: Prediction of Autumn Precipitation over the Middle and Lower Reaches of the Yangtze River Basin Based on Climate Indices. Climate 8(4), 53. https://doi.org/10.3390/cli8040053

Rezaei Banafshe, M., Hossein Alipour Ghazi, H., Jaffari Shendi, F., and *Alimohammadi, M.*, 2015: Synoptic analysis of heavy rainfall in northwest of iran (with an emphasis on patterns of atmospheric thickness). *Geograp. Plan, 19(53)*, 117–135.

Rezaei, B., Jahanbakhsh, M.S., BayatiKhatibi, M., and *Zeinali, B.*, 2010: Prediction of Autumn and Winter rainfall in the Western half of Iran, using the Mediterranean SST in Summer and Autumn. *Nat. Geogr. Studies 42(4)*, 47–62.

Rezai, P. and *Abed, H.*, 2010: Survey Least Temperature Change Trend in Station Rasht Synoptic with Accent on Glacial Period. *Geograp. Environ Observ 2*, 39–48.

Rousta, I., Doostkamian, M., Haghighi, E., and *Mirzakhani, B.*, 2016: Statistical-synoptic analysis of the atmosphere thickness pattern of iran's pervasive frosts. *Climate, 4*(3), 41. https://doi.org/10.3390/cli4030041

Rousta, I., Doostkamian, M., Olafsson, H., Ghafarian Malamiri, H. R., Zhang, H., Taherian, A. M., ... and *Monroy-Vargas, E.R.*, 2019: On the relationship between the 500 hPa height fluctuations and the atmosphere thickness over Iran and the Middle East. *Tethys, 16*, 3–14.

Sabziparvar, A.A., 1991: Investigation of Flood Generating Systems in Southwest Iran. M.Sc. Thesis, Institute of Geophysics, University of Tehran.

Sari Sarraf Behrooz, Rajaei Abdolhamid, Mesri Alamdari Parichehr, 2010: The Role of Topographic and Geographical Variables of Talesh Mountain in the Distribution of Regional Precipitation. *J. Geogr. Region. Plan 32*, 191–218.

Sohrabi, M., Fakheri, F., and *Bozorg, H.*, 2020: Investigating the effect of autumn and winter precipitation shifts on annual rainfed yield using time-precipitation index. *Water Soil 26*.

Ventura, F., Pisa, P.R., and *Ardizzoni, E.*, 2002: Temperature and precipitation trends in Bologna (Italy) from 1952 to 1999. *Atmos. Res. 61*(3), 203–214. https://doi.org/10.1016/S0169-8095(01)00135-1

Zappa, G., Ceppi, P., and *Shepherd, T.G.*, 2020: Time-evolving sea-surface warming patterns modulate the climate change response of subtropical precipitation over land. Proceedings of the National Academy of Sciences 117(9), 4539–4545. https://doi.org/10.1073/pnas.1911015117

DOI:10.28974/idojaras.2023.3.2

IDŐJÁRÁS

Quarterly Journal of the Hungarian Meteorological Service
Vol. 127, No. 3, July – September, 2023, pp. 285–298

Estimating the sunshine duration using multiple linear regression in Kocaeli, Turkey

Mine Tulin Zateroglu

University of Cukurova
Vocational School of Technical Sciences
(01350) Adana/Turkey

Author E-mail: mtzateroglu@cu.edu.tr

(Manuscript received in final form September 27, 2022)

Abstract— This study aims to estimate and evaluate the characteristic behavior of sunshine duration for long-term records. Sunshine duration and other climate variables such as cloudiness, precipitation, relative humidity, etc., have been measured in meteorological stations for a long time all over the world. But in some cases, such as missing data or unavailable station, the estimation of sunshine duration play a crucial role. Statistical models can be used to predict the sunshine duration over climate variables. To evaluate the behavior of sunshine duration, several climate variables were analyzed for different time scales. The data used in this study were collected from a ground-based meteorological station. In the first, all data were arranged according to different time scales as monthly, seasonal, and annual average values. Prediction models were constructed for each time scale. This study used multiple linear regression (MLR) to build the models and the Pearson correlation analysis to determine the relations between the climate elements. The created models for estimating sunshine duration were validated as well. According to the results, MLR can be utilized and recommended for the prediction of the sunshine duration over climate variables.

Key-words: sunshine duration, estimating, climate variables, Pearson correlation analysis, MLR

1. Introduction

Sunshine duration, which is a key element for solar radiation, has been widely studied over the recent years. The energy that comes from solar radiation is clean and environmentally friendly. Sunshine duration is highly related to solar radiation via the Angström-Prescott model that is utilized for predicting the amount of daily global solar radiation.

The measurement of sunshine duration is made pointwise at meteorological stations. In places, where there is no station and no measurement can be made, the sunshine duration values are estimated using different methods such as regression analysis and interpolation techniques. Sunshine duration is correlated to climate variables in the atmospheric environment. Some researchers used climate variables to determine their relationship to sunshine duration and to estimate the value of sunshine duration. An empirical formula was presented to estimate the sunshine duration using the cloud amount data (*Reddy*, 1974). Similarly, *Stanghellini* (1981) developed an empirical formula to predict the monthly sunshine duration via daily mean cloudiness values. *Chagnon* (1981) determined that a high amount of cirrus-type clouds originating from jet planes caused a decrease in sunshine duration. Sunshine duration is negatively related to cloudiness (*Angell et al*., 1984; *Essa* and *Etman*, 2004; *Hoyt*, 1977; *Palle* and *Butler*, 2001; *Robaa*, 2008; *Sanchez-Lorenzo et al*., 2009; *Weber*, 1994; *You et al*., 2010). Besides, similarly to cloudiness, relative humidity was also found as negatively correlated to sunshine duration (*Aksoy*, 1999; *Yang et al*., 2009a; *You et al*., 2010; *Zateroglu*, 2021a). Furthermore, sunshine duration was declared that positively correlated with wind speed (*Yang et al*., 2009a, 2009b). Additionally, *Sanchez-Lorenzo et al*. (2009) expressed a positive relationship between sunshine duration and atmospheric pressure. Some studies were shown that sunshine duration was negatively related to precipitation (*Yang et al*., 2009a; *You et al*., 2010; *Zateroglu*, 2021a). *Aksoy* (1999) evaluated the changes in sunshine duration over the changes in other climate parameters for Ankara in Turkey. *Yildirim et al*. (2013) investigated the trends of observed sunshine duration data and found a decrease in sunshine duration due to anthropogenic air pollution. Furthermore, air pollutants such as particulate matter and sulfur dioxide influence the sunshine duration and are associated with environmental parameters in the atmospheric periphery over urban areas (*Zateroglu*, 2021b, 2021c and 2022). Additionally, particulate matter and sulfur dioxide decrease the amount of sunshine duration (*Zateroglu*, 2021a). Also, the Pasquill–Gifford–Turner (PGT) scheme, which is used in predicting vertical and horizontal dispersion of a plume in air pollution models, considers the steady-state atmospheric conditions such as the quantity of solar radiation, fractional cloudiness, horizontal surface wind speed, and also vertical temperature gradient (*USEPA*, 1993; *Venkatram*, 1996). The air pollutants reflect and scatter solar radiation and then reduce the surface temperature. Sunshine duration is related to solar radiation with the Ansgtröm-

Prescott formula which is used for estimating the global solar radiation; so sunshine duration is associated with air pollutants (*Zateroglu*, 2022).

Sunshine duration is measured at meteorological stations but anyway, in some cases, measurements cannot be done due to some conditions such as remote areas, geographical problems, and not existing or insufficient stations. Different methods have been used to predict climate elements in climatological studies. Linear regression analysis was used to estimate sunshine duration (*Stanghellini*, 1981). This method was preferred in terms of compatibility with climate data, ease of operation, and efficient outcomes. Sunshine duration data were obtained from the Campbell-Stokes instrument. This equipment records the sunshine data by burning a specific card upon which sun rays were focused via a glass sphere of the sunshine recorder (*WMO*, 1996).

The main purpose of the present study was to gain the prediction models for sunshine duration over a statistical approach. Several climate variables were used as variables in building models. This study focuses on the 1961–2010 period. Monthly mean values of daily climate elements were taken for estimating the sunshine duration measured by a ground-based meteorological station. Furthermore, the accuracy of the empirical models obtained from the statistical analysis was evaluated via validation parameters of the regression. Finally, performance indices were implemented for the suitability of the prediction models. The findings were discussed and interpreted over the results of validation indicators.

2. Study area and data

This study was conducted for Kocaeli in the northwestern region of Turkey. The province is located between 29°22'E–30°21'E longitudes, 40°31'N– 41°13'N latitudes at 76 m altitude. There are intensive industrial activities and transportation facilities in the area. The population of the urban area is continually increasing as a result of developing industrialization. In the province, a temperate climate prevails on the Izmit Gulf coasts and the Black Sea coast, and a harsher climate prevails in the mountainous areas. It can be said that the climate of Kocaeli constitutes a transition between the Mediterranean climate and the Black Sea climate. In the city center, summers are hot and less rainy, and winters are rainy, snowy, and cold from time to time. There are some differences between the climate of Kocaeli's coasts facing the Black Sea and the coasts facing the Izmit Gulf. While sometimes sweltering heat is experienced on the gulf coasts in summer, the Black Sea coasts are cooler. According to the long-term records, the annual mean maximum air temperature is 19.8 °C, the annual mean minimum air temperature is 10.8 °C, the annual average monthly precipitation is 815.2 mm, annual average rainy days is 150.1, the number of annual mean sunshine duration is 5.7 hour, the annual average relative humidity is 71.7%, and the annual mean

wind speed is 1.6 m/s. The average annual precipitation on the Black Sea coast exceeds 1,000 mm. This amount decreases in the south; and falls below 800 mm (784.6 mm). On the slopes of the mountains facing the gulf, the climate is similar to the Black Sea coast. The amount of precipitation is also different in this section. Winds blow from the north and northeast in winter and from the northeast in summer.

In the present study, daily values of climate elements such as sunshine duration (SD), cloudiness (CLD), relative humidity (RHUM), wind speed (WS), precipitation (PREC), evaporation (EVAP), atmospheric pressure (PRES), minimum air temperature (TMIN), and maximum air temperature (TMAX) were obtained from the ground-based observation station at Izmit/Kocaeli. The measurements were realized by the Turkish State Meteorological Service (TSMS). Monthly average values of climate variables were computed over daily data. The values of relative sunshine duration were calculated for prediction models. The arranged data were analyzed by using a statistical approach, then the obtained statistical models were validated.

3. Methods

The relative sunshine duration *RSD* is defined as the ratio of the measured (*S*) and maximum possible daily (S_o) sunshine duration and its value varies between 0 and 1. S_o is calculated using the formula as follows (*Duffie* and *Beckman*, 1991; *Goswami*, 2015; *Kalogirou*, 2014):

$$S_0 = \left(\frac{2}{15}\right) cos^{-1}(-tan\delta tan\varphi) \,, \tag{1}$$

$$\delta = 23.45 * sin\left(\frac{360}{365}(284 + d)\right), \tag{2}$$

where φ is the latitude angle (-90≤ φ ≤+90) and depends on the location of interest, δ defines the solar declination angle between the equatorial plane and incoming solar rays, and d determines the number of days of the year (begins from January 1).

The Pearson correlation coefficient is a scale which denotes the strength of the linear correlation between variables. This metric determines not only the quantity but also the direction of the relation. It is computed as follows:

$$r(s_i, s_j) = \frac{Cov(s_i, s_j)}{\sigma(s_i)\sigma(s_j)} \quad , \tag{3}$$

where s_i and s_j are the measured values of the two climate variables, $\sigma(s_i)$ and $\sigma(s_j)$ are the standard deviations, and $Cov(s_i, s_j)$ denotes the covariance of s_i

and s_j. $r(s_i, s_j)$ demonstrates the correlation coefficient between the *RSD* and either climate variable. According to value of the Pearson correlation coefficient, the relations are categorized as low (value in 0.0–0.49), moderate (value in 0.5–0.69) and high (value in 0.7–1.0).

Regression-based techniques have been utilized in the estimation studies of climate parameters. To build the models for the climate and the other atmospheric elements, the multiple linear regression (MLR) method is commonly preferred for estimation among the several statistical methods. In this statistical approach, the method processes the dataset that fit the normal distribution. Climate data is appropriate for this analysis. MLR represents the relationships between dependent (response) and independent (predictor or explanatory) variables. In this study, *RSD* is the dependent variable, the other climate elements are the independent variables. The method reveals the number of changes in *RSD* as a percentage that is explained by other climate variables. The relationship between dependent and independent variables obtained from MLR analysis is defined as a mathematical model:

$$Y = a_0 + a_1X_1 + a_2X_2 + \ldots\ldots\ldots + a_rX_r + \mathcal{E} \ , \tag{4}$$

where Y expresses the dependent variable which consists of a measured data matrix with dimension (n x 1), n is the number of measurements, X_1, X_2, ……, X_r define the independent variables, X determines the measured data matrix with dimension ($n \times r$), r denotes the number of independent variables, a_o denotes the constant, a_1, a_2, ……, a_r demonstrate the regression coefficients, a is the coefficient matrix with dimension ($r \times 1$), $\mathcal{E}$ determines the predicted error term. To minimize the error term, the values of constant and regression coefficients are computed by the least squares method utilizing the coefficient matrix a, which is determined by formula $a = (X^TX)^{-1}(X^TY)$. X^T is the transpose of matrix X. The significance levels of constant and regression coefficients are determined over the t value and F distribution. In MLR analysis, the accuracy of the models is judged by two indicators named the coefficient of determination (R^2) and the standard error of estimation (*SEE*). R^2 denotes a measure of how well the predicted model fits the data used. It is expressed as the percent value changes from 0 to 1. SEE gives the amount of difference between actual and estimated values.

$$R^2 = 1 - \frac{\sum(P_k - \overline{M_k})^2}{\sum(M_k - \overline{M_k})^2} \ , \tag{5}$$

$$SEE = \sqrt{\frac{\sum(M_k - P_k)^2}{n-2}} \ , \tag{6}$$

where P_k and M_k determine the predicted and measured values, respectively, and n is the number of measurements. The level of the confidence interval was taken into account as 95% in constructing the empirical models.

To be evaluated on the same scale, all climate data were standardized before constructing the figures. The values of climate variables were transformed to normalized values (vary between 0 and 1) concerning the following formula:

$$I_i = \frac{I_j - I_{min}}{I_{max} - I_{min}} \ , \tag{7}$$

where I_j expresses the observed value, I_i determines the normalized value of I_j. I_{min} is the minimum value and I_{max} is the maximum value of the related dataset.

To verify the suitability of the prediction, some error terms are applied to the built models. The widely used performance indices, the root mean square error (RMSE), mean bias error (MBE), mean absolute error (MAE), percentage mean absolute error (MAPE), normalized mean square error (NMSE), fractional bias (FB), and index of agreement (IOA) were utilized to interpret the accuracy of the twelve models for months. These seven indices were calculated by the following formulas:

$$RMSE = \sqrt{\frac{\sum_{k=1}^{n}(P_k - M_k)^2}{n}}, \tag{8}$$

$$NMSE = \frac{\overline{(M_k - P_k)^2}}{\overline{M_k} * \overline{P_k}} \ , \tag{9}$$

$$MBE = \frac{\sum_{k=1}^{n}(P_k - M_k)}{n} \ , \tag{10}$$

$$MAE = \frac{\sum_{k=1}^{n}|P_k - M_k|}{n}, \tag{11}$$

$$MAPE = \frac{100}{n}\sum_{k=1}^{n}\frac{|P_k - M_k|}{M_k} \ , \tag{12}$$

$$FB = \frac{(\overline{M_k} - \overline{P_k})}{0.5 * (\overline{M_k} + \overline{P_k})}, \tag{13}$$

$$IOA = 1 - \frac{\sum_{k=}^{n}(P_k - M_k)^2}{\sum_{k=1}^{n}(|P_k - \bar{M}_k| + |M_k - \bar{M}_k|)^2} \ , \tag{14}$$

where P_k, and M_k denote the predicted and measured values respectively, $\overline{M_k}$ determines the mean value of the measured values, and n defines the number of measurements.

The performance indices shown in Eqs. (8)-(14) may be used to evaluate the efficiency of the prediction models. Commonly, as much as small (i.e., close to zero) for the value of RMSE, MBE, MAE, MAPE, NMSE, and FB, but as far as big (i.e., near 1) for the value of IOA are acceptable for the success of the

predictions. The values of FB are limited by -2 to +2. Positive values of FB describe a constructed model under-estimation, and the negative values describe a constructed model over-estimation.

To determine the distribution of climate variables, one-sample Kolmogorov-Smirnov test was implemented on a dataset for the normality test. The SPSS (Statistical Package for Social Science) package program was utilized to examine the statistical analysis.

4. Results and discussion

Pearson correlation analysis was used to reveal the statistically significant correlations between relative sunshine duration and climate variables. The values shown in *Table 1* were expressed in the directions such as positive and negative, and magnitudes of the relations for all months, i.e., from December to November (DE, JA, FE, MR, AP, MA, JN, JL, AU, SE, OC, NO). For EVAP, there were no available (NA) data for the months JA, FE, and MR. According to *Table 1*, RSD was correlated with CLD, RHUM, and PREC negatively, whereas it was correlated with WS, EVAP, PRES, TMIN, and TMAX positively despite the ignored exception cases. The statistically significant correlation coefficients were represented in bold in *Table 1*. In all months, CLD, RHUM, and PREC (except MR) have significant correlations with RSD on moderate and high levels for CLD, and low and moderate levels for RHUM and PREC. RSD was associated with WS and TMAX on weak levels, and with PRES on weak and moderate levels.

Table 1. Pearson correlation matrix for RSD

Time scale	CLD	RHUM	WS	PREC	EVAP	PRES	TMIN	TMAX
DE	**-0.674****	**-0.443****	-0.01	**-0.334***	0.075	**0.500****	-0.093	-0.009
JA	**-0.725****	**-0.336***	0.002	**-0.500****	NA	**0.517****	-0.069	-0.239
FE	**-0.749****	**-0.415****	-0.125	**-0.570****	NA	0.251	0.214	0.277
MR	**-0.834****	**-0.620****	-0.154	-0.014	NA	0.245	0.071	**0.349***
AP	**-0.844****	**-0.596****	0.021	**-0.500****	**0.437****	**0.406****	0.119	0.197
MA	**-0.796****	**-0.679****	0.114	**-0.527****	**0.772****	0.176	0.028	**0.281***
JN	**-0.775****	**-0.682****	0.194	**-0.387****	**0.608****	0.26	-0.095	0.278
JL	**-0.718****	**-0.602****	0.117	**-0.493****	**0.583****	0.023	0.043	0.163
AU	**-0.866****	**-0.671****	**0.305***	**-0.517****	**0.679****	-0.087	0.103	**0.449****
SE	**-0.808****	**-0.482****	0.245	**-0.488****	**0.735****	-0.02	0.128	0.242
OC	**-0.784****	**-0.631****	**0.352***	**-0.463****	**0.777****	-0.042	0.279	**0.427****
NO	**-0.831****	**-0.617****	0.064	**-0.534****	**0.412***	0.001	0.279	**0.329***

* Correlation is significant at the 0.05 level ($p<0.05$)
** Correlation is significant at the 0.01 level ($p<0.01$)

Besides, the variations of monthly correlation coefficients between RSD and each climate parameter were plotted in *Fig. 1*. It was seen that the Pearson correlation coefficients for CLD and RHUM varied similarly. Additionally, the changes in the correlation coefficient for TMIN and TMAX were shown as nearly close characteristics. The correlation coefficients of EVAP suddenly began to decrease from two months, MA and OC. For PREC, the coefficient sharply has a minimum value in MR. The highest statistically significant correlations were found for CLD in AU as high, RHUM in JN as moderate, WS in OC as low, PREC in FE as moderate, EVAP in OC as high, PRES in JA as moderate, TMAX in AU as low.

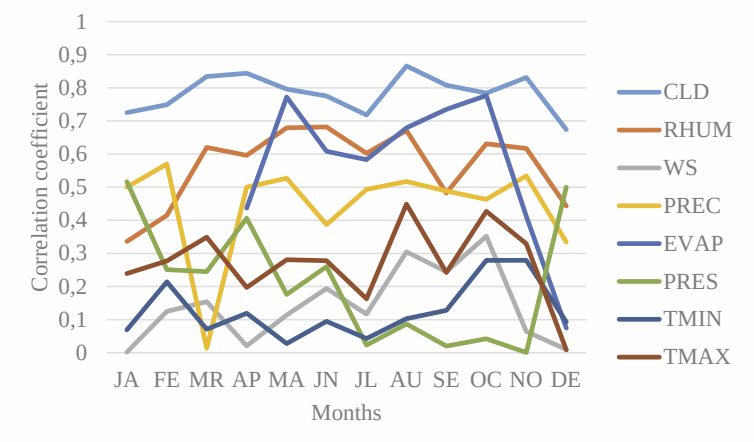

Fig. 1. Variations of correlation coefficients between RSD and each climate variable.

The monthly variations of climate variables were represented as normalized values in *Fig.2 (a-h)*. The normalized values of related climate variables were given below the table. As seen in *Fig.2. a, b*, RSD has high values in JN, JL, and AU and low values in DE, JA, and FE contrary to CLD and RHUM. RSD was changed reversely with CLD and RHUM. When RSD increased/decreased, CLD and RHUM decreased/increased. PREC and PRES behaved similarly against RSD as changed oppositely (*Fig. 2. c, d*).

The characteristics of monthly TMAX and TMIN had close behavior to the changes in RSD (*Fig.2. e, f*). Although some monthly data were missing, the variations in EVAP was completely compatible with RSD (*Fig. 2. g*). According to *Fig. 2 h*, the variation of WS showed different features compared to RSD. The amount of change in the increasing and decreasing behaviours of WS was not in the same portion as in RSD.

(a) cloudiness

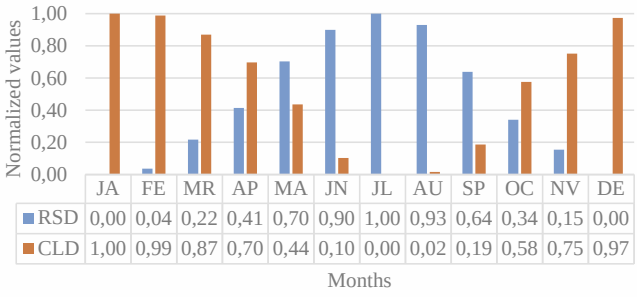

	JA	FE	MR	AP	MA	JN	JL	AU	SP	OC	NV	DE
RSD	0,00	0,04	0,22	0,41	0,70	0,90	1,00	0,93	0,64	0,34	0,15	0,00
CLD	1,00	0,99	0,87	0,70	0,44	0,10	0,00	0,02	0,19	0,58	0,75	0,97

(b) relative humidity

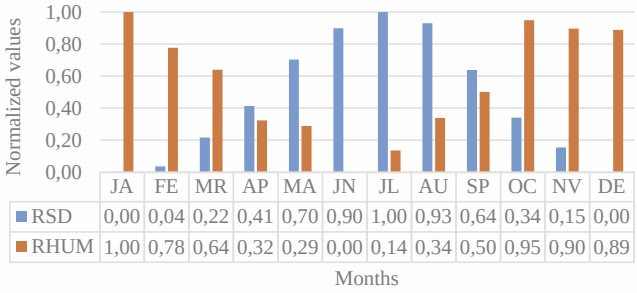

	JA	FE	MR	AP	MA	JN	JL	AU	SP	OC	NV	DE
RSD	0,00	0,04	0,22	0,41	0,70	0,90	1,00	0,93	0,64	0,34	0,15	0,00
RHUM	1,00	0,78	0,64	0,32	0,29	0,00	0,14	0,34	0,50	0,95	0,90	0,89

(c) precipitation

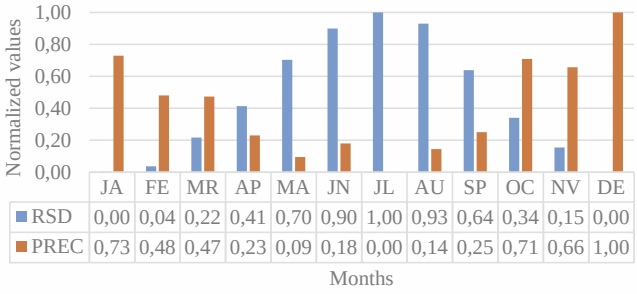

	JA	FE	MR	AP	MA	JN	JL	AU	SP	OC	NV	DE
RSD	0,00	0,04	0,22	0,41	0,70	0,90	1,00	0,93	0,64	0,34	0,15	0,00
PREC	0,73	0,48	0,47	0,23	0,09	0,18	0,00	0,14	0,25	0,71	0,66	1,00

(d) atmospheric pressure

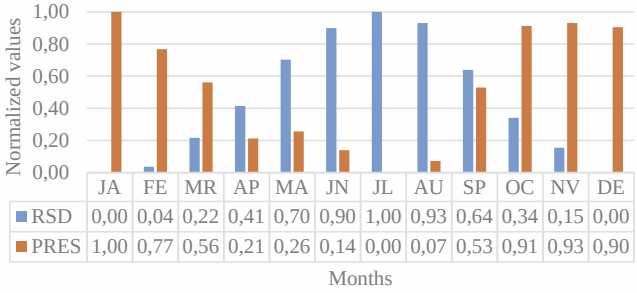

	JA	FE	MR	AP	MA	JN	JL	AU	SP	OC	NV	DE
RSD	0,00	0,04	0,22	0,41	0,70	0,90	1,00	0,93	0,64	0,34	0,15	0,00
PRES	1,00	0,77	0,56	0,21	0,26	0,14	0,00	0,07	0,53	0,91	0,93	0,90

Fig. 2. Monthly normalized values for the RSD and the climate variables.

(e) maximum air temperature

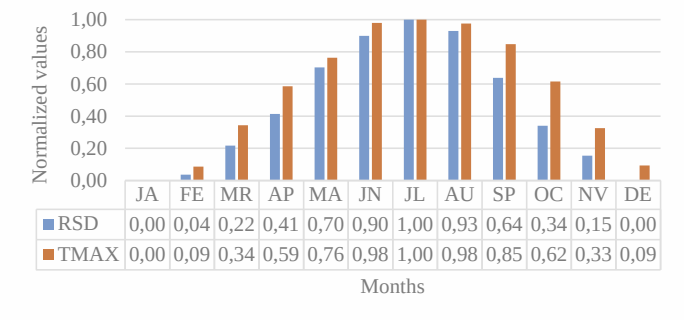

	JA	FE	MR	AP	MA	JN	JL	AU	SP	OC	NV	DE
RSD	0,00	0,04	0,22	0,41	0,70	0,90	1,00	0,93	0,64	0,34	0,15	0,00
TMAX	0,00	0,09	0,34	0,59	0,76	0,98	1,00	0,98	0,85	0,62	0,33	0,09

(f) minimum air temperature

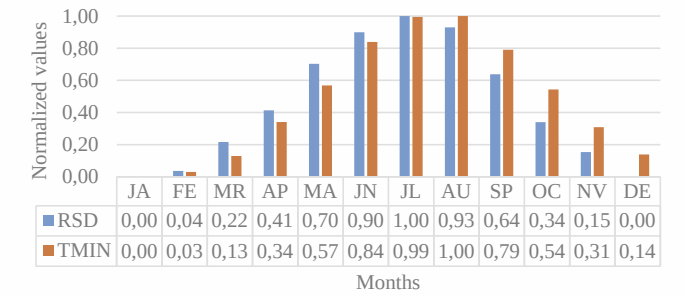

	JA	FE	MR	AP	MA	JN	JL	AU	SP	OC	NV	DE
RSD	0,00	0,04	0,22	0,41	0,70	0,90	1,00	0,93	0,64	0,34	0,15	0,00
TMIN	0,00	0,03	0,13	0,34	0,57	0,84	0,99	1,00	0,79	0,54	0,31	0,14

(g) evaporation

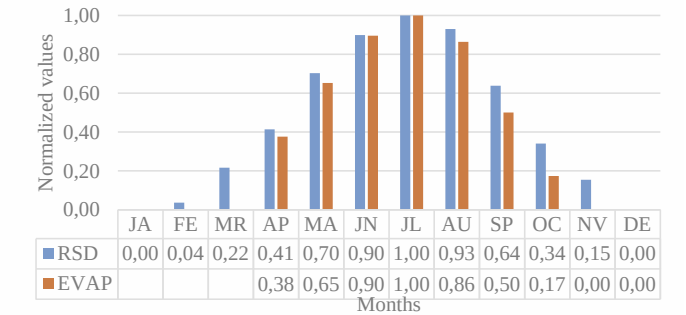

	JA	FE	MR	AP	MA	JN	JL	AU	SP	OC	NV	DE
RSD	0,00	0,04	0,22	0,41	0,70	0,90	1,00	0,93	0,64	0,34	0,15	0,00
EVAP				0,38	0,65	0,90	1,00	0,86	0,50	0,17	0,00	0,00

(h) wind speed

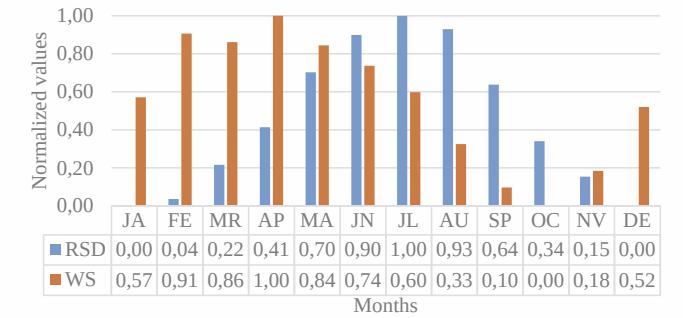

	JA	FE	MR	AP	MA	JN	JL	AU	SP	OC	NV	DE
RSD	0,00	0,04	0,22	0,41	0,70	0,90	1,00	0,93	0,64	0,34	0,15	0,00
WS	0,57	0,91	0,86	1,00	0,84	0,74	0,60	0,33	0,10	0,00	0,18	0,52

Fig. 2. Continue

To obtain a quantitative prediction of RSD, MLR analysis was performed. From this analysis, twelve empirical models were derived to estimate the RSD over several climate variables (*Table 2*). To specify the best predictors, the stepwise regression technique, which is one of the MLR methods, was implemented on the dataset. The superiority of this method was that the estimation of RSD was gained by statistically significant climate variables in the analysis. The order of the variables written in the prediction models also indicated their order of importance. Concerning *Table 2*, the best predictor for all months was CLD except for OC and EVAP. The sequel of sequencing could be expressed for the winter months as WS and PREC for DE; and PREC and WS for JA and FE. In MR, CLD was accompanied by RHUM and PRES. EVAP was in second-order in AP and MA, subsequently for TMIN and RHUM, respectively. For the remaining months, RHUM, PREC, TMIN, and EVAP were the second-order predictors that explain the RSD.

Table 2. Prediction models for RSD

Month	Model	R	R2	AdjR^2	SEE
JA	0.6397-0.0581*CLD-0.0007*PREC+0.0491*WS	0.842	0.709	0.685	0.04454
FE	0.7576-0.0696*CLD-0.0011*PREC+0.0465*WS	0.902	0.814	0.800	0.04232
MR	-4.0243-0.0496*CLD-0.0062*RHUM+0.0051*PRES	0.885	0.784	0.767	0.03772
AP	0.61-0.0514*CLD+0.0014*EVAP-0.0076*TMIN	0.892	0.795	0.775	0.03546
MA	0.7458-0.0479*CLD+0.0015*EVAP-0.0028*RHUM	0.913	0.833	0.817	0.03237
JN	1.0879-0.0539*CLD-0.0044*RHUM	0.878	0.772	0.758	0.03254
JL	0.8644-0.0618*CLD-0.0006*PREC	0.820	0.672	0.653	0.04030
AU	1.1272-0.0889*CLD-0.0109*TMIN	0.886	0.785	0.769	0.02824
SP	0.5268-0.0447*CLD+0.0022*EVAP	0.873	0.762	0.748	0.03622
OC	0.4889+0.0031*EVAP-0.0462*CLD	0.906	0.821	0.810	0.0358
NV	1.2586-0.0585*CLD-0.0074*RHUM	0.921	0.849	0.838	0.03866
DE	-7.5471-0.0597*CLD+0.0677*WS+0.008*PRES	0.798	0.637	0.609	0.04640

To achieve the accuracy of the prediction models, the value of R^2 is the best scale to indicate the success of the linear regression models. Mostly, R^2 and adjusted (Adj) R^2 were evaluated together to interpret the models. If the two values were close to each other, it was declared that the constructed model was appropriate. According to *Table 2*, R^2 and AdjR^2 values were nearly close to each other, so all models could be expressed as appropriate models. The calculated R^2 values were obtained as generally high levels except for JL and DE as moderate ones. For all time scales, SEE values were gained as small values desired for the suitable models.

To confirm of the concluded empirical models, the monthly mean values of RSD were computed for the period mentioned above. For either month, the predicted RSD value was calculated over the related climate elements by using the deduced model. Predicted and measured values of RSD were compared by implementing the performance indices (*Table 3*). The lower the RMSE, MBE, MAE, MAPE, NMSE, and FB and the higher the IOA, the smaller the model error and the preferable the estimation performance. The performance indices showed that the obtained regression models were appropriate to estimate the RSD for given time scales.

Table 3. Statistical indicators

Term	RMSE	MBE	MAE	MAPE	NMSE	FB	IOA
JA	0.06218	0.01591	0.04369	9.17987	0.05805	0.04387	0.82250
FE	0.06297	0.02162	0.03555	6.64318	0.04567	0.11522	0.88391
MR	0.06187	0.01492	0.04013	7.27445	0.03354	0.04414	0.82524
AP	0.04978	-0.00845	0.03684	3.21047	0.01450	-0.00259	0.86526
MA	0.04064	0.00443	0.03166	2.34710	0.00641	-0.00486	0.91476
JN	0.03373	0.00291	0.02714	1.84488	0.00320	-0.01214	0.90923
JL	0.04618	-0.00643	0.03628	1.98324	0.00531	-0.02072	0.84372
AU	0.04553	0.00776	0.03206	1.93990	0.00488	-0.00332	0.89146
SP	0.048	-0.00819	0.03694	2.30729	0.00718	-0.03572	0.86043
OC	0.06071	0.00194	0.03976	3.88605	0.02006	-0.04139	0.84605
NV	0.05497	0.0000021	0.04073	4.67938	0.02273	-0.01660	0.89559
DE	0.05748	-0.02059	0.04595	7.41340	0.05761	-0.15991	0.77577

5. Conclusıon

In this study, the statistical modeling of the sunshine duration was implemented because of its importance in many applications, especially in predicting solar radiation. This study presents an analysis of the estimation of the monthly mean sunshine duration. The MLR analysis method is widely used in estimating the climate variables. Correlation analysis expresses the relations as strength and direction between RSD and climate elements mentioned as CLD, RHUM, WS, PREC, EVAP, TMIN, and TMAX. RSD was correlated with CLD, RHUM, and PREC negatively, while with WS, EVAP, PRES, TMIN, and TMAX positively. The level of strength of the relations differed as weak, moderate, and high order according to the time scales. Further, the constructed prediction models were obtained as compatible with the climate elements. Climate variables selected in the models explained the RSD successfully. Additionally, some cases may affect

the accuracy of prediction models. For instance. measurements cannot be made accurately due to equipment calibration problems or climatic conditions. RHUM or/and PREC can affect the sunshine recorder and the sensitivity of the equipment. This may cause inaccurate measurements of sunshine duration. Besides, it should be noted that the amount of CLD is measured as visual observations by the observer, and this may cause measurement errors. Finally, the results for the statistical indicators demonstrated that the MLR method can be used for estimating the sunshine duration data for a specific location accurately.

Furthermore, according to the Pasquill-Gifford-Turner protocol, solar radiation. vertical air temperature gradient, CLD, and WS are highly associated with air pollutants; so air pollutants may affect the sunshine duration and can cause variations in its quantity because of the relationship between sunshine duration and solar radiation.

Additonally, the North Atlantic Oscillation (NAO) affects the region of the Black Sea. The NAO influences climate parameters, especially rainfall and air temperature. Therefore, because of the interactions between sunshine duration and other climate elements. NAO may influence the amount of sunshine duration in Kocaeli.

References

Aksoy, B., 1999: Analysis of changes in sunshine duration data for Ankara. Turkey. *Theor. Appl.Climatol.64* (3-4). 229–237. https://doi.org/10.1007/s007040050125

Angell, J.K., Korshover, J., and *Cotton, G.F.*, 1984: Variation in United States Cloudiness and Sunshine. 1950-82. *J. Appl. Meteorol.23.* 752–761. https://doi.org/10.1175/1520-0450(1984)023<0752:VIUSCA>2.0.CO;2

Changnon, S.A., 1981: Midwestern Cloud. Sunshine and Temperature Trends since 1901: Possible Evidence of Jet Contrail Effects. *J. Appl.Meteorol. 20*. 496–508. https://doi.org/10.1175/1520-0450(1981)020<0496:MCSATT>2.0.CO;2

Duffie, J.A. and *Beckman W.A.*, 1991: Solar Engineering of Thermal Processes. John Wiley & Sons. New York. NY. USA. 2nd edition.

Essa, K.S. and *Etman. M.S.*, 2004: On the Relation Between Cloud Cover Amount and Sunshine Duration. *Meteorol. Atmos. Phys. 87*. 235–240. https://doi.org/10.1007/s00703-003-0046-7

Goswami, D.Y., 2015: Principles of Solar Engineering. CRC Press. Taylor and Francis Group. Boca Raton. London. New York. 3rd edition.

Hoyt, D.V., 1977: Percent of Possible Sunshine and the Total Cloud Cover. *Month.Weather Rev. 105*, 648–652. https://doi.org/10.1175/1520-0493(1977)105<0648:POPSAT>2.0.CO;2

Kalogirou, S.A., 2014: Solar Energy Engineering Processes and Systems. Elsevier Inc. Amsterdam. Netherlands. 2nd edition. 815 pp.

Palle, E. and *Butler, C.J.*, 2001: Sunshine Records From Ireland: Cloud Factors and Possible Links to Solar Activity and Cosmic Rays. *Int. J. Climatol. 21*. 709–729. https://doi.org/10.102/joc.657

Reddy, S.J., 1974: An empirical method for estimating sunshine from total cloud amount. *Solar Energy 15*(4), 281–285. https://doi.org/10.1016/0038-092X(74)90017-6

Robaa, S.M., 2008: Evaluation of Sunshine Duration From Cloud Data in Egypt. *Energy 33*, 785–795. https://doi.org/10.1016/j.energy.2007.12.001

Sanchez-Lorenzo. A.. Calbo. J.. Brunetti. M.. and *Deser. C.*. 2009: Dimming / Brightenning over the Iberian Peninsula: Trends in Sunshine Duration and Cloud Cover and Their Relations with Atmospheric Circulation. *J. Geophys. Res. 114*. https://doi.org/10.1029/2208JD011394

Stanghellini, C.A., 1981: Simple Method for Evaluating Sunshine Duration by Cloudiness Observations. *J. Appl. Meteorol. 20,* 320–323. https://doi.org/10.1175/1520-0450(1981)020<0320:ASMFES>2.0.CO;2

USEPA, 1993: Selection Criteria for Mathematical Models Used in Exposure Assessments: Atmospheric Dispersion Models. United States Environmental Protection Agency. Office of Research and Development Washington. DC 20460. EPA/600/8-91/038.

Venkatram, A., 1996: An examination of the Pasquill-Gifford-Turner dispersion scheme. *Atmos. Environ.30*(8). 1283–1290. https://doi.org/10.1016/1352-2310(95)00367-3

Weber, G.R., 1994: On the Seasonal Variation of Local Relationships Between Temperature. Temperature Range. Sunshine and Cloudiness. *Theor. Appl. Climatol. 50*(1–2). 15–22. https://doi.org/10.1007/BF00864898

WMO, 1996: Guide to meteorological instruments and methods of observations. 6th ed. WMO. No.8. Geneva.

Yang, Y.H., Zhao. N., Hao. X.H., and *Li. C.Q.,* 2009a: Decreasing trend of sunshine hours and related driving forces in North China. *Theor. Appl. Climatol. 97,* 91–98. https://doi.org/10.1007/s00704-008-0049-x

Yang, Y., Zhao. N., Hu, Y., and *Zhou, X.,* 2009b: Effect of Wind Speed on Sunshine Hours in Three Cities in Northern China. *Climate Research 39.* 149–157. https://doi.org/10.3354/cr00820

Yildirim, U., Yilmaz, I.O., and *Akinoglu, B.G.,* 2013: Trend analysis of 41 years of sunshine duration data for Turkey. *Turkish J. Engineer. Environ. Sci. 37.* 286–305. https://doi.org/10.3906/muh-1301-11

You, Q., Kang, S., Flugel, W.A., Lorenzo, A.S., Yan, Y., Huang, J., and *Vide, J.M.,* 2010: From Brightening to Dimming in Sunshine Duration over the Eastern and Central Tibetan Plateau (1961–2005). *Theor. Appl. Climatol. 101,* 445–457. https://doi.org/10.1007/s00704-009-0231-9

Zateroglu, M.T., 2021a: Statistical Models For Sunshine Duration Related To Precipitation and Relative Humidity. *Eur. J.f Sci. Technol. 29.* 208–213. https://doi.org/10.31590/ejosat.1022962

Zateroglu, M.T., 2021b: Assessment of the effects of air pollution parameters on sunshine duration in six cities in Turkey. *Fresenius Environ. Bull. 30*(02A). 2251–2269.

Zateroglu, M.T., 2021c: The Role of Climate Factors on Air Pollutants (PM_{10} and SO_2). *Fresenius Environ. Bull. 30,* 12029–12036.

Zateroglu, M.T., 2022: Modelling The Air Quality Index For Bolu. Turkey. *Carpathian J. Earth Environ. Sci. 17,* 119 –130. https://doi.org/10.26471/cjees/2022/017/206

DOI:10.28974/idojaras.2023.3.3

IDŐJÁRÁS

Quarterly Journal of the Hungarian Meteorological Service
Vol. 127, No. 3, July – September, 2023, pp. 299–319

Research trend the in meteorology and atmospheric sciences category based on essential science indicators during 2011–2021

Bao-Zhong Yuan[1,*] and **Jie Sun**[2]

[1]*College of Plant Science and Technology*
Huazhong Agricultural University
Wuhan city, Hubei province, PR China, 430070

[2] *Library of Huazhong Agricultural University*
Wuhan city, Hubei province, PR China, 430070

**Corresponding author E-mail: yuanbz@mail.hzau.edu.cn*

(Manuscript received in final form October 25, 2022)

Abstract— This study analyzed 1,636 top papers in the subject category of meteorology and atmospheric sciences about eleven years from 2011 to 2021, which included 1,636 highly cited papers and 24 hot papers in the field belonged to 20 Web of Science categories and 14 research areas. All top papers, written in English, were from 13,878 authors, 2,913 organizations, and 124 countries or territories, and published in 72 journals in the field. The top five journals are the *Nature Climate Change* (15.9% of the studied paper), *Atmospheric Chemistry and Physics* (12.1%), *Journal of Climate* (7.0%), *Bulletin of the American Meteorological Society* (6.7%), and *Journal of Geophysical Research Atmospheres* (4.6%), each published more than 76 papers. Top five countries were the USA, England, PR China, Germany, and France. Furthermore, top five organizations of National Oceanic and Atmospheric Administration (NOAA), National Center for Atmospheric Research (NCAR), National Aeronautics and Space Administration (NASA), Chinese Academy of Sciences, and University Colorado were popular based on contribution of articles more than 134 papers each. All keywords were separated into eight clusters for different research topic. Visualizations offer exploratory information on the current state in a scientific field or discipline, as well as can indicate possible developments in the future.

Key-words: bibliometric analysis, essential science indicators (ESI), meteorology and atmospheric sciences, top papers, VOSviewer

1. Introduction

According to the category description for meteorology and atmospheric sciences in Scope Notes of Science Citation Index Expanded, it covers those resources that deal with the atmosphere and its phenomena, especially weather and weather forecasting. Resources in this category are concerned with the atmosphere's temperature, density, winds, clouds, precipitation and other characteristics, as well as the structure and evolution of the atmosphere in terms of external influences and the basic laws of physics. This category also includes resources dealing with climatology (*Clarivate*, 2022, Categories & Collections (Scope Notes)).

Bibliometric analysis are useful tools to collect, analyze, and get a better understanding of the progress in specific areas of science and technology, and to assess the outcomes of research efforts and investments (*Eito-Brun*, 2021). Bibliometrics technique has been adopted in Web of Science category of meteorology and atmospheric sciences such as, atmospheric simulation trends in meteorology and atmospheric science journals (*Li*, 2018), scientific production on coastal communities' social vulnerability to climate change and to the impact of extreme events (*Lima* and *Bonetti*, 2020), disaster and climate change resilience (*Rana*, 2020), multidimensional flood risk management under climate changes (*da Silva et al*., 2020), research on carbon price in emissions trading scheme (*Ji et al.*, 2019), tsunami in the last 15 years (*Jain et al*., 2021), mapping the evolution and current trends in climate change adaptation science (*Nalau* and *Verrall*, 2021), knowledge mapping analysis of integrated disaster risk management in a changing climate (*Wang et al*., 2021), evolution of disaster nursing research in the past 30 years (1990–2019) (*Molassiotis et al*., 2021), a quantitative approach to the scientific production on radar altimetry (*Eito-Brun*, 2021), waste-to-energy technologies towards circular economy (*Boloy et al*., 2021), bibliometric analysis of global trends on soil moisture assessment using the remote sensing research study from 2000 to 2020 (*Badaluddin et al*., 2021), a large-scale bibliometric analysis of global climate change research between 2001 and 2018 (*Fu* and *Waltman*, 2022), the use of local climate zones in the urban environment (*Aslam* and *Rana*, 2022), coastal impacts of storm surges on a changing climate (*Leal et al*., 2022), disasters triggered by natural hazards and terrorism (*Battikh et al*., 2022), bibliometric analysis of rice and climate change publications based on Web of Science (*Yuan* and *Sun*, 2022a), and others.

Top papers are the sum of hot papers and highly cited papers, based on Clarivate Analytics' Essential Science Indicators (ESI). A bibliometric evaluation of highly cited papers with high-level representation was conducted during the period from 1999 to 2009 based on the essential science indicators (ESI) database (*Fu et al*., 2011), highly cited papers in the field of Economics and Business based on the Essential Science Indicators database (*Zhang et al.*, 2018), highly cited papers in operations research and management science from 2008 to 2017 (*Liao*

et al., 2019), highly cited papers in environmental sciences (*Ma et al*., 2020), macro-level collaboration network analysis and visualization with Essential Science Indicators (*Yang et al*., 2020). *Sun* and *Yuan* have analyzed the top papers in library and information science (*Sun* and *Yuan*, 2020), agronomy category (*Sun* and *Yuan*, 2021), green and sustainable science and technology category (*Yuan* and *Sun*, 2019), scientific research on maize or corn (*Yuan* and *Sun*, 2020), research trend and status of forestry category based on Essential Science Indicators during 2010–2020 (*Yuan* and *Sun*, 2021), trend and status of food science and technology category based on the Essential Science Indicators during 2011–2021(*Yuan* and *Sun*, 2022b), and others.

The purpose of this paper was to use bibliometric methods to analyze top papers in the subject category of meteorology and atmospheric sciences during 11-year-long period from 2011 to 2021 through publication year, category, author, affiliations, country, journals, all keywords, and other key features. Co-authorship network visualization of authors, organizations, and countries, co-occurrence network visualization of all keywords were done by the VOSviewer software tool.

2. Materials and methods

2.1. Essential Science Indicators (ESI)

Article counts for ESI are derived from the Web of Science (WoS) core collection over an 11-year-long period. Here, the database has been updated on March 10, 2022, to cover the period from January 1, 2011 to December 31, 2021 (Clarivate, Essential Science Indicators Help, 2022).

2.2. Data collection

Data collection was completed on the single day on March 28, 2022 to avoid the bias. Firstly, it was conducted an advanced search in the WoS category of meteorology and atmospheric sciences. Then, the results were used to identify the highly cited papers and hot papers in the field (Hot papers are papers that receive citations soon after publication, relative other papers of the same field and age.). There were 1,636 top papers from the WoS Core Collection. The records were downloaded and saved as plain text format by selecting the export format "full records and cited references", and then imported into VOSviewer (version 1.6.18, 2022, Leiden University, Leiden, the Netherlands) for further citation analysis. The impact factors (IF 2021 and IF 5year) were taken from the Journal Citation Report (JCR 2021) that was updated on June 28, 2022 (Clarivate, Journal Citation Reports ™ 2021, 2022). The Journal Citation Reports™ includes journals from the Science Citation Index Expanded (SCIE) and the Social Science Citation Index (SSCI).

2.3. VOSviewer

VOSviewer is a freely available computer program developed to construct and view bibliometric maps with detailed approach in an easy-to-interpret way (www.vosviewer.com). In this work, VOSviewer were used to show the international collaboration between the authors, organizations, countries and the research trends through all keywords (*Van Eck* and *Waltman*, 2010). The graphs represent a network of items through circles, whose size differs according to the significance of the element, whereas the network connections represent the proximity of the link between items. The distance position of the circles and distinct colors are used to cluster the elements. In this paper, default parameters values of the VOSviewer are usually used in the analysis (*Van Eck* and *Waltman*, 2022).

3. Results and discussion

3.1. Document types and language of publication

From the WoS Index, all of the 1,636 top papers were identified in SCIE (1,633 papers, ratio of total papers is 99.817%), SSCI (391, 23.9%), and Conference Proceeding Citation Index-Science (CPCI-S, 7, 0.428%). The document types of all 1,636 top papers were articles (1,440, 88.02%), review articles (196, 11.98%), and also included data papers (19, 1.161%) and proceedings papers (7, 0.428%). Among the total 1,636 top papers, there were 24 hot papers and 1,636 highly cited papers, which means that the 24 hot papers are both hot papers and highly cited papers. All top papers were published in English language.

3.2. Publication output

Fig. 1 shows the top paper of the meteorology and atmospheric sciences category for eleven years from 2011 to 2021. The mean publication was 148.73 each year, and the highest value was 186 in 2013. The *h*-index was initially proposed as a measure of a researcher's scientific output based on counting the number of publications (N) by that researcher cited N or more times (*Hirsch*, 2005). For the total 1,636 papers, the *h*-index is 342, and the average citation per item is 279.87 till to March 28, 2022.

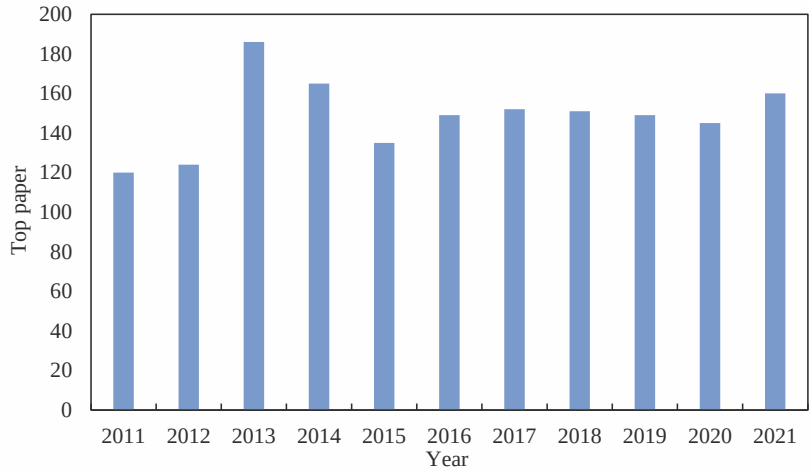

Fig. 1. Number of top papers for the meteorology and atmospheric sciences category per year from 2011 to 2021.

3.3. Web of Science categories and research areas

Based on the WoS categories, the total 1,636 papers were all in the meteorology and atmospheric sciences category, they also belong to other 19 WoS subject categories and total 14 research areas (*Table 1*).

The top six categories included meteorology atmospheric sciences (1,636 papers, 100% of 1,636 papers), environmental sciences (724, 44.254%), environmental studies (320, 19.56%), geosciences multidisciplinary (148, 9.046%), agronomy (67, 4.095%) and forestry (67, 4.095%). The top five research areas included meteorology atmospheric sciences (1,636 papers, 100% of 1,636 papers), environmental sciences ecology (779, 47.616%), geology (148, 9.046%), agriculture (67, 4.095%) and forestry (67, 4.095%). Journals or papers may be classified into two or more categories in the WoS, showed the multidisciplinary character of this research field (*Elango* and *Ho*, 2017).

Table 1. WoS categories and research areas for the meteorology and atmospheric sciences category during 2011-2021

Rank	WoS categories			Research areas		
	Categories	**No. papers**	**% Total papers**	**Areas**	**No. papers**	**% Total papers**
1	Meteorology Atmospheric Sciences	1,636	100	Meteorology Atmospheric Sciences	1,636	100
2	Environmental Sciences	724	44.254	Environmental Sciences Ecology	779	47.616
3	Environmental Studies	320	19.56	Geology	148	9.046
4	Geosciences Multidisciplinary	148	9.046	Agriculture	67	4.095
5	Agronomy	67	4.095	Forestry	67	4.095
6	Forestry	67	4.095	Water Resources	45	2.751
7	Water Resources	45	2.751	Engineering	27	1.65
8	Oceanography	21	1.284	Oceanography	21	1.284
9	Astronomy Astrophysics	11	0.672	Astronomy Astrophysics	11	0.672
10	Engineering Chemical	9	0.55	Geochemistry Geophysics	5	0.306
11	Engineering Mechanical	9	0.55	Biophysics	4	0.244
12	Engineering Aerospace	7	0.428	Physiology	4	0.244
13	Engineering Environmental	6	0.367	Remote Sensing	1	0.061
14	Geochemistry Geophysics	5	0.306	Telecommunications	1	0.061
15	Biophysics	4	0.244			
16	Engineering Ocean	4	0.244			
17	Physiology	4	0.244			
18	Engineering Civil	1	0.061			
19	Remote Sensing	1	0.061			
20	Telecommunications	1	0.061			

3.4. Core journals

All the 1,636 top papers were published in 72 journals. The top 20 core journals are displayed in *Table 2* with total articles each more than 14 top papers. The table showed the journal impact factor as IF 2021 and IF 5year, quartile in category (QC) and quartile rank (QR) among the total 94 journals in the meteorology and atmospheric sciences category from the Journal Citation Reports ™ 2021.

The top 5 journals, top 10 journals, top 15 journals, and top 20 journals published about 46.454%, 64.302%, 78.238%, and 84.84% of the total 1,636 top papers, respectively. The top five journals are the *Nature Climate Change* (260, 15.892%), *Atmospheric Chemistry and Physics* (199, 12.164%), *Journal of Climate* (115, 7.029%), *Bulletin of the American Meteorological Society* (110, 6.724%) and *Journal of Geophysical Research Atmospheres* (76, 4.645%), each published more than 76 papers. Based on the results of quartile category in *Table 2*, among the top 20 journals, sixteen journals were in quartile 1, three journals were in quartile 2 and one journal was in quartile 3.

Table 2. The top 20 core journals on meteorology and atmospheric sciences category research indexed in the WoS

Rank	Journal	TP	Ratio (%)	IF 2021	IF 5year	QC	QR
1	*Nature Climate Change*	260	15.892	28.66	32.35	Q1	1
2	*Atmospheric Chemistry and Physics*	199	12.164	7.197	7.32	Q1	12
3	*Journal of Climate*	115	7.029	5.38	6.549	Q1	20
4	*Bulletin of the American Meteorological Society*	110	6.724	9.116	10.009	Q1	6
5	*Journal of Geophysical Research Atmospheres*	76	4.645	5.217	5.302	Q1	22
6	*Atmospheric Environment*	69	4.218	5.755	6.027	Q1	19
7	*Agricultural and Forest Meteorology*	67	4.095	6.424	7.021	Q1	17
8	*Environmental Research Letters*	53	3.24	6.947	8.414	Q1	13
9	*Wiley Interdisciplinary Reviews Climate Change*	52	3.178	10.072	10.452	Q1	3
10	*Earth System Science Data*	51	3.117	11.815	12.88	Q1	2
11	*Atmospheric Research*	48	2.934	5.965	5.97	Q1	18
12	*Climate Dynamics*	48	2.934	7.901	4.742	Q2	24
13	*Climatic Change*	48	2.934	5.174	6.058	Q1	23
14	*International Journal of Climatology*	44	2.689	3.651	4.914	Q2	45
15	*Atmospheric Measurement Techniques*	40	2.445	4.184	4.473	Q2	40
16	*Journal of Advances in Modeling Earth Systems*	39	2.384	8.469	7.008	Q1	8
17	*Quarterly Journal of the Royal Meteorological Society*	22	1.345	7.237	5.303	Q1	11
18	*Natural Hazards*	18	1.1	3.158	3.685	Q3	58
19	*Global Biogeochemical Cycles*	15	0.917	6.5	7.067	Q1	16
20	*Earths Future*	14	0.856	8.852	9.274	Q1	7

Note: TP: Total publications; Ratio: ratio of 1,636 (%); IF 2021: journal impact factor in 2021; IF5 year: journal impact factor of 5 years; QC: quartile in category; QR: quartile rank of 94 journals in the meteorology and atmospheric sciences category from the Journal Citation Reports ™ 2021.

According to the citation sources analyzed by the VOSviewer, for the publication data in the citation of 72 journals, there were 43 journals that meet the thresholds of 5 publications, and were connected to each other in *Fig. 2*. The network map of citation for 43 journals in the field of meteorology and atmospheric sciences category is shown six clusters with different colors in *Fig. 2*, the size of circles reflects a total number of journal publication records. Journals in the same color cluster usually suggested that they published the similar content papers and had close relations with each other. The first cluster (red) had twelve journals and centered as *Journal of Climate*, the second cluster (green) had nine journals and centered as *Atmospheric Chemistry and Physics*, the third cluster (blue) had eight journals and centered as *Nature Climate Change*, the fourth cluster (yellow) had eight journals and centered as *Earth System Science Data*, the fifth cluster (violet) had four journals and centered as *Atmospheric Research*, and the sixth cluster (light blue) had two journals both the *Atmospheric Research* and *Climate Risk Management*.

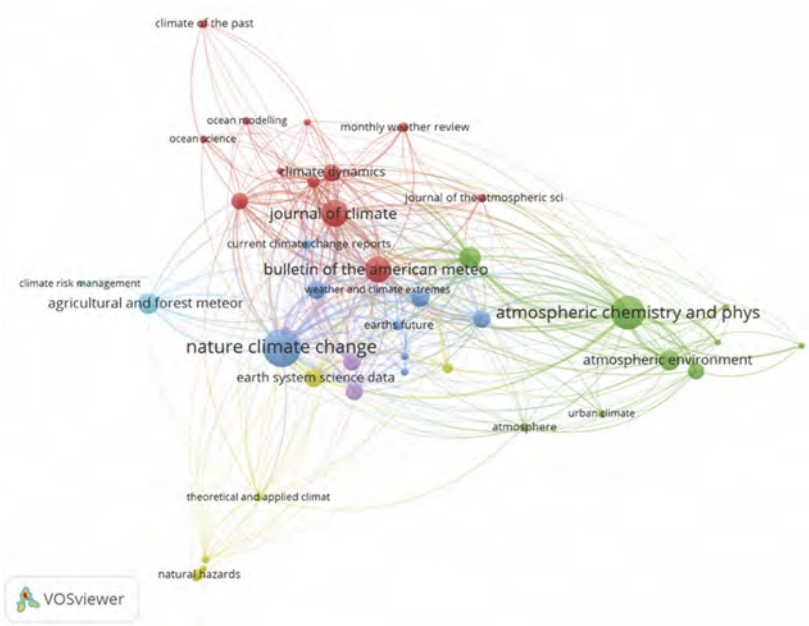

Fig. 2. Network visualization maps of citation journals in the field of meteorology and atmospheric sciences category based on WoS with 43 circles and 6 clusters.

3.5. Authors co-authorship analysis

A total of 13,878 authors have dedicated to all 1,636 top papers, and 291 authors met the thresholds of five publications, but 283 authors were connected with each

other and were separated into ten clusters. The network of the authors co-authorship analysis is represented in *Fig. 3*. Authors in the same cluster usually suggested that they studied in a similar field or worked at the same institute or had close cooperation with each other. The strong linkages between authors show that within the cluster, the collaboration is strong.

The details of the author information in the published articles from 2011 to 2021 along with citation, average citations, affiliations, and countries are provided in *Table 3*. The top five authors published more than 15 papers. Based on the average citations, each published paper of the top five mostly cited authors were cited more than 479.7 times.

There were five authors from the USA, the organizations were the State University of New York, Stanford University, University of Colorado, National Center for Atmospheric Research (NCAR), National Oceanic and Atmospheric Administration (NOAA); three authors from the Netherlands, the organizations were the University of Utrecht and the Vrije Universiteit Amsterdam; two authors from Tsinghua University of China; two authors from the University of Exeter and the Imperial College London of England; one author from the Commonwealth Scientific and Industrial Research Organisation (CSIRO) of Australia; one author from the University of Paris Saclay of France; one author from Center for International Climate Research, Norway; one author from the Environment and Climate Change Canada.

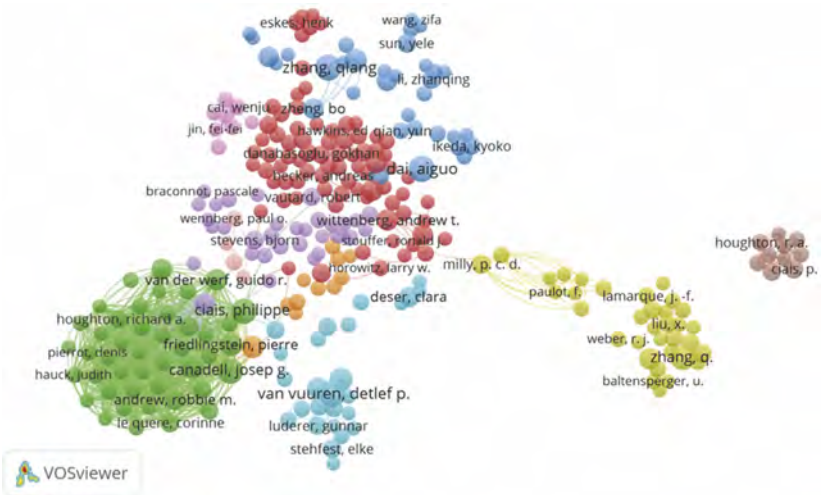

Fig. 3. Network visualization map of top authors in meteorology and atmospheric sciences category from 2011 to 2021.

Table 3. The top sixteen most prolific authors in the field of meteorology and atmospheric sciences category from 2011 to 2021

Rank	Author	Papers	Citations	Average citations	Affiliations	Country
1	Dai, Aiguo	16	7,675	479.7	State University of New York	USA
2	Van Vuuren, Detlef P.	16	9,096	568.5	University of Utrecht	Netherlands
3	Zhang, Qiang	16	3,177	198.6	Tsinghua University	China
4	Canadell, Josep G.	15	6,669	444.6	CSIRO Oceans & Atmosphere	Australia
5	Ciais, Philippe	15	6,833	455.5	University of Paris Saclay	France
6	Riahi, Keywan	13	6,416	493.5	University of Utrecht	Netherlands
7	Friedlingstein, Pierre	12	6,294	524.5	University of Exeter	England
8	He, Kebin	12	2,664	222.0	Tsinghua University	China
9	Jackson, Robert B.	12	4,092	341.0	Stanford University	USA
10	Peters, Glen P.	12	5,036	419.7	enter for International Climate Research	Norway
11	Jimenez, J. L.	11	2,878	261.6	University of Colorado	USA
12	Rogelj, Joeri	11	3,405	309.5	Imperial College London	England
13	Trenberth, Kevin E.	11	5,573	506.6	National Center Atmospheric Research	USA
14	van der Werf, Guido R.	11	4,972	452.0	Vrije Universiteit Amsterdam	Netherlands
15	Wittenberg, Andrew T.	11	3,635	330.5	National Oceanic and Atmospheric Administration (NOAA)	USA
16	Zhang, Xuebin	11	2,737	248.8	Environment and Climate Change	Canada

3.6. Countries/regions co-authorship analysis

Co-authorship with countries as unit is the relation of items based on the number of co-authors in papers highlighting their respective countries. There were 124 countries or regions that contributed 1,636 top papers from 2011 to 2021 based on WoS, and 56 countries or regions that met the requirement threshold of five papers.

Table 4 represents the list of the top 20 countries or regions that published more than 55 papers. Among the 20 countries, the USA, England, Peoples

Republic of China, Germany, and France were the major article contributors. From the average citations, the top five countries were South Korea, Austria, Japan, Sweden, and England, whose citations are more than 311.7 times per paper.

Table 4. Top 20 countries/regions publishing top papers in the field of meteorology and atmospheric sciences category from 2011 to 2021.

Rank	Countries/Regions	Records Count	Cluster	Total link strength	Citations	Average citations
1	USA	984	3	2,837	286,090	290.7
2	England	459	3	2,314	143,077	311.7
3	Peoples Republic of China	419	1	1,333	85,528	204.1
4	Germany	368	2	2,130	110,255	299.6
5	France	272	2	1,800	70,562	259.4
6	Australia	243	1	1,441	66,309	272.9
7	the Netherlands	222	2	1,401	62,128	279.9
8	Canada	212	3	1,258	59,941	282.7
9	Japan	181	3	1,305	73,050	403.6
10	Switzerland	177	2	1,217	51,249	289.5
11	Italy	164	2	1,224	41,545	253.3
12	Spain	145	2	1,083	36,937	254.7
13	Norway	136	2	1,074	41,023	301.6
14	Austria	115	2	827	54,576	474.6
15	Sweden	107	2	842	39,494	369.1
16	Finland	83	2	686	19,858	239.3
17	Belgium	67	2	506	14,419	215.2
18	Denmark	63	2	596	15,947	253.1
19	South Korea	58	1	411	29,216	503.7
20	Scotland	55	3	498	15,497	281.8

There were 56 countries or regions that met the requirement threshold of five papers(*Fig. 4*). The VOSviewer divided these circles into three clusters. According to *Fig. 4*, the first cluster consisted of twenty-seven countries or regions (red color) including the Peoples Republic of China, Australia, South Korea, India, Brazil, South Africa, Russia, Saudi Arabia, Malaysia, Argentina, Iran, Mexico, Chile, Singapore, Taiwan, Turkey, Colombia, Peru, Indonesia, Pakistan, Vietnam, Kenya, Romania, Egypt, Morocco, Ecuador, Estonia. The

second cluster consisted of twenty-two countries or regions (green color) including Germany, France, the Netherlands, Switzerland, Italy, Spain, Norway, Austria, Sweden, Finland, Belgium, Denmark, Greece, Portugal, Israel, Ireland, Poland, Czech Republic, Hungary, Cyprus, Slovenia, Croatia. The third cluster consisted of seven countries (blue color) including USA, England, Canada, Japan, Scotland, New Zealand, Wales. Taiwan as a region of China showed the stronger research ability in the field.

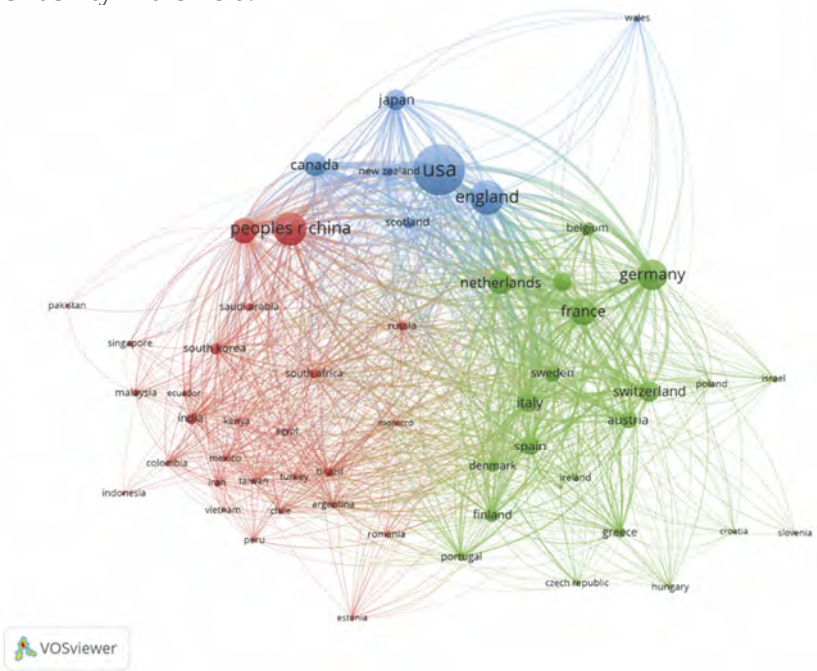

Fig. 4. The country co-authorship network of the meteorology and atmospheric sciences related top papers from 2011 to 2021 with 56 nodes and 3 clusters.

3.7. Organizations (author affiliation) co-authorship analysis

The affiliations presented were described on the profile of each researcher in WoS. They were updated according to the last paper published by the author until March 28, 2022. A total of 2,913 organizations had 1,636 top papers, there were 437 organizations met the minimum thresholds of five citations.

Table 5 represents the top 21 organizations and institutions ranked by the number of total publications (more than 52 papers), and also showed the total link of strength, citations, average citations, and country. These 21 organizations were mainly in USA (11 organizations), England (5 organizations), China (3 organizations), Germany (1 organization), and the Netherlands (1 organization). Furthermore, top five organizations of NOAA, NCAR, NASA,

Chinese Academy of Sciences, and University Colorado were popular based on contribution of articles more than 134 papers each. Similarly, in case of average citations of papers, the University of Leeds, University of Utrecht, NCAR, NOAA and University of Maryland, showed the higher average citations, more than 346.1 times per paper.

Table 5. Top twenty-one organizations published papers in the field of meteorology and atmospheric sciences category from 2011 to 2021.

Rank	Organizations	Records	Total link strength	Citations	Average citations	Country
1	National Oceanic and Atmospheric Administration	205	1940	73149	356.8	USA
2	Natlional Center for Atmospheric Research	181	1395	66657	368.3	USA
3	National Aeronautics and Space Administration (NASA)	163	1658	46048	282.5	USA
4	Chinese Academy of Sciences	160	902	32581	203.6	China
5	University of Colorado	134	1581	41081	306.6	USA
6	Columbia University	104	1167	23698	227.9	USA
7	University of Maryland	97	1179	33571	346.1	USA
8	University of Reading	82	853	19147	233.5	England
9	Princeton University	75	595	19748	263.3	USA
10	University of Washington	70	829	18074	258.2	USA
11	Tsinghua University	64	349	13279	207.5	China
12	University ofExeter	64	859	18851	294.5	England
13	Met Office Hadley Center	63	1042	20643	327.7	England
14	CALTECH	61	784	11297	185.2	USA
15	Max Planck Institute	60	1066	17600	293.3	Germany
16	Nanjing University	57	324	8172	143.4	China
17	Colorado State University	55	521	13187	239.8	USA
18	University of Leeds	53	518	30054	567.1	England
19	University of Oxford	53	515	11054	208.6	England
20	University of Calif Irvine	52	702	15428	296.7	USA
21	University of Utrecht	52	728	21182	407.3	Netherlands

Among the total 2,913 organizations, there were 437 organizations which met the minimum threshold of five papers, and connected to each other (*Fig. 5*). The VOSviewer software divided these 437 institutes into seven clusters with different colors. Within the context of network formation, organizations tend to form bonds with other institutions in the same region.

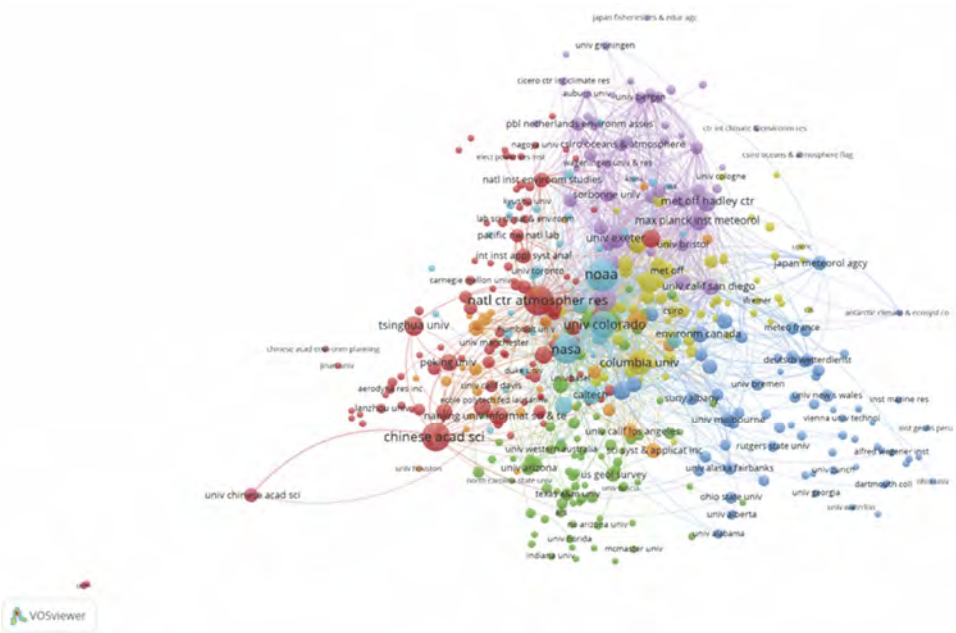

Fig.5. The organizations co-authorship network of the meteorology and atmospheric sciences related publications from 2011 to 2021 with 437 circles and 7 clusters.

3.8. All keywords co-occurrence analysis

For a specific scientific field study, keyword plays a large role as it can reflect the root contents of articles, and the compilation of keywords can reveal the pattern and trends of specific academic research (*Badaluddin et al.*, 2021). To analyze the co-occurrence of the keywords, author keywords, keywords plus, and all keywords as unit were chosen and analyzed.

For the author keywords by full counting method for co-occurrence analysis, there were total 2,097 author keywords, and 72 keywords which met the threshold level of more than five times, and they were separated into eight cluster. The top twenty-four co-occurrence author keywords were climate change, precipitation, drought, China, remote sensing, CMIP6, PM2.5, climate models, climate, climate variability, CMIP5, air pollution, air quality, Covid-19, source apportionment, data assimilation, extreme events, trends, ENSO, arctic, particulate matter, carbon cycle, global warming, and agriculture, each keywords occurred more than 10 times.

For the keywords plus by full counting method for co-occurrence analysis, there were total 4,864 keywords plus, and 503 keywords which met the threshold level of more than five times, and they were separated into seven cluster. The top twenty-three co-occurrence keywords plus were variability, model, climate change, temperature, climate, impact, precipitation, trends, impacts, United

States, emissions, circulation, rainfall, ocean, sensitivity, sea-surface temperature, particulate matter, projections, air pollution, performance, soil moisture, source apportionment, and El Nino, each keywords plus occurred more than 40 times.

For the all keywords by full counting method for co-occurrence analysis, there were total 6,466 all keywords, only 599 keywords met the threshold level of more than five times included in the map. There are eight main clusters that represent different viewpoints on the meteorology and atmospheric sciences category research (*Fig. 6*). The size of the node is proportional to the frequency of occurrence of the keyword, and the thickness of the line represents the intensity of co-occurrence between individual keywords (*Leal et al*., 2022). The top twenty co-occurrence all keywords were variability, model, climate change, temperature, precipitation, climate, impact, trends, climate change, impacts, United States, rainfall, emissions, circulation, China, drought, ocean, particulate matter, sensitivity, CMIP5, each all keywords occurred more than 50 times. The same data in *Fig. 6* were then arranged by a period of meteorology and atmospheric sciences category research as overlay map for most frequent all keywords (*Fig. 7*). Blue colors indicated earlier research topics, whereas, yellow and green colors indicated more recent topics of interest. Yellow and green circles present those which are research fronts.

Here, for 599 all keywords, about twenty keywords were listed and ranked in each cluster based on *Fig. 6*.

The first cluster (red) has 161 all keywords and focused on source apportionment of emissions and air pollution, and the 20 most frequently used keywords are United States, emissions, particulate matter, source apportionment, pollution, air pollution, PM2.5, transport, aerosols, air quality, aerosol, black carbon, secondary organic aerosol, optical properties, ozone, retrieval, tropospheric ozone, mortality, boundary layer, chemical composition, *et al*., each keywords occurred more than 20 times.

The second cluster (green) has 107 all keywords and represents climate change impacts, and are 20 most frequently used keywords climate change, climate change, impacts, CO_2, patterns, energy, scenarios, carbon, uncertainty, land, vegetation, responses, vulnerability, adaptation, risk, agriculture, time-series, land-use, framework, management, each key-words occurred more than 19 times.

The third cluster (blue) has 91 all keywords and is focused on climate variability and circulation impact, and the 22 most frequently used keywords are variability, climate, impact, circulation, ocean, sea-surface temperature, El-Nino, sea ice, interannual variability, ENSO, weather, atmospheric circulation, surface temperature, North-Atlantic, southern ocean, climate variability, sea-level rise, pacific, atmosphere, north-atlantic Oscillation, each keywords occurred more than 18 times.

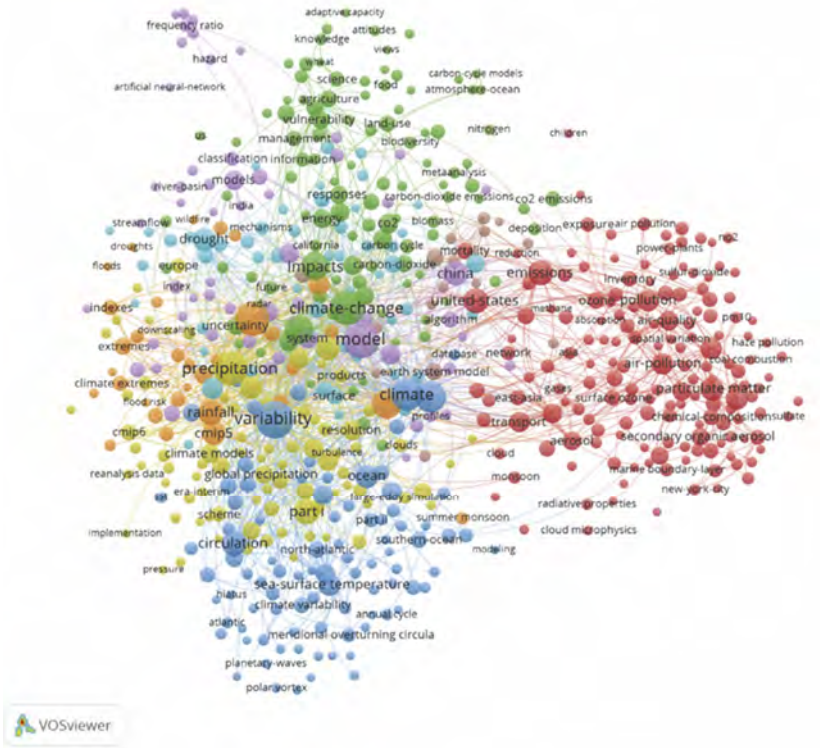

Fig. 6. VOSviewer co-occurrence network visualization mapping of all keywords (minimum 5 occurrences) in the meteorology and atmospheric sciences category from 2011 to 2021. Co-occurrence network of all keywords includes author keywords and keywords plus. The size of the circles correlates with the number of articles using that keyword such that a higher number of articles is represented by a bigger circle. Circle color denotes different clusters.

The fourth cluster (yellow) has 83 all keywords and represents precipitation, and the 20 most frequently used keywords are precipitation, part i, sensitivity, performance, simulations, resolution, simulation, data assimilation, climate models, parameterization, global precipitation, general-circulation model, reanalysis, Madden-Julian oscillation, CMIP6, convection, scheme, numerical weather prediction, Europe, assimilation, each keywords occurred more than 16 times.

The fifth cluster (violet) has 58 all keywords and is focused on climate models, and the 20 most frequently used keywords are model, China, satellite, water, system, models, prediction, validation, events, remote sensing, algorithm, extreme precipitation, area, classification, energy balance, fluxes, index, air temperature, trmm, basin, each keywords occurred more than 12 times.

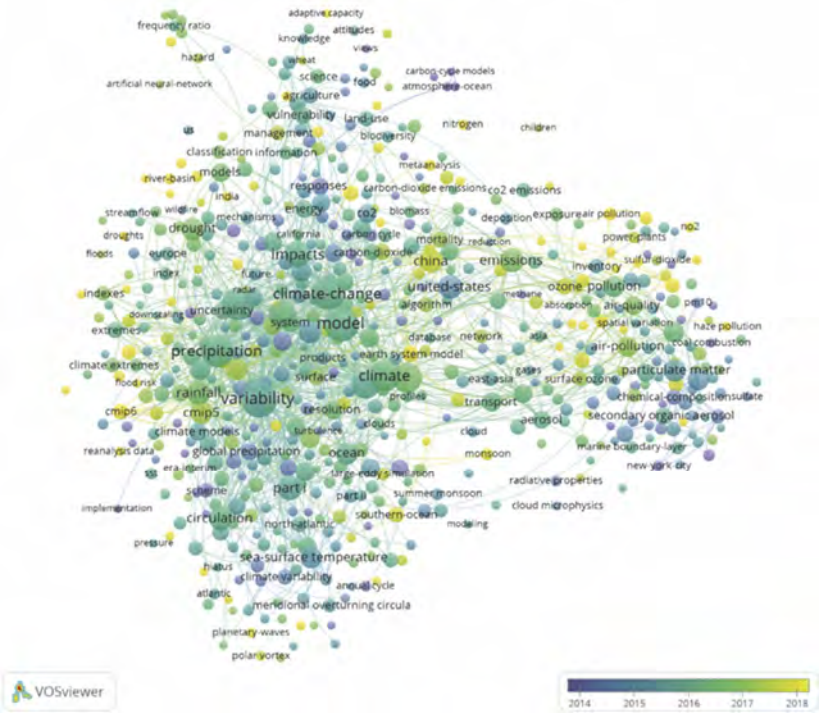

Fig. 7. VOSviewer co-occurrence overlay visualization mapping of all keywords in the meteorology and atmospheric sciences research (minimum of five occurrences) from 2011 to 2021.

The sixth cluster (light blue) has 51 all keywords and is focused on drought and soil moisture, and the 22 most frequently used keywords are drought, soil moisture, MODIS, surface, carbon-dioxide, water-vapor, dynamics, forest, evapotranspiration, evaporation, stomatal conductance, photosynthesis, NDVI, mechanisms, Tibetan Plateau, potential evapotranspiration, runoff, snow, soil, global warming, carbon cycle, spatial variability, each keywords occurred more than 10 times.

The seventh cluster (orange) has 32 all keywords and is focused on the temperature change trends, and the 20 most frequently used keywords are temperature, trends, rainfall, CMIP5, projections, ensemble, extremes, hydrological cycle, frequency, indexes, climate extremes, 20th century, dataset, future changes, increase, summer, extreme events, attribution, region, climate change impacts, each keywords occurred more than 11 times.

The eighth cluster (brown) has 16 all keywords and is focused on global climate change on earth system model, and the keyword are earth system model, atmospheric CO_2 cycle, dioxide emissions, environment simulator JULES, leaf area index, anthropogenic CO_2 uptake, land-use change, global climate, fire

emissions, land-cover change, model description, dependence, flux variability, South-America, terrestrial ecosystems, each keywords occurred more than 5 times.

3.9. The most frequently cited articles

Although many articles have been published, a relatively small number of individuals account for a large proportion of the citations within the period. The annual citations of the eight papers showed an increasing trend after the year of publication (*Fig. 8*). Here, the total citations for the most frequently cited articles were more than 3,123. The eight papers were authored by *Dee et al*. (2011), *Taylor et al*. (2012), *Alvares et al*. (2013), *Harris et al*. (2014), *Fick* and *Hijmans* (2017), *van Vuuren et al*. (2011), *Rienecker et al.* (2011), *Bond et al*. (2013). The total citations of the eight most cited papers were 16971, 9215, 4079, 4073, 3544, 3538, 3339, and 3123. From the publication year to 2022, the average number of citations per year of the most cited eight papers were 1414.25, 837.73, 407.9, 452.56, 590.67, 294.83, 278.25, 312.3. Among the eight articles, the highest average citation per year (1,414.25, blue color) was observed for the article of *Dee et al.* (2011) published in the *Quarterly Journal of the Royal Meteorological Society* (*Fig. 8*).

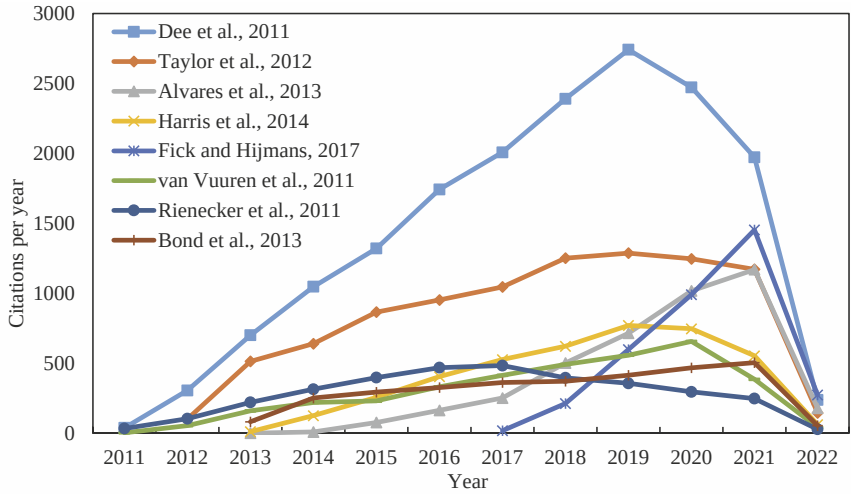

Fig. 8. Comparison of the citations per year of the most cited eight papers from their initial publications to March 28, 2022.

4. Conclusions

This study analyzed 1,636 top papers in the subject category of meteorology and atmospheric sciences published in the period from 2011 to 2021, which included 1,636 highly cited papers and 24 hot papers in the field and belonged to 20 Web of Science categories and 14 research areas. All top papers written in English were from 13,878 authors, 2,913 organizations and 124 countries or territories, and published in 72 journals. The top five journals are the *Nature Climate Change*, *Atmospheric Chemistry and Physics*, *Journal of Climate*, *Bulletin of the American Meteorological Society*, and *Journal of Geophysical Research Atmospheres*. Top five countries and regions were the USA, England, Peoples Republic of China, Germany, and France. Top five organizations were the National Oceanic and Atmospheric Administration (NOAA), National Center for Atmospheric Research (NCAR), National Aeronautics and Space Administration (NASA), Chinese Academy of Sciences, and University of Colorado. The top five authors were *Aiguo Dai*, *Detlef P. Van Vuuren*, *Qiang Zhang*, *Josep G. Canadell*, and *Philippe Ciais*. All keywords were separated into eight clusters for different research topic. This work is also useful for student identifying graduate schools and for researchers selecting journals.

Acknowledgments: This research was funded by the National Key Research and Development Program of China (2022YFD2300205), and the Hubei Agricultural Science and Technology Innovation Center Program (2021-620-000-001-032).

References

Alvares, C.A., Stape, J.L., Sentelhas, P.C., de Moraes Goncalves. J.L., and *Sparovek, G.*, 2013: Koppen's climate classification map for Brazil. *Meteorol. Zeit. 22*(6), 711-728 https://doi.org/10.1127/0941-2948/2013/0507

Aslam, A. and *Rana, I.A.*, 2022: The use of local climate zones in the urban environment: A systematic review of data sources, methods, and themes. *Urban Climate 42*, 101120. https://doi.org/10.1016/j.uclim.2022.101120

Badaluddin, N.A., Lion, M., Razali, S.M., and *Khalit, S.I.*, 2021: Bibliometric Analysis of Global Trends on Soil Moisture Assessment Using the Remote Sensing Research Study from 2000 to 2020, *Water Air Soil Pollut. 232*(7), 271. https://doi.org/10.1007/s11270-021-05218-9

Battikh, J.Y., Bodolica, V., and *Wood, M.O.*, 2022: Disasters triggered by natural hazards and terrorism: A bibliometric network analysis into the intellectual structure of a cross-disciplinary research field. *Int. J. Disaster Risk Reduct. 77*, 103045. https://doi.org/10.1016/j.ijdrr.2022.103045

Boloy, R.A.M., Reis, A.D., Rios, E.M., Martins, J.D.S., Soares, L.O., Machado, V.A.D., and *de Moraes, D.R.*, 2021: Waste-to-Energy Technologies Towards Circular Economy: a Systematic Literature Review and Bibliometric Analysis, *Water Air Soil Pollut. 232*(7), 306. https://doi.org/10.1007/s11270-021-05224-x

Bond, T.C., Doherty, S.J., Fahey, D.W., Forster, P.M., Berntsen, T., DeAngelo, B.J., Flanner, M.G., Ghan, S., Karcher, B., Koch, D., Kinne, S., Kondo, Y., Quinn, P.K., Sarofim, M.C., Schultz, M.G., Schulz, M., Venkataraman, C., Zhang, H., Zhang, S., Bellouin, N., Guttikunda, S.K., Hopke, P.K., Jacobson, M.Z., Kaiser, J.W., Klimont, Z., Lohmann, U., Schwarz, J.P., Shindell, D., Storelvmo, T., Warren, S.G., and *Zender, C.S.*, 2013: Bounding the role of black carbon in the climate system: A scientific assessment. *J. Geophys. Res.-Atmospheres, 118*(11), 5380–5552. https://doi.org/10.1002/jgrd.50171

Clarivate, 2022: Journal Citation Reports ™ 2021 https://jcr.clarivate.com/jcr/browse-journals
Clarivate, 2022: Categories & Collections (Scope Notes), Web of Science Master Journal List, https://mjl.clarivate.com/help-center
Clarivate, 2022: Essential Science Indicators Help: About Essential Science Indicators, http://esi.help.clarivate.com/Content/home.htm
da Silva, L.B.L., Alencar, M.H., and de *Almeida, A.T.*, 2020: Multidimensional flood risk management under climate changes: Bibliometric analysis, trends and strategic guidelines for decision-making in urban dynamics. *Int. J. Disaster Risk Reduct. 50*, 101865. https://doi.org/10.1016/j.ijdrr.2020.101865
Dee, D.P., Uppala, S.M., Simmons, A.J., Berrisford, P., Poli, P., Kobayashi, S., Andrae, U., Balmaseda, M.A., Balsam, G., Bauer, P., Bechtold, P., Beljaars, A.C.M., van de Berg, L., Bidlot, J., Bormann, N., Delsol, C., Dragani, R., Fuentes, M., Geer, A.J., Haimberger, L., Healy, S.B., Hersbach, H., Holm, E.V., Isaksen, L., Kallberg, P., Koehler, M., Matricardi, M., McNally, A.P., Monge-Sanz, B.M., Morcrette, J.J., Park, B.K., Peubey, C., de Rosnay, P., Tavolato, C., Thepaut, J.N., and *Vitart, F.*, 2011: The ERA-Interim reanalysis: configuration and performance of the data assimilation system. *Quart. J. Roy. Meteorol. Soc. 137*(656), 553–597. https://doi.org/10.1002/qj.828
Eito-Brun, R., 2021: A quantitative approach to the scientific production on radar altimetry, *Adv. Space Res. 68*(2), 1216–1224. https://doi.org/10.1016/j.asr.2019.11.029
Elango, B. and *Ho, Y.S.*, 2017: A bibliometric analysis of highly cited papers from India in Science Citation Index Expanded. *Current Science, 112*(8), 1653–1658. https://doi.org/10.18520/cs/v112/i08/1653-1658
Fick, S.E. and *Hijmans, R.J.*, 2017: World Clim 2: new 1-km spatial resolution climate surfaces for global land areas. *Int. J. Climatol. 37*(12), 4302–4315. https://doi.org/10.1002/joc.5086
Fu, H.Z., Chuang, K.Y., Wang, M.H., and *Ho, Y.S.*, 2011: Characteristics of research in China assessed with Essential Science Indicators. *Scientometrics 88*(3), 841–862. https://doi.org/10.1007/s11192-011-0416-8
Fu, H.Z. and *Waltman, L.*, 2022: A large-scale bibliometric analysis of global climate change research between 2001 and 2018. *Climatic Change 170*(3-4), 36. https://doi.org/10.1007/s10584-022-03324-z
Harris, I., Jones, P.D., Osborn, T.J., and *Lister, D.H.*, 2014: Updated high-resolution grids of monthly climatic observations-the CRU TS3.10 Dataset. *Int. J. Climatol. 34(*3), 623–642. https://doi.org/10.1002/joc.3711
Hirsch, J.E., 2005: An index to quantify an individual's scientific research output. *Proc. Natl. Acad. Sci. U. S. A., 102*(46),16569–16572. https://doi.org/10.1073/pnas.0507655102
Jain, N., Virmani, D., and *Abraham, A.*, 2021: Tsunami in the last 15 years: a bibliometric analysis with a detailed overview and future directions. *Nat. Hazards 106*(1), 139–172. https://doi.org/10.1007/s11069-020-04454-2
Ji, C.J., Li, X.Y., Hu, Y.J., Wang, X.Y., and *Tang, B.J.*, 2019. Research on carbon price in emissions trading scheme: a bibliometric analysis, *Nat. Hazards 99*(3), 1381–1396. https://doi.org/10.1007/s11069-018-3433-6
Leal, K.B., Robaina, L.E.D., and *De Lima, A.D.*, 2022: Coastal impacts of storm surges on a changing climate: a global bibliometric analysis. *Nat. Hazards 114*, 1455–1476. https://doi.org/10.1007/s11069-022-05432-6
Li, J.F., 2018: Bibliometric Analysis of Atmospheric Simulation Trends in Meteorology and Atmospheric Science Journals: Update. *Croatica Chemica Acta, 91*(1), 109–113. https://doi.org/10.5562/cca3210
Liao, H.C., Tang, M., Li, Z.M., and *Lev, B.*, 2019: Bibliometric analysis for highly cited papers in operations research and management science from 2008 to 2017 based on Essential Science Indicators. *Omega-Int. J. Manage. Sci. 88*, 223–236. https://doi.org/10.1016/j.omega.2018.11.005
Lima, C.O., and *Bonetti, J.*, 2020: Bibliometric analysis of the scientific production on coastal communities' social vulnerability to climate change and to the impact of extreme events. *Nat. Hazards 102*(3), 1589–1610. https://doi.org/10.1007/s11069-020-03974-1

Ma, Q., Li, Y.D., and *Zhang, Y.*, 2020: Informetric Analysis of Highly Cited Papers in Environmental Sciences Based on Essential Science Indicators, *Int. J. Environ. Res. Public Health 17*(11), 3781. https://doi.org/10.3390/ijerph17113781

Molassiotis, A., Guo, C.L., Abu-Odah, H., West, C., and Loke, A.Y., 2021: Evolution of disaster nursing research in the past 30 years (1990–2019): A bibliometric and mapping analysis. *Int. J. Disaster Risk Reduct. 58*, 102230. https://doi.org/10.1016/j.ijdrr.2021.102230

Nalau, J. and *Verrall, B.*, 2021: Mapping the evolution and current trends in climate change adaptation science. *Climate Risk Manage. 32*, 100290. https://doi.org/10.1016/j.crm.2021.100290

Rana, I.A., 2020: Disaster and climate change resilience: A bibliometric analysis. *Int. J. Disaster Risk Reduct. 50*, 101839. https://doi.org/10.1016/j.ijdrr.2020.101839

Rienecker, M.M., Suarez, M.J., Gelaro, R., Todling, R., Bacmeister, J., Liu, E., Bosilovich, M.G., Schubert, S.D., Takacs, L., Kim, G.K., Bloom, S., Chen, J.Y., Collins, D., Conaty, A., Da Silva, A., Gu, W., Joiner, J., Koster, R.D., Lucchesi, R., Molod, A., Owens, T., Pawson, S., Pegion, P., Redder, C.R., Reichle, R., Robertson, F.R., Ruddick, A.G., Sienkiewicz, M., and *Woollen, J.*, 2011: MERRA: NASA's Modern-Era Retrospective Analysis for Research and Applications. *J. Climate, 24*(14), 3624–3648. https://doi.org/10.1175/JCLI-D-11-00015.1

Sun, J. and *Yuan, B.Z.*, 2021: Trend and research status of Agronomy based on the Essential Science Indicators during 2009–2019. *Agronomy J. 113*(2), 2184–2194. https://doi.org/10.1002/agj2.20628

Sun, J. and *Yuan, B.Z.*, 2020: Bibliometric mapping of top papers in Library and Information Science based on the Essential Science Indicators Database. *Malaysian J. Libr. Inform. Sci. 25*(2), 61–76. https://doi.org/10.22452/mjlis.vol25no2.4

Taylor, K.E., Stouffer, R.J., and *Meehl, G.A.*, 2012: An overview of CMIP5 and the experiment design. *Bull. Amer. Meteorol. Soc. 93*(4), 485–498. https://doi.org/10.1175/BAMS-D-11-00094.1

Van Eck, N.J. and *Waltman, L.*, 2010: Software survey: VOSviewer, a computer program for bibliometric mapping. *Scientometrics 84*(2), 523–538. https://doi.org/10.1007/s11192-009-0146-3

Van Eck, N.J. and *Waltman, L.*, 2022: Manual for VOSviewer version 1.6.18, Leiden University, Leiden, the Netherlands. https://www.vosviewer.com

Van Vuuren, D.P., Stehfest, E., den Elzen, M.G.J., Kram, T., van Vliet, J., Deetman, S., Isaac, M., Goldewijk, K.K., Hof, A., Beltran, A.M., Oostenrijk, R., and *van Ruijven, B.*, 2011: RCP2.6: exploring the possibility to keep global mean temperature increase below 2 degrees C. *Climatic Change 109* (1–2), 95–116. https://doi.org/10.1007/s10584-011-0152-3

Wang, L.H., Gong, Z.W., Shi, L.N., Hu, Z.W., and *Shah, A.A.*, 2021: Knowledge mapping analysis of research progress and frontiers in integrated disaster risk management in a changing climate. *Nat. Hazards 107*(3), 2033–2052. https://doi.org/10.1007/s11069-020-04465-z

Yang, D.H., Wang, Y., Yu, T., and *Liu, X.Y.*, 2020: Macro-level collaboration network analysis and visualization with Essential Science Indicators: A case of social sciences. *Malaysian J. Libr. Inform. Sci. 25*(1), 121–138. https://doi.org/10.22452/mjlis.vol25no1.7

Yuan, B.Z. and *Sun, J.*, 2019: Bibliometric and mapping of top papers in the subject category of green and sustainable science and technology based on ESI, *COLLNET J. Scientometrics Inform. Manage. 13*(2), 269–289. https://doi.org/10.1080/09737766.2020.1716643

Yuan, B.Z. and *Sun, J.*, 2020: Mapping the scientific research on maize or corn: a bibliometric analysis of top papers during 2008–2018. *Maydica 65*(2): M17.

Yuan, B.Z. and *Sun, J.*, 2021: Research trend and status of forestry based on essential science indicators during 2010 – 2020: a bibliometric analysis. *Appl. Ecol. Environ. Res. 19*(6), 4941–4957. https://doi.org/10.15666/aeer/1906_49414957

Yuan, B.Z. and *Sun, J.*, 2022a: Trend and status of Food Science and Technology category based on the Essential Science Indicators during 2011–2021. *Food Sci. Technol 42*, e91321. https://doi.org/10.1590/fst.91321

Yuan, B.Z. and *Sun, J.*, 2022b: Bibliometric analysis of rice and climate change publications based on Web of Science. *Theor. Appl. Climatol. 150*, 347–362. https://doi.org/10.1007/s00704-022-04169-3

Zhang, N., Wan, S.S., Wang, P.L., Zhang, P., and *Wu, Q.*, 2018: A bibliometric analysis of highly cited papers in the field of Economics and Business based on the Essential Science Indicators database. *Scientometrics 116*, 1039–1053. https://doi.org/10.1007/s11192-018-2786-7

DOI:10.28974/idojaras.2023.3.4

IDŐJÁRÁS

Quarterly Journal of the Hungarian Meteorological Service
Vol. 127, No. 3, July – September, 2023, pp. 321–346

Impacts of large scale climate drivers on precipitation in Sindh, Pakistan using machine learning techniques

Sapna Tajbar*, **Ali Mohammad Khorshiddoust**, and **Saeed Jahanbakhsh Asl**

Department of Climatology
University of Tabriz
Tabriz 51664, East Azerbaijan, Iran

**Corresponding author E–mail: sapnatajbar@gmail.com*

(Manuscript received in final form August 8, 2022)

Abstract— Sindh province of Pakistan has a long history of severe droughts. Several large scale climate drivers (LSCD) are known for their effect on precipitation worldwide but studies in the Sindh region are missing; wide variety of LSCDs and lagged associative information. This study aimed to identify the significant LSCDs in Sindh province of Pakistan and improve the forecast skill of monthly precipitation by employing the principal component analysis (PCA), artificial neural network (ANN), Bayesian regularization neural network (BRNN), and multiple regression analysis (MRA), while considering the 12 months lagged LSCDs such as Nino-1+2, Nino-3, Nino-3.4, Nino-4, Quasi-Biennial Oscillation (QBO) at 30 and 50hPa (QBOI and QBOII), sea surface temperature (SST), 2m air temperature (T2M), 500 hPa and 850 hPa geopotential heights (H500 and H850), surface and 500 hPa zonal velocity (SU and U500), latent and sensible heat fluxes over land (LHFOL and SHFOL), and surface specific humidity (SSH). Global Land Data Assimilation System (GLDAS), Tropical Rainfall Measuring Mission (TRMM), Modern-Era Retrospective Analysis for Research and Application (MERRA-2), NOAA, Freie University Berlin, and Hadley Centre Sea Ice and Sea Surface Temperature (HadISST) datasets were used. Results manifested that significant LSCDs with 99% confidence level were SU, U500, T2M, SST, SHFOL, LHFOL, SSH, and H850. During test period, compared with MR models of 0.39 to 0.64 and principal components of 0.31 to 0.57, the ANN and BRNN models had better predictive skills with correlation coefficients of 0.57 to 0.83 and 0.52 to 0.76, respectively. It can be concluded that the ANN and BRNN models enable us to predict monthly precipitation in Sindh region with lagged LSCDs.

Key-words: artificial neural network, Bayesian regularization neural network, LSCD, multiple regression analysis, sea surface temperature, Sindh province of Pakistan

1. Introduction

Precipitation is a complex global atmospheric process, which is dependent on space and time, its increase or decrease can have several impacts on the society in the form of floods and droughts, and is not easy to predict (*Kumar et al.,* 2021). Due to the visible random characteristics of precipitation series, they are mostly described by a stochastic process (*Chinchorkar et al.,* 2012). It plays an important role in the economy of Pakistan being an agricultural country (*Aamir* and *Hassan,* 2018), where agriculture sector contributes 26% to the gross domestic product (*Rehman et al.,* 2015). In Pakistan, precipitation as well as thermal regimes have experienced variations particularly in the recent couple of decades when sharp jump of global atmospheric temperatures was noticed (*Rasul et al.,* 2012). The southern part of Pakistan which comprises of Sindh and Balochistan provinces has an arid climate and usually receive less amount of precipitation throughout the year as compared to other parts of the country. This study's main focus is Sindh province which has a long history of severe droughts and is the second important province in terms of agriculture. It has a considerable agricultural base along the Indus River (*Solomon,* 2019). Annual total rainfall is only 160 mm. Very less amount falls during the winter season (13 mm normal), while chief amount falls during the summer season and is highly variable. Its rainfall is a result of the monsoon depressions which forms in the Bay of Bengal and occasionally moves westward into the lower Sindh (*Muslehuddin* and *Faisal,* 2006).

The first and important stage for the management of water resources at any region is to identify the prospective climate variables which are affecting the future water resource situation (*Gholami Rostam et al.,* 2020). Worldwide, various large scale climate phenomena influence the occurrence of precipitation (*Hossain et al.,* 2015), and numerous studies have been carried out in this context, but such studies over the Sindh province of Pakistan are few (*Rashid,* 2004; *Mahmood et al.,* 2006; *Sarfaraz,* 2007; *Iqbal* and *Athar,* 2018). *Sarfaraz* (2007) discussed the monsoon over Pakistan by investigating its features and components that is El Nino Southern Oscillation (ENSO), heat low, Southern Oscillation Index, Tropical Easterly Jet, Low-level Jet, westerly Sub-tropical Jet, Tibetan anticyclone over Himalayas at 200 hPa, and high pressure region over the Indian Ocean. *Rashid* (2004) plotted normalized standard deviation (NSD) versus time to know the association between distinct intensities of El Nino and rainfall. *Mahmood et al.* (2006) dealt with the impacts of El Nino on summer monsoon rainfall over Pakistan and calculated percent rainfall departure and correlation coefficients. They found that the deficiency in rainfall is significant during August in Sindh province. *Iqbal* and *Athar* (2018) studied the variability and teleconnections of precipitation over Pakistan using percentile analysis, Mann-Kendall trend test, Sen's slope estimator, and correlation techniques. They found that ENSO did not show significant impact.

Various researches around the world identified different LSCDs and used Machine learning techniques such as artificial neural networks (ANN), Bayesian regularization neural networks (BRNN), and multiple regression models for the prediction of precipitation (*Awan* and *Maqbool*, 2010; *Shukla et al.*, 2011; *Mekanik et al.*, 2013; *Venkata Ramana et al.*, 2013; *Ahmadi et al.*, 2014; *Kashiwao et al.*, 2017; *Lee et al.*, 2018; *Doranalu Chandrashekar et al.*, 2019). In the current study, artificial neural networks and Bayesian regularization neural networks are selected as they are known for their capability of finding the complex non-linear associations between the input and output parameters without taking into consideration the nature of the physical processes. As the processes influencing the rainfall are non-linear and highly complex, therefore they can help in solving the complexity (*Adamowski* and *Sun*, 2010).

To the best of author's knowledge, there are no detailed studies in Sindh province in this regard. Past studies in the region are limited in their approaches; firstly because of the absence of wide variety of LSCDs. The El Nino Southern Oscillation with some other climate variables has been discussed, and only one study analyzed the effect of the Quasi-Biennial Oscillation(QBO) phenomena on precipitation which is known for its impacts in different regions around the world. Secondly, none of the studies investigated the time extent in which the LSCDs effect the prediction of monthly precipitation. To forecast precipitation, it is essential to have the lagged associative information. In addition to this, the usage of LSCDs as potential predictors for the future precipitation has not given much attention. Finally, the monthly prediction of precipitation is not carried out using powerful machine learning techniques while utilizing LSCDs; the studies have either used linear regression analysis or probabilistic/categorical analysis. Therefore, there is a need of further research.

The main objective of the present study is to identify the significant LSCDs in Sindh province of Pakistan and improve the forecast skill of monthly precipitation by application of the principal component analysis, artificial neural network, Bayesian regularization neural network and multiple regression analysis while considering the lagged association of LSCDs. This paper is arranged in four sections; Section 1 gives a brief introduction, Section 2 explains the study area and data used with methods of prediction. Section 3 presents the results of the application of models and the discussion of the results. Concluding remarks are mentioned in Section 4.

2. Materials and methods

2.1. Study area

Sindh province is located between 23–35° and 28–30°N and 66–42° and 71–1°E (*Muslehuddin* and *Faisal*, 2006). It is bordered by Punjab in the north, the Indian states of Gujarat and Rajasthan in the east, the Arabian Sea in the south, and

Balochistan in the west (*Fig. 1*). Its landscape comprises mostly of alluvial plains surrounding the Indus River, but along with the border with India and mountains of Kirthar in the west side, it encompasses the Thar desert (*Solomon*, 2019). The province is located in a region that is subtropical; it is cold in the winter and hot in the summer. During the months of December and January, the minimum temperature of 2 ^{o}C occurs and during May and August the maximum temperature of 46 ^{o}C occurs. About 178 mm annual average rainfall falls mainly during July and August. The region lies between two monsoons such as the southwest monsoon from the Indian Ocean, and the northeast or retreating monsoon from the Himalayan mountains (*SWP*, 2021).

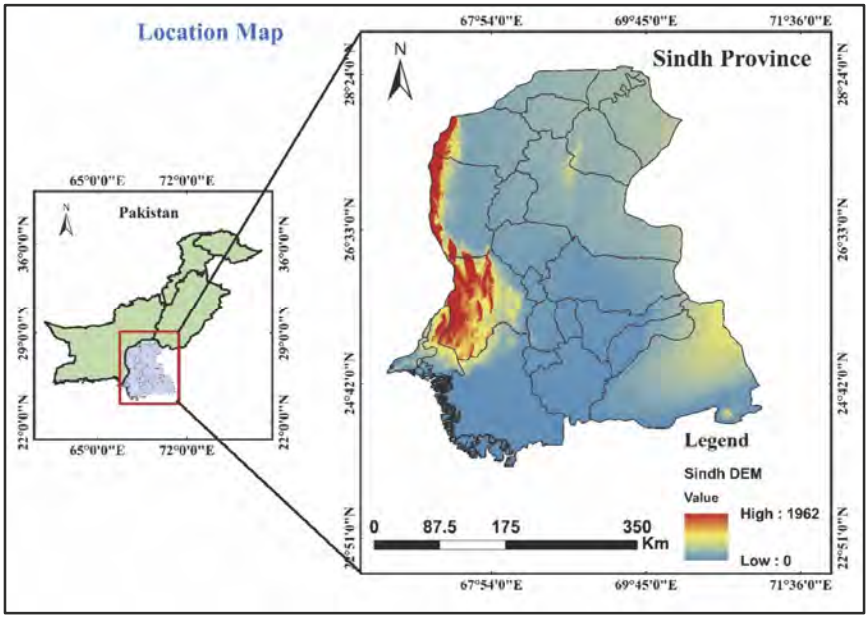

Fig. 1. Location of the study area.

2.2. Data used

2.2.1. Precipitation

The Global Land Data Assimilation System (GLDAS) is producing a series of land surface conditions such as moisture of the soil and temperature of the surface as well as fluxes such as sensible heat flux and evaporation products simulated by the Community Land Model (CLM), as well as the Mosaic, Noah, and Variable Infiltration Capacity (VIC) land surface models (*Fang et al.*, 2009). Monthly precipitation data of GLDAS from 1983 to 2020 and the Tropical Rainfall Measuring Mission (TRMM) from 1998 to 2019 with spatial resolution at

$0.25^o \times 0.25^o$ was used. GLDAS precipitation data was in $kgm^{-2}s^{-1}$ which was converted to mm. TRMM records data by utilizing three instruments, precipitation radar (PR), the TRMM microwave image (TMI), and the visible infrared scanner (VIRS) (*Begum et al.*, 2021). GLDAS and TRMM data services are provided at the NASA Giovanni portal.[1]

2.2.2. Climate indices

2m air temperature (T2M), 500 hPa and 850 hPa geopotential heights (H500 and H850), mean sea level pressure (SLP), surface zonal velocity (SU), 500 hPa zonal velocity (U500), latent heat flux over land (LHFOL), sensible heat flux over land (SHFOL), and surface specific humidity (SSH) were downloaded from Modern-Era Retrospective Analysis for Research and Application (MERRA-2) model at the NASA Giovanni portal.[1] It provides data at $0.5^o \times 0.625^o$ spatial resolution from 1980 till present. *Fig. 2* shows the climate domains depicting the points where potential predictor data were extracted from MERRA-2. From MERRA-2 model, different variables were selected for different districts on the basis of their correlation with precipitation (*Table 1*). Climate indices from other sources were used same for all districts. The NOAA monthly Optimum Interpolation (OI) Sea Surface Temperature (SST) version 2.0 ($1^o \times 1^o$ resolution) data covering 89.5N-89.5S and 0.5E-359.5E region was downloaded from the NOAA Physical Sciences Laboratory and is available from December 1981onwards.[2] The QBO index of Freie University Berlin, which is the mean monthly zonal wind components computed for the levels of 10, 15, 20, 30, 40, 50, and 70 hPa at three radiosonde stations close to the equator, i.e., Canton Island, Gan Island in Maledives, and Singapore are accessible from 1953 onwards. QBO at 30 hPa (QBOI) and 50 hPa (QBOII) were utilized.[3] Nino-1+2, Nino-3, Nino-3.4, and Nino-4 were obtained from the NOAA Global Climate Observing System (GCOS) Working Group on Surface Pressure (WG-SP) which calculated all indices at $1^o \times 1^o$ from the Hadley Centre Sea Ice and Sea Surface Temperature (HadISST).[4] Nino-1+2 is the Nino SST eastern-most region from 0N-10S and 90W-80W. Nino-3, Nino-3.4, and Nino-4 are the area-averaged SSTs from 5S-5N and 150W-90W, 5S-5N and 170-120W, and 5S-5N and 160E-150W, respectively and are available from 1870. In the current study, all datasets were downloaded for the period of 1982 to 2020.

[1] https://giovanni.gsfc.nasa.gov/giovanni/
[2] https://psl.noaa.gov/data/gridded/data.noaa.oisst.v2.html
[3] https://www.geo.fu-berlin.de/met/ag/strat/produkte/qbo/qbo.dat
[4] https://psl.noaa.gov/gcos_wgsp/Timeseries/

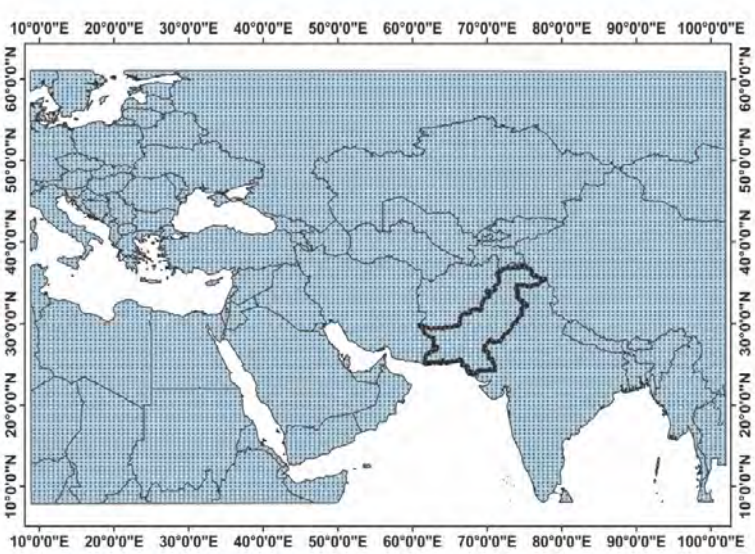

Fig. 2. Climate domains depicting the points where potential predictor data are extracted from MERRA-2.

Table 1. Selected variables for different districts from MERRA-2 model

Districts	Variables	Districts	Variables
Badin	H850, SSH, LHFOL, and SHFOL	Kashmore	T2M, LHFOL, and SHFOL
Dadu	T2M, LHFOL, and SHFOL	Larkana	H850, LHFOL, and SHFOL
Ghotki	H850, LHFOL, and SHFOL	Mithi	U500, SSH, LHFOL, and SHFOL
Hyderabad	U500, SSH, LHFOL, and SHFOL	Sanghar	SSH, LHFOL, and SHFOL
Jacobabad	SSH, LHFOL, and SHFOL	Shikarpur	T2M, LHFOL, and SHFOL
Jamshoro	U500, SSH, LHFOL, and SHFOL	Thatta	U500, SSH, LHFOL, and SHFOL
Karachi	SU, SSH, LHFOL, and SHFOL	Umerkot	SSH, LHFOL, and SHFOL

2.3. Methods

The techniques applied in this study are robust and are utilized in many studies around the world. Detailed explanations are given below. *Fig. 3* shows the flow chart of adopted methodology.

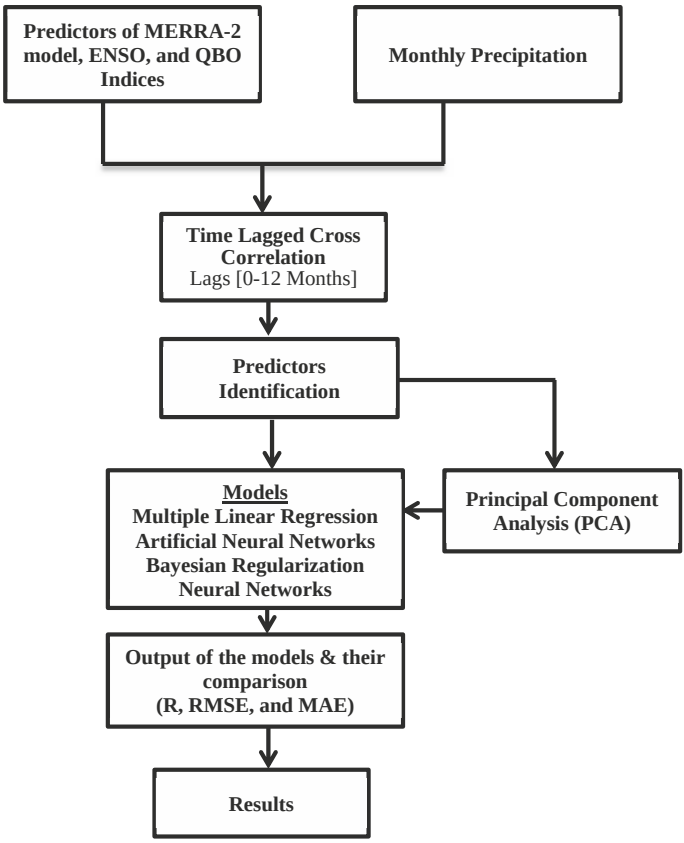

Fig. 3. Flow chart of the adopted methodology for monthly precipitation estimation teleconnected with large scale climate drivers.

2.3.1. Cross correlations

To show lagged association between the LSCDs and precipitation, the cross correlation method was employed. This method is useful when we want to align two time series in a way that one is delayed with respect to other and their peaks occurs at a lag where both series match up best (correlate well) (*Menke* and *Menke*, 2009). In the present study, monthly cross-correlations were computed between the LSCDs and the precipitation up to 12 months range for different districts, and the best correlations were identified at different lags. The formula is:

$$r_m = \frac{\sum(x_i - \bar{x})(y_i - m - \bar{y})}{\sqrt{\sum(x_i - \bar{x})^2 \sum(y_i - m - \bar{y})^2}}, \quad (1)$$

where r_m shows the m lag time and $\{x_i\}$ and $\{y_i\}$ are random variables (*Taweesin* and *Seeboonruang*, 2019). Heatmaps were prepared in Origin 2021b software to show significant lagged correlations in different districts.

2.3.2. Principal component analysis (PCA)

World widely multivariate data analysis is carried out using principal component analysis (PCA) (*Shukla et al.*, 2011). It transforms several correlated parameters into a smaller number of uncorrelated parameters which are called principal components (PCs). It is suitable for the application where data records are few compared to the complexity of the model. The number of free parameters is large in ANN models, and if the training set is not large enough to accommodate for the suitable optimization of those parameters, then overfitting occurs (*Shukla et al.*, 2011; *Doranalu Chandrashekar et al.*, 2019). In the present study, the number of predictors is 10 in some districts and 11 in other, and hence the number of neurons is 10 and 11, respectively, in the input layer. The output layer possesses only one neuron. Due to the inadequate number of present data points, the free parameters optimization without the danger of overfitting is not possible, and PCA can help by reducing the number of predictors. Dataset of 456 points (1983–2020) was divided into two parts, 75% (1983–2011) for training and 25% (2012–2020) for testing. PCA was applied using a Python script on the training data only. The eigen vector which corresponds to the predictors covariance matrix's highest eigen value was determined. Selected PCs were then used to represent the data in two and three dimensional spaces (different locations selected PCs were different in number). The first two principal components explained maximum variances for all districts, and the third one was considered in some districts. 114 points (test points for ANN and BRNN) were still in 10 and 11 dimensional spaces. We projected them one at a time on the ascertained eigen vector which gave us test points in two- and three-dimensional spaces. *Table 2* and *Fig. 4* show the variances and eigen values for each of the components calculated by PCA.

Table 2. Eigen values of principal component analysis

Districts		PC1	PC2	PC3	PC4	PC5	PC6
	Eigenvalue	1.7203	1.2491	0.8954	0.1572	-	-
Badin	Variability (%)	42.7716	31.0547	22.2631	3.9104	-	-
	Cumulative (%)	42.7716	73.8264	96.0895	100	-	-
	Eigenvalue	1.7562	0.9804	0.2658	-	-	-
Dadu	Variability (%)	58.4917	32.6549	8.8532	-	-	-
	Cumulative (%)	58.4917	91.1467	100	-	-	-
	Eigenvalue	2.9136	0.8340	0.1485	0.0608	-	-
Ghotki	Variability (%)	73.6290	21.0779	3.7546	1.5383	-	-
	Cumulative (%)	73.6290	94.7070	98.4616	100	-	-
	Eigenvalue	2.0521	0.7845	0.1682	-	-	-
Hyderabad	Variability (%)	68.2920	26.1091	5.5988	-	-	-
	Cumulative (%)	68.2920	94.4011	100	-	-	-
	Eigenvalue	1.8909	1.0050	0.0747	-	-	-
Jacobabad	Variability (%)	63.6520	33.8302	2.5176	-	-	-
	Cumulative (%)	63.6520	97.4823	100	-	-	-
	Eigenvalue	3.8062	1.1217	0.7665	0.2232	0.0235	0.0125
Jamshoro	Variability (%)	63.9286	18.8402	12.8751	3.7498	0.3957	0.2102
	Cumulative (%)	63.9286	82.7689	95.6441	99.3940	99.7897	100
	Eigenvalue	2.6010	0.9405	0.4006	0.1090	-	-
Karachi	Variability (%)	64.2021	23.2158	9.8894	2.6925	-	-
	Cumulative (%)	64.2021	87.4179	97.3074	100	-	-
	Eigenvalue	1.8909	1.0050	0.0747	-	-	-
Kashmore	Variability (%)	63.6520	33.8302	2.5176	-	-	-
	Cumulative (%)	63.6520	97.4823	100	-	-	-
	Eigenvalue	2.6994	1.0496	0.5963	0.4172	0.1364	-
Larkana	Variability (%)	55.0995	21.4259	12.1729	8.5161	2.7854	-
	Cumulative (%)	55.0995	76.5254	88.6984	97.2145	100	-
	Eigenvalue	1.7168	1.2600	0.8968	0.2341	-	-
Mithi	Variability (%)	41.7938	30.6744	21.8311	5.7004	-	-
	Cumulative (%)	41.7938	72.4683	94.2995	100	-	-
	Eigenvalue	2.0521	0.7845	0.1682	-	-	-
Thatta	Variability (%)	68.2920	26.1091	5.5988	-	-	-
	Cumulative (%)	68.2920	94.4011	100	-	-	-
	Eigenvalue	2.1588	1.2723	0.5007	0.0747	-	-
Shikarpur	Variability (%)	53.8809	31.7562	12.4977	1.8650	-	-
	Cumulative (%)	53.8809	85.6371	98.1349	100	-	-
	Eigenvalue	1.7168	1.2600	0.8968	0.2341	-	-
Sanghar	Variability (%)	41.7983	30.6744	21.8311	5.7004	-	-
	Cumulative (%)	41.7938	72.4683	94.2995	100	-	-
	Eigenvalue	1.9619	1.2582	0.7409	0.0739	-	-
Umerkot	Variability (%)	48.6216	31.1820	18.3628	1.8334	-	-
	Cumulative (%)	48.6216	79.8037	98.1665	100	-	-

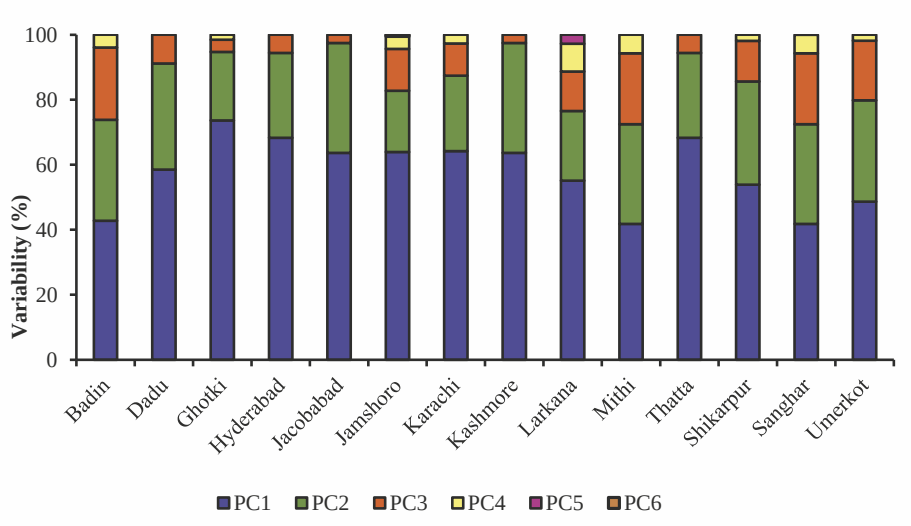

Fig. 4. Explained variability (%) of the principal components (PC1, PC2, PC3, PC4, PC5, and PC6).

2.3.3. Multiple regression analysis (MRA)

The data was normalized in the range of 0 and 1 using the following equation, which is a min-max formula.

$$\bar{x}_i = \frac{x_i - x_{min}}{x_{max} - x_{min}} \tag{2}$$

where $\bar{x}_i$ represents normalized values, x_i are given values, x_{min} represents minimum value and x_{max} represents maximum value. 75% of the data was used for training and 25% for testing. Distinct regression models (*Wilks*, 1995) were developed using stepwise MRA. *Table 3* shows these regression models for each district.

Table 3. Summary of the best multiple regression models

Districts	Equation	r	VIF	DW
Badin	$Y_t = 0.003 + 0.151SST_{t-12} - 0.113H850_{t-12} + 0.183SST_{t-1} + 0.044SST_{t-6}$	0.59	1.53	2.05
Dadu	$Y_t = -0.053 + 0.190SST_{t-11} + 0.127SST_{t-2} + 0.046LHFOL_{t-7}$	0.47	1.27	2.15
Ghotki	$Y_t = 0.024 + 0.397SST_{t-11} - 0.215SST_{t-10} - 0.346SHFOL_{t-2} + 0.381LHFOL_{t-11}$	0.58	1.52	2.07
Hyderabad	$Y_t = -0.105 + 0.246SST_{t-12} + 0.094SST_{t-2} + 0.086SSH_{t-7}$	0.54	1.40	2.04
Jacobabad	$Y_t = -0.059 + 0.519SST_{t-11} - 0.291SST_{t-10} + 0.127LHFOL_{t-8}$	0.46	1.26	2.16
Jamshoro	$Y_t = 0.393 - 0.492SHFOL_{t-2} + 0.375SST_{t-1} + 0.208SST_{t-11} - 0.355SST_{t-8} - 0.218LHFOL_{t-7} - 0.130SSH_{t-6}$	0.65	1.72	2.05
Karachi	$Y_t = 0.102 + 0.150SST_{t-12} + 0.404SST_{t-1} - 0.279SST_{t-8} - 0.243SSH_{t-2}$	0.60	1.56	1.99
Kashmore	$Y_t = -0.068 + 0.572SST_{t-11} - 0.300SST_{t-10} + 0.119LHFOL_{t-8}$	0.51	1.36	2.13
Larkana	$Y_t = 0.080 + 0.188SST_{t-11} - 0.201H850_{t-1} + 0.131H850_{t-9} - 0.137SHFOL_{t-1} + 0.193SST_{t-1}$	0.55	1.43	2.07
Mithi	$Y_t = -0.031 + 0.272SST_{t-11} - 0.219SST_{t-8} + 0.183SST_{t-6} + 0.113SST_{t-1}$	0.62	1.62	2.02
Sanghar	$Y_t = -0.035 + 0.124SST_{t-1} + 0.190SST_{t-6} + 0.252SST_{t-11} - 0.191SST_{t-8}$	0.59	1.53	2.07
Shikarpur	$Y_t = -0.086 + 0.520SST_{t-11} - 0.292SST_{t-10} + 0.138LHFOL_{t-8} + 0.164SST_{t-1}$	0.49	1.32	2.08
Thatta	$Y_t = -0.105 + 0.089SSH_{t-7} + 0.108SST_{t-2} + 0.232SST_{t-12}$	0.54	1.40	2.04
Umerkot	$Y_t = 0.065 - 0.470SST_{t-8} + 0.503SST_{t-1} + 0.338SSH_{t-11} - 0.232SHFOL_{t-2}$	0.59	1.54	2.05

Significant lagged climate indices were included as predictors. Another set of models were developed using the selected PCs for different districts in MRA. These models are presented in *Table 4*.

Table 4. Summary of the best PC based multiple regression models

Districts	Equation	r	VIF	DW
Badin	Y_t = 0.031 – 0.036PC1 +0.000PC2	0.48	1.29	2.02
Dadu	Y_t = 0.040 – 0.030PC1 – 0.004PC2	0.40	1.19	2.11
Ghotki	Y_t = 0.061 + 0.035PC1 + 0.017PC2	0.45	1.25	2.21
Hyderabad	Y_t = 0.029 - 0.029PC1 – 0.009PC2	0.44	1.24	2.09
Jacobabad	Y_t = 0.069 + 0.033PC1 – 0.001PC2	0.32	1.11	2.15
Jamshoro	Y_t = 0.027 + 0.019PC1 – 0.006PC2	0.43	1.23	2.05
Karachi	Y_t = 0.025 + 0.019PC1 + 0.020PC2	0.43	1.23	2.05
Kashmore	Y_t = 0.072 + 0.044PC1 – 0.005PC2	0.40	1.19	2.22
Larkana	Y_t = 0.061 – 0.036PC1 + 0.002PC2	0.46	1.26	2.09
Mithi	Y_t = 0.047 – 0.043PC1 + 0.037PC2 + 0.002PC3	0.57	1.47	2.02
Sanghar	Y_t = 0.043 – 0.038PC1 – 0.038PC2 +0.003PC3	0.54	1.40	2.08
Shikarpur	Y_t = 0.066 + 0.038PC1 + 0.005PC2 + 0.007PC3	0.38	1.17	2.05
Thatta	Y_t = 0.027 + 0.027PC1 + 0.007PC2	0.45	1.25	2.05
Umerkot	Y_t = 0.048 + 0.045PC1 + 0.011PC2	0.48	1.29	2.04

Verification of the multicollinearity is significant in the MR modeling, which is observed in case of highly correlated predictors and can result in substantial variation in the estimates of the parameter in response to small variations in the data or the model. The utilized indicators are tolerance (*T*) and variance inflation factor (*VIF*):

$$Tolerance = 1–R^2 \quad , \quad VIF = \frac{1}{Tolerance}, \tag{3}$$

where R^2 represents the coefficient of multiple determination:

$$R^2 = \frac{SSR}{SST} = 1 - \frac{SSE}{SST}, \tag{4}$$

where *SST* represents the total sum of squares, *SSR* represents the regression sum of squares, and *SSE* shows the error sum of squares. Tolerance value less than 0.20–0.10 or a *VIF* value greater than 5–10 shows the problem of multicollinearity (*Lin,* 2008). To assess the errors independence of the models, the Durbin-Watson test was used which looks for the serial correlations between errors and ranges from 0–4. Values >3 or <1 create problems (*Field,* 2009).

2.3.4. Artificial neural network (ANN)

Multi-layer feed-forward neural network with back propagation algorithm was used for the prediction of monthly precipitation with the first two PCs in most cases and three PCs in some cases as the predictors. The model comprised three layers, the input layer having two neurons and three neurons in some cases, the output layer having one neuron, and one hidden layer were selected, and the number of neurons was determined by a trial and error method. It is known that a single hidden layer is ample to estimate any non-linear function to arbitrary accuracy (*Cybenko,* 1989). The number of neurons in hidden layer significantly affects the performance of the model, for example, less number causes underfitting, while greater number causes overfitting (*Hussain,* 2020). The ANN model development process is 1) to find suitable data set for input, 2) to ascertain the hidden layers number as well as neurons, and 3) to train, validate, and test the network. It can be expressed mathematically as:

$$y_j = f_2[\sum_{j=1}^{J} w_i \, f_1\left(\sum_{i=1}^{I} w_i \, x_i\right)] \,, \tag{5}$$

where the output of the network is represented by y_j, the input by x_i, w_i and w_j represent the weights between the input neurons and the hidden layer and between the hidden layer and output neurons, respectively, the activation functions for the hidden layer and output layer are f_1 and f_2, respectively. Sigmoidal and linear kinds of transfer functions are appropriate for the hidden and output layers (*Maier* and *Dandy,* 2000). In the current study, f_1 is a sigmoid function, which is basically a nonlinear function, and f_2 is a linear purelin function, given as:

$$f_1 = \frac{1}{1+e^{-x}} \,, \tag{6}$$

$$f_2(x) = x. \tag{7}$$

The models of ANN were trained employing the Levenberg-Marquardt technique, and the early stop approach was employed to avoid the chance of overfitting while training and validating. In this method, the training process stops when the validation set error start to increase, while the training set error is still reducing (*Mekanik et al.*, 2013; *Luk et al.*, 2021). *Fig. 5* shows schematic diagram of the ANN.

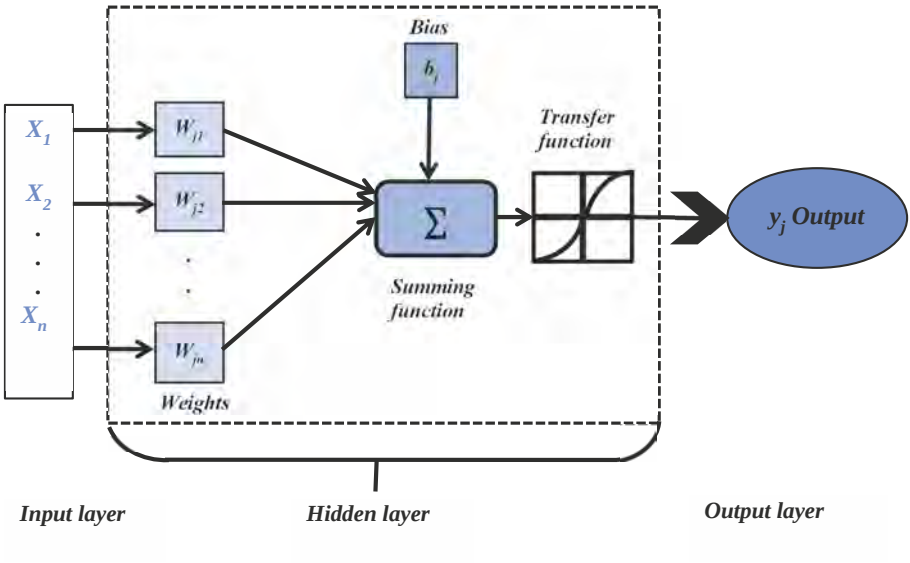

Fig. 5. Schematic diagram of the artificial neural network (ANN).

2.3.5. Bayesian regularization neural network (BRNN)

The Bayesian regularization neural network (BRNN) is the version of artificial neural networks (ANN), which is a more powerful method as compared to the conventional ANN. A common error function (E_d) of ANN utilizing early stop technique can be represented as:

$$E_D(D|w,M) = \sum_{i=1}^{n}(t_i - \hat{t}_i)^2 \,, \tag{8}$$

where *w* represents the weight, *M* represents the structure of ANN, *n* represents the size of training data, t_i represents the i_{th} target, whereas $\hat{t}_i$ represents the output. ANN's immature convergence results in overfitting. Its regularization in using Bayesian technique helps optimization of the ANN parameters by utilizing their prior values. For this reason, an additional term (E_w) is incorporated as:

$$E_D(D|w,M) = \sum_{i=1}^{n}(t_i - \hat{t}_i)^2 + E_w \,, \tag{9}$$

where E_w deals with the unrealistic weights for better generalization and cautious conversion. This kind of optimization method is utilized to minimize the function:

$$F = \beta E_D(D|w,M) + \alpha E_w(w|M) \,, \tag{10}$$

where $E_w(w|M)$ represents the sum of ANN architecture square, and α and β show the hyperparameters for the optimization process (*Ye et al.,* 2021). This technique decreases a combination of squared errors and weights and identifies the accurate combination. It does not require validation set and is potentially suitable algorithm for limited data (*Beale et al.,* 2011). In the current study, the same PCs used in ANN were utilized in BRNN. Scripts were developed for both ANN and BRNN in the MATLAB R2015a environment.

To validate the performance of all developed models, the TRMM dataset was used. It was similarly normalized, and the PCs were calculated by projecting the data points on the previous ascertained eigen vectors. In the last, time series graphs and radar charts were prepared for comparison.

2.3.6. Model evaluation

The constructed models were evaluated using three performance metrics such as root mean square error (*RMSE*), mean absolute error (*MAE*), and correlation coefficient (*R*) between the GLDAS precipitation values and models predicted values as well as between TRMM precipitation values and models predicted values. They can be expressed as follows.

$$RMSE = \sqrt{\frac{\sum_{i=1}^{n}(Yi-Xi)^2}{n}}, \tag{11}$$

$$MAE = \frac{\sum_{i=1}^{n}|Y_i-X_i|}{n}, \tag{12}$$

$$\mathrm{R} = \frac{\sum_{i=1}^{n}(X_i-\overline{X})(Y_i-\overline{Y})}{\sqrt{\sum_{i=1}^{n}(X_i-\overline{X})^2\sum_{i=1}^{n}(Y_i-\overline{Y})^2}}, \tag{13}$$

where *Yi* are the predicted values, *Xi*are the GLDAS or TRMM values, $\overline{X}$ is the mean GLDAS or TRMM value, and $\overline{Y}$ is the mean predicted value.

3. Results and discussion

3.1. Identification of significant large scale climate drivers

The cross-correlations between monthly precipitation and LSCD values are presented in *Fig. 6*. We observe that in Badin district, five LSCDs (H850, SST, SSH, LHFOL, and SHFOL) have significant positive (negative) cross-correlations at various lags with 99% confidence interval, revealing that there exists a direct (inverse) physical association. Dadu, Kashmore, and Shikarpur

districts have four (T2M, LHFOL, SHFOL, and SST), Ghotki and Larkana have four (H850, LHFOL, SHFOL, and SST), Hyderabad, Jamshoro, Thatta and Mithi have five (U500, SSH, LHFOL, SHFOL, and SST), Jacobabad, Sanghar, and Umerkot have four (SSH, LHFOL, SHFOL, and SST), and Karachi has five (SSH, LHFOL, SHFOL, SST, and SU) significant LSCDs.

We notice that for most of the LSCDs, the relationship is persistent and statistically significant at lags 1, 2, and 4 to 12, with the strongest correlations in the SST, LHFOL, SSH, and U500. For H850, we observe that at lags 1, 2, and 12, the correlation was negative, while from 8 to 11 it was positive. In case of SSH, T2M, LHFOL, SHFOL, SST, and SU, positive correlation was observed from lags 1 to 3 and 10 to 12, while negative from 4 to 9. For U500, it was positive at lags 4 to 9, while negative at 1 to 3 and 10 to 12. Moreover, this analysis showed that the cross-correlations of Nino-1+2, Nino-3, Nino-3.4, Nino-4, QBOI, and QBOII were not significant in the Sindh region, and the most significant LSCDs were SU, U500, T2M, SST, SHFOL, LHFOL, SSH, and H850.

Till now, some studies were carried out in Sindh province (*Mahmood et al.*, 2006; *Iqbal* and *Athar*, 2018; *Bhutto* and *Wei*, 2009) and the last mentioned study (*Iqbal* and *Athar*, 2018) obtained the same results for the Sindh region, but they found concurrent correlations, and did not find antecedent correlations (lagged correlations) where the QBO as well as ENSO did not show correlation with the monthly precipitation of Sindh province stations. The lagged association was only discussed by one study for the period of 1960–1990, and some of the used climate indices (Nino-1+2 and Nino-4) were not significant over the region which is in accordance with this study (*Muslehuddin et al.*, 2005).

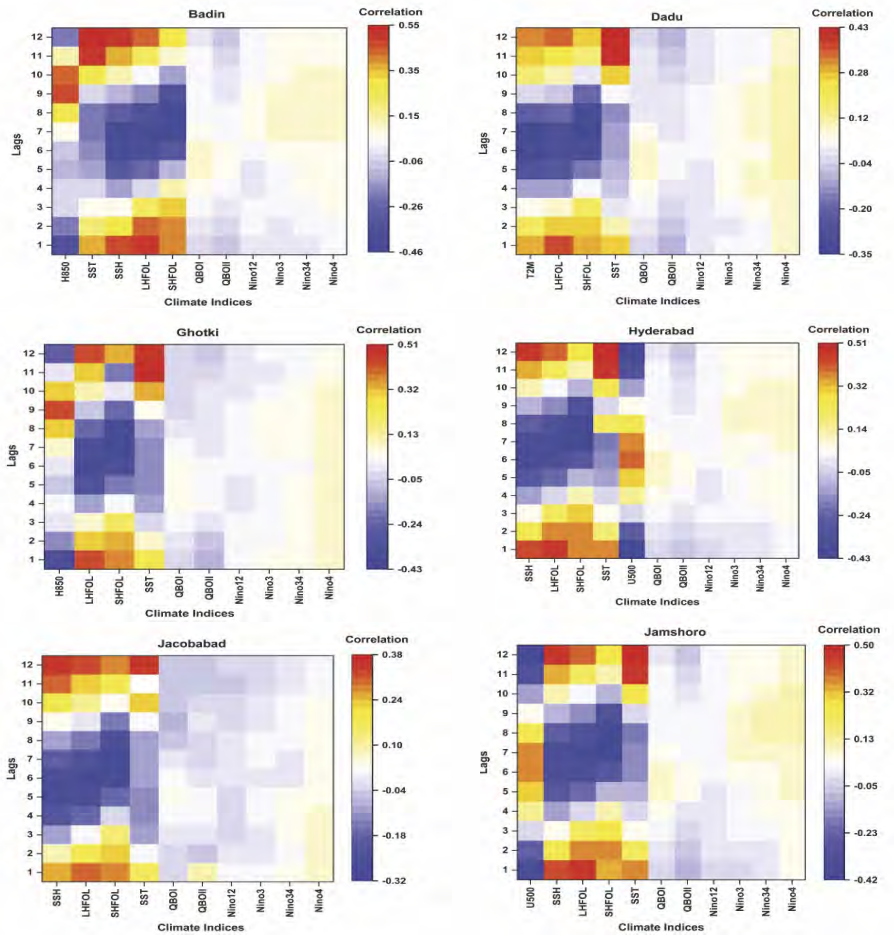

Fig. 6. Correlations of lagged climate indices and monthly precipitation for the first 6 districts.

3.2. Results of multiple regression analysis

In the present study, MLR equations were developed using the identified significant LSCDs at different lag times to predict monthly precipitation. The models were selected as the best models, when they did not violate the limits of statistical significance and recorded lower errors. *Table 3* shows the best developed multiple regression (MR) models using lagged LSCDs for each district, with Pearson correlation (*r*), variance inflation factor (*VIF*), and Durbin-Watson

statistics (*DW*), and similarly, *Table 4* shows the same statistics for MR models developed with PC components (MR-PC). It can be seen that the *VIF* values are just above one which shows that there is no multicollinearity among the predictors, and the *DW* statistics confirmed the goodness-of-fit of the models as the residuals have no autocorrelation. *Table 5* manifests the performance of MR and MR-PC models. The highest Pearson correlation was observed for Mithi district in both sets of the models. In training case, it was 0.62 and 0.57, and in test case it was 0.64 and 0.57, respectively. Overall, MR models performed better than MR-PC models, and all districts' *RMSE* and *MAE* values are relatively low. In the research of *Muslehuddin et al.* (2005), MR models were developed for Sindh, Pakistan with correlation values ranging from 0.53–0.71 which is in accordance with the results of the current study. Studies around the world evaluated oceanic and atmospheric climate indices were lagged at period of several months as predictors of precipitation. In the study of *Taweesin* and *Seeboonruang* (2019), MR models were prepared for Thailand with and without lagged LSCDs, and it was noticed that the rainfall's response to climatic factors was delayed and the models were capable of forecasting monthly rainfall accurately. In the study of *Kim et al.* (2020) in South Korea, it was observed that the models predicted some summer seasons well, but satisfactorily performed during other seasons and long periods which were ascribed to irregular characteristics of rainfall such as heavy rains resulted by monsoonal front and typhoon. The reasons could be a failure to identify the associated climate index signal or in the historical data, or the absence of a significant teleconnection between the climate indices and precipitation. It was also stated that, because of the models statistical nature, the predictability is most likely to be decreased if distinct statistical characteristics climate phenomena appear in the predictors or predictands instead like the past. In the study of *Choubin et al.* (2014) MR model was used also, and it was found that the fluctuations or standard deviation of the observed station data cannot be predicted by the models, therefore, it is not able to forecast droughts and wet years. Some other studies were also carried out (*Hossain et al.*, 2015; *Shukla et al.*, 2011; *Mekanik et al.*, 2013).

Table 5. Performance of the regression models

Districts	Training						Test					
	Correlation		RMSE		MAE		Correlation		RMSE		MAE	
	MR	MR-PC	MR	MR-PC	MR	MR-PC	MR	MR-PC	MR	MR-PC	MR	MR-PC
Badin	0.59	0.50	0.08	0.09	0.03	0.04	0.55	0.49	0.08	0.08	0.04	0.04
Dadu	0.47	0.39	0.09	0.09	0.04	0.05	0.39	0.36	0.11	0.11	0.06	0.06
Ghotki	0.59	0.45	0.12	0.13	0.06	0.06	0.50	0.43	0.13	0.14	0.07	0.08
Hyderabad	0.54	0.45	0.08	0.09	0.03	0.04	0.45	0.44	0.10	0.09	0.05	0.04
Jacobabad	0.46	0.34	0.13	0.14	0.08	0.08	0.41	0.31	0.17	0.19	0.10	0.10
Jamshoro	0.65	0.43	0.07	0.08	0.03	0.03	0.52	0.45	0.08	0.08	0.04	0.05
Karachi	0.60	0.42	0.07	0.08	0.03	0.03	0.44	0.31	0.08	0.09	0.04	0.04
Kashmore	0.51	0.41	0.13	0.14	0.07	0.08	0.45	0.37	0.16	0.17	0.09	0.10
Larkana	0.55	0.46	0.12	0.12	0.07	0.07	0.41	0.38	0.15	0.15	0.08	0.08
Mithi	0.62	0.57	0.10	0.10	0.04	0.05	0.64	0.57	0.09	0.10	0.05	0.06
Sanghar	0.59	0.54	0.10	0.10	0.04	0.05	0.57	0.49	0.10	0.11	0.06	0.06
Shikarpur	0.49	0.39	0.13	0.14	0.07	0.08	0.39	0.31	0.16	0.17	0.09	0.09
Thatta	0.54	0.44	0.08	0.08	0.03	0.03	0.46	0.46	0.08	0.07	0.04	0.04
Umerkot	0.59	0.49	0.11	0.12	0.05	0.05	0.56	0.51	0.11	0.12	0.06	0.06

3.3. Results of artificial neural networks and Bayesian regularization neural networks analysis

Table 6 shows the performance of ANN and BRNN models based on correlation, *RMSE* and *MAE* errors for the training and test cases. The highest correlation coefficient of ANN and BRNN for training case was 0.76 and 0.74 for Mithi district. In the test case, the highest for ANN was 0.83 for Badin and 0.76 for Mithi. All districts' *RMSE* and *MAE* values were relatively low for both types of models. The training case correlation coefficient varied between 0.46–0.76 for ANN and 0.40–0.74 for BRNN. *RMSE* ranged between 0.05–0.14 for ANN and 0.06–0.13 for BRNN. MAE ranged between 0.02–0.09 for ANN and 0.03-0.08 for BRNN. In the test case, correlation coefficient ranged between 0.57–0.83 for ANN and 0.61–0.76 for BRNN. *RMSE* varied between 0.04–0.12 for ANN and 0.07–0.14 for BRNN. *MAE* varied between 0.03–0.07 for ANN models and 0.03-0.08 for BRNN models. The higher values of correlation coefficient of ANN and BRNN models manifest that both models are capable of finding the pattern and trend of the GLDAS precipitation compared to MR and MR-PC models. There is no study in the Sindh region for comparison, but some research carried out in Pakistan and across the world is mentioned here. In the study of *Choubin et al.* (2014), multilayer perceptron (MLP) neural network was employed with MR and ANFIS models for Iran, and the lagged LSCDs were used as inputs. The MLP model showed better performance than the other two models, which is in

agreement with the results of the current study, because the MLP utilizes the Levenberg-Marquardt technique which is faster and powerful than the ANFIS with gradient decent technique for computing the membership function parameters. In the study of *Bello* and *Mamman* (2018), a linear and an ANN model were developed for Kano, Nigeria, and it was found that the ANN is preferable and can be used confidently with the ENSO indices. Similar results were obtained by *Shukla et al.* (2011) and *Doranalu Chandrashekar et al.* (2019) over India. In the study of *Ahmed et al.*, (2015), an MLP was utilized to downscale the rainfall in the Balochistan region of Pakistan. The observed and downscaled rainfall showed good agreement, while it was found that the model underpredicted the variance of rainfall. The study of *Awan* and *Maqbool* (2010) over Islamabad Pakistan revealed better performance of neural network approaches in terms of accuracy, greater lead time, and fewer requirements of resources. In the study of *Ye at al.* (2021), it was observed that BRNN performed well compared with other models but was not capable to reproduce extreme rainfall showing that it cannot be utilized for extreme rainfall and flash flood, prediction, and it overpredicted low rainfall.

Table 6. Performance of ANN and BRNN models

Districts	**Training**						**Test**					
	Correlation		**RMSE**		**MAE**		**Correlation**		**RMSE**		**MAE**	
	ANN	**BRNN**	**ANN**	**BRNN**	**ANN**	**BRNN**	**ANN**	**BRNN**	**ANN**	**BRNN**	**ANN**	**BRNN**
Badin	0.62	0.60	0.06	0.07	0.03	0.04	0.83	0.63	0.08	0.08	0.04	0.03
Dadu	0.57	0.49	0.09	0.08	0.05	0.04	0.61	0.64	0.07	0.10	0.04	0.05
Ghotki	0.64	0.60	0.11	0.12	0.05	0.06	0.66	0.62	0.12	0.10	0.05	0.06
Hyderabad	0.69	0.64	0.08	0.07	0.04	0.03	0.71	0.63	0.04	0.09	0.03	0.04
Jacobabad	0.46	0.40	0.14	0.13	0.09	0.08	0.57	0.61	0.09	0.17	0.07	0.08
Jamshoro	0.65	0.62	0.06	0.07	0.02	0.03	0.79	0.75	0.09	0.07	0.04	0.03
Karachi	0.68	0.46	0.07	0.06	0.03	0.03	0.66	0.68	0.09	0.09	0.04	0.04
Kashmore	0.60	0.46	0.12	0.13	0.07	0.08	0.61	0.61	0.12	0.14	0.07	0.08
Larkana	0.55	0.52	0.11	0.11	0.06	0.07	0.62	0.70	0.12	0.11	0.06	0.07
Mithi	0.76	0.74	0.08	0.08	0.04	0.04	0.79	0.76	0.12	0.09	0.04	0.04
Sanghar	0.65	0.72	0.08	0.09	0.05	0.04	0.74	0.70	0.09	0.08	0.05	0.04
Shikarpur	0.50	0.50	0.14	0.12	0.08	0.07	0.60	0.52	0.16	0.16	0.08	0.08
Thatta	0.65	0.62	0.05	0.06	0.02	0.03	0.74	0.70	0.07	0.09	0.03	0.03
Umerkot	0.62	0.58	0.10	0.11	0.05	0.05	0.65	0.71	0.07	0.10	0.04	0.05

3.4. *Evaluation of model generalization ability on the TRMM set*

After calibration and validation of the models, to assess the generalization capability of the constructed MR, MR-PC, ANN, and BRNN models, the TRMM dataset was used for the period of 1998–2019 (*Fig. 7*). It can be seen that MR and MR-PC models are showing relatively low performance as compared to ANN and BRNN. The correlation coefficient values for the MR and MR-PC based models ranged between 0.22–0.57 and 0.17–0.56, respectively. *RMSE* ranged between 0.11–0.20 and 0.11–0.21. *MAE* varied between 0.06–0.15 and 0.05–0.13. ANN and BRNN models' correlation coefficient varied between 0.27–0.65 and 0.28–0.60, respectively. *RMSE* ranged between 0.10–0.14 and 0.11–0.14 while *MAE* ranged between 0.05–0.08 and 0.04–0.08.

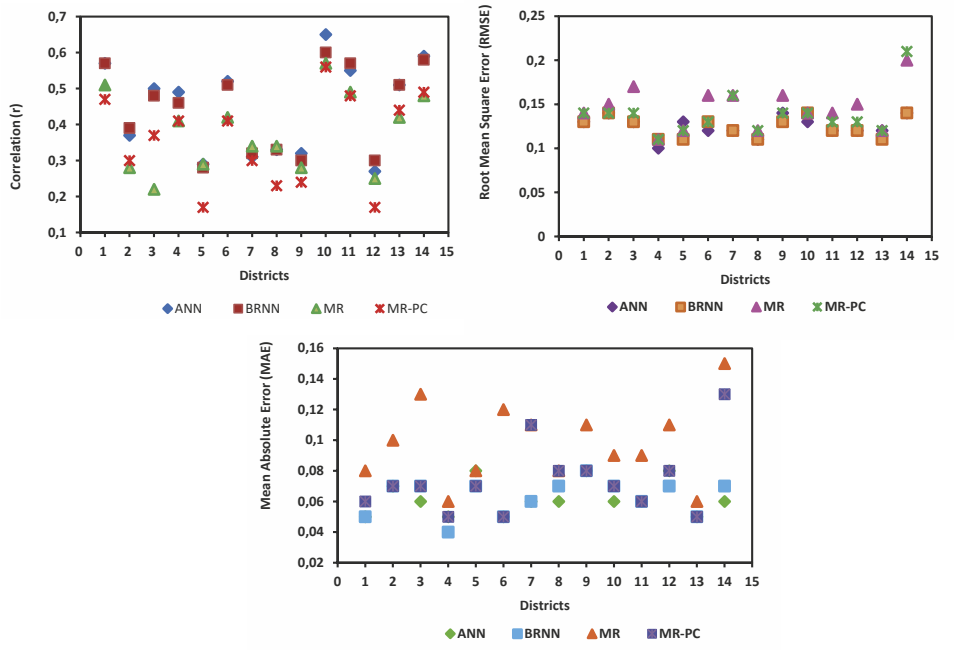

Fig. 7. Performance of ANN, BRNN, and multiple regression models for the test set (TRMM dataset).

3.5. *Comparison of the models*

Fig. 8 shows comparisons between all four types of models (MR, MR-PC, ANN, and BRNN). To summarize results, only two out of the fourteen districts are

graphically presented. ANN and BRNN outperformed the other models, and in general, the regression models showed underestimation of the actual observations also discussed by *Mekanik et al.* (2013). However, it is noted that these models were not able to predict the extreme precipitation, which means that they are not applicable for extreme precipitation prediction. This is in accordance with the findings of *Ye et al.* (2021). *Fig. 9(a-f)* represents the radar charts of overall performance, where the first two charts are showing the correlation over two sets of the 14 districts (*Fig. 9a* and *b*). Correlation of the ANN with GLDAS precipitation is higher in most of the districts followed by BRNN and MLR, while MLR-PC one is low. To check the errors of the models, two radar charts of root mean square error (*RMSE*) (*Fig. 9c* and *d*) and two of the mean absolute error (*MAE*) (*Fig. 9e* and *f*) are also presented, which are manifesting low errors for ANN, BRNN, and MR and highest for MR-PC.

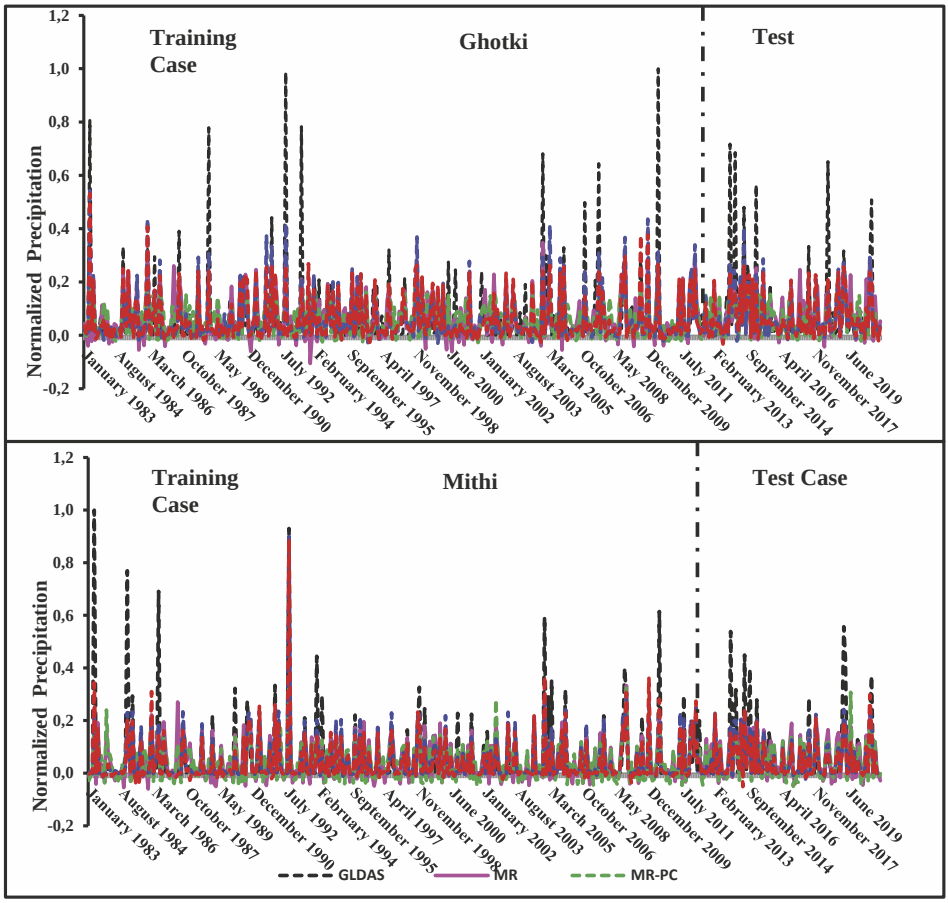

Fig. 8. Comparing ANN and BRNN models with MR and MR-PC models over two districts of Sindh province.

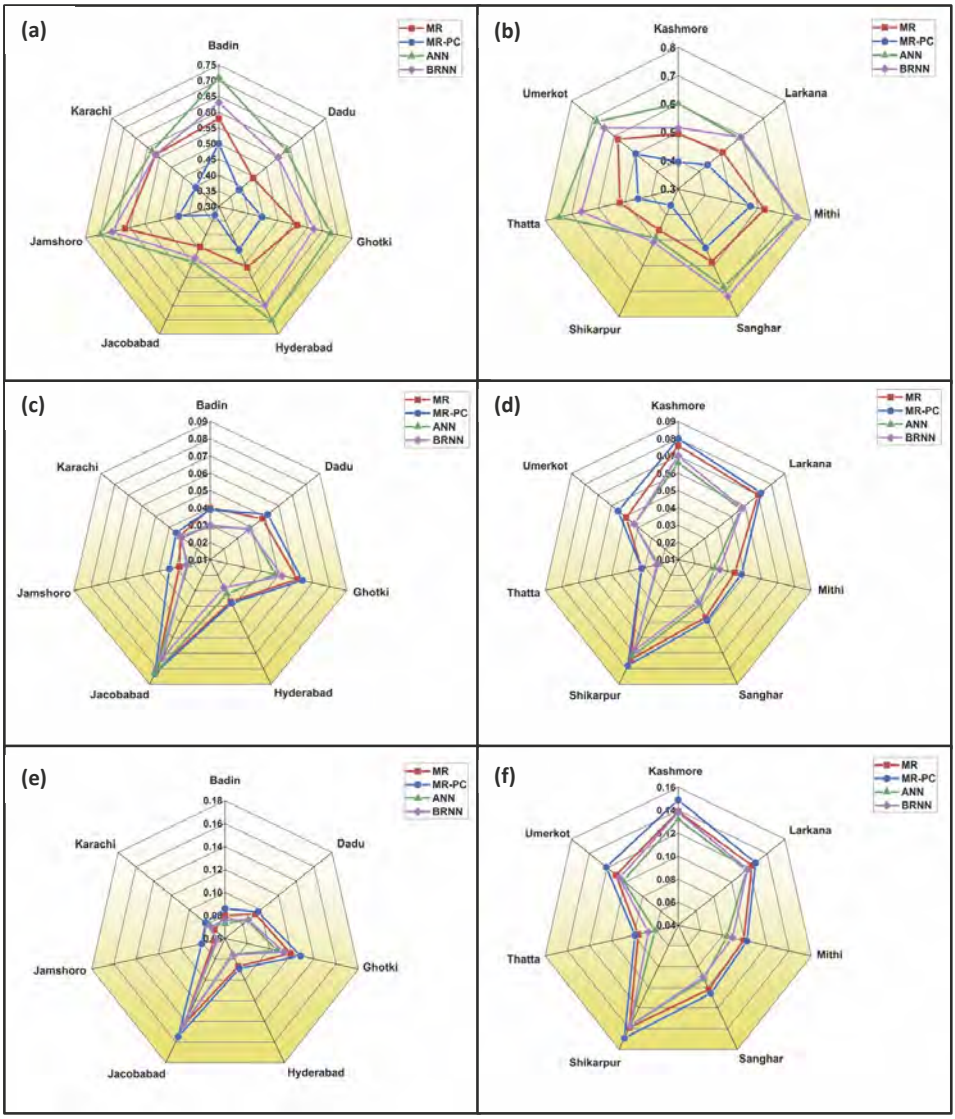

Fig. 9. Radar charts of GLDAS and predicted precipitation values by MR, MR-PC, ANN, and BRNN during 1983-2020; (a and b) correlation (c and d) mean absolute error, and (e and f) root mean square error.

4. Conclusion

This study focused on the identification of significant LSCDs in Sindh province of Pakistan, and improved the forecast skill of monthly precipitation by application of principal component analysis, artificial neural network, Bayesian

regularization neural network, and multiple regression analysis while taking into account the lagged association of LSCDs. Nino-1+2, Nino-3, Nino-3.4, Nino-4, SST, QBOI, QBOII, T2M, H500, H850, SU, U500, LHFOL, SHFOL, and SSH were selected as LSCDs. The significant LSCDs identified by a cross correlation analysis with 99% confidence level were SU, U500, T2M, SST, SHFOL, LHFOL, SSH, and H850. It was noticed that for most of the LSCDs, the relationship was persistent and statistically significant at lags 1, 2, and 4 to 12 with the strongest correlations in the SST, LHFOL, SSH, and U500. To predict monthly precipitation using lagged LSCDs and principal components, MR models were developed. The models that did not violate the limits of statistical significance and multicollinearity and had lower errors were selected. MR models performed better than MR-PC. Highest correlation was observed for Mithi district in both model sets. In the training case it was 0.62 and 0.57 and in the test case it was 0.64 and 0.57, respectively. ANN and BRNN models were developed using selected PC components and gave higher correlations as compared to regression models indicating their capability of finding the pattern and trend of the observations. They generally manifested lower errors and were more reliable for the purpose of prediction in the region. However, they were not able to predict very high precipitation events, which means that they are not applicable for extreme precipitation prediction. The highest correlation coefficient of ANN and BRNN for the training case was 0.76 and 0.74 for Mithi district. In the test case, the highest for ANN was 0.83 for Badin and 0.76 for Mithi. Their generalization ability was tested on TRMM dataset. In conclusion, this study divulged the possibility of monthly precipitation forecasting using ANN and BRNN and lagged LSCDs for the study region. It is explicit that the response of precipitation to climatic factors is delayed. Future studies are needed to be carried out for the improvement of prediction of the extreme and lower precipitation events with the addition of new climatic indices.

Acknowledgements: This study is a part of the first author's doctoral research work conducted at the University of Tabriz, Iran. The authors would like to acknowledge the NASA Goddard Earth Sciences Information Services Center (GES DISC) for giving access to the GLDAS model satellite precipitation data and the MERRA-2 model, the Freie University Berlin, and the NOAA Global Climate Observing System (GCOS) Working Group on Surface Pressure (WG-SP) for the HadISST data for the research purpose on free basis.

References

Ahmed, K., Shahid, S., Haroon, S.B., and *Wang, X.J.,* 2015: Multilayer perceptron neural network for downscaling rainfall in arid region: A case study of Baluchistan, Pakistan. *J. Earth Sys. Sci.* 124, 325–1341. https://doi.org/10.1007/s12040-015-0602-9

Aamir, E., and *Hassan, I.,* 2018: Trend analysis in precipitation at individual and regional levels in Baluchistan, Pakistan. In IOP Conference Series: Material Science and Engineering 414, 1st International Conference on Advances in Engineering and Technology (ICAET-2018). https://doi.org/10.1088/1757-899X/414/1/012042

Adamowski, J., and *Sun, K.*, 2010: Development of a coupled wavelet transform and neural network method for flow forecasting of non-perennial rivers in semi-arid watersheds. *J. Hydrol. 390*, 85–91. https://doi.org/10.1016/j.jhydrol.2010.06.033

Ahmadi, A., Moridi, A., Lafdani, E.K., and *Kianpisheh, G.*, 2014: Assessment of climate change impacts on rainfall using large scale climate variables and downscaling models – A case study. *J. Earth Sys. Sci. 123*, 1603–1618. https://doi.org/10.1007/s12040-014-0497-x

Awan, J.A., and *Maqbool, O.*, 2010: Application of Artificial Neural Networks for monsoon rainfall prediction. In 2010 6th International Conference on Emerging Technologies (ICET). 27–32.

Bello, A.A., and *Mamman, M.B.*, 2018: Monthly rainfall prediction using artificial neural network: A case study of Kano, Nigeria. *Environ. Earth Sci. Res. J. 5*(2), 37–41. https://doi.org/10.18280/eesrj.050201

Begum, B., Tajbar, S., Khan, B., and *Rafiq, L.*, 2021: Identification of relationships between climate indices and precipitation fluctuation in Peshawar City-Pakistan. *J. Res. Environ. Earth Sci. 10*, 264–278.

Beale, M.H., Hagan, M.T., and *Demuth, H.B.*, 2011: Neural network toolbox TM7: User's guide.

Bhutto, A., and *Wei, M.*, 2009: Impact of ENSO on summer monsoon in southern parts of Pakistan. In 2009 1st International Conference on Information Science and Engineering (ICISE). 4903–4906. https://doi.org/10.1109/ICISE.2009.654

Choubin, B., Khalighi-Sigaroodi, S., Malekian, A., and *Kisi, O.*, 2014: Multiple linear regression, multi-layer perceptron network and adaptive neuro-fuzzy inference system for forecasting precipitation based on large-scale climate signals. *Hydrol. Sci. J. 61*, 1001–1009. https://doi.org/10.1080/02626667.2014.966721

Chinchorkar, S.S., Patel, G.R., and *Sayyad, F.G.*, 2012: Development of monsoon model for long range forecast rainfall explored for Anand (Gujarat-India). *Int. J. Wat. Res. Environ. Engineer. 4*, 322–326.

Cybenko, G., 1989: Approximation of superpositions of a sigmoidal function. *Mathemat. Control. Sign. Sys. 2*, 303–314. https://doi.org/10.1007/BF02551274

Doranalu Chandrashekar, V., Shetty, A., and *Patel, G.C.M.*, 2019: Estimation of monsoon seasonal precipitation teleconnection with El Niño-Southern Oscillation sea surface temperature indices over the Western Ghats of Karnataka. *Asia-Pacific J. Atm. Sci.(2019)* https://doi.org/10.1007/s13143-019-00133-w

Field, A., 2009: *Discovering statistics using SPSS*, 3rd edn. Sage Publications Ltd, London.

Fang, H., Beaudoing, H.K., Rodell, M., Teng, W.L., and *Vollmer, B.E.*, 2009: Global Land Data Assimilation System (GLDAS) products, services and application from NASA Hydrology Data and Information Services Center (HDISC). In ASPRS 2009 Annual Conference. 151–159.

Gholami Rostam, M., Sadatinejad, S.J., and *Malekian, A.*, 2020: Precipitation forecasting by large-scale climate indices and machine learning techniques. *J. Arid Land* 12, 854–864. https://doi.org/10.1007/s40333-020-0097-3

Hossain, I., Rasel, H.M., Imteaz, M.A., and *Pourakbar, S.*, 2015: Effects of climate indices on extreme rainfall in Queensland, Australia. In 21st International Congress on Modelling and Simulation MODSIM. 1984–1990.

Hussain, M., 2020: Spatiotemporal construction safety planning by integrating Building Information Modeling (BIM) with Artificial Intelligence (AI). Dissertation, Sungkyunkwan University, South Korea.

Iqbal, M.F., and Athar, H., 2018: Variability, trends, and teleconnections of observed precipitation over Pakistan. *Theor. Appl. Climatol. 134*, 613–632. https://doi.org/10.1007/s00704-017-2296-1

Kumar, R., Singh, M.P., Roy, B., and *Shahid, A.H.*, 2021: A comparative assessment of metaheuristic optimized extreme learning machine and deep neural network in multi-step-ahead long-term rainfall prediction for all-Indian regions. *Wat. Res. Manage. 35*, 1927–1960. https://doi.org/10.1007/s11269-021-02822-6

Kashiwao, T., Nakayama, K., Ando, S., Ikeda, K., Lee, M., and *Bahadori, A.*, 2017: A neural network-based local rainfall prediction system using meteorological data on the Internet: A case study using data from the Japan Meteorological Agency. *Appl. Soft Comput. J. 56*, 317–330. https://doi.org/10.1016/j.asoc.2017.03.015

Kim, C-G., Lee, J., Lee, J.E., Kim, N.W., and *Kim, H.,* 2020: Monthly precipitation forecasting in the Han River Basin, South Korea, using large-scale teleconnections and multiple regression models. *Water 12*(6), 1590. https://doi.org/10.3390/w12061590

Lee, J., Kim, C.G., Lee, J.E., Kim, N.M., and *Kim, H.,* 2018: Application of artificial neural networks to rainfall forecasting in the Geum River Basin, Korea. *Water 10*(10), 1448. https://doi.org/10.3390/w10101448

Luk, K.C., Ball, J.E., and *Sharma, A.,* 2000: A study of optimal model lag and spatial inputs to artificial neural network for rainfall forecasting. *J. Hydrol. 227*, 56–65. https://doi.org/10.1016/S0022-1694(99)00165-1

Lin, F.J., 2008: Solving multicollinearity in the process of fitting regression model using the nested estimate procedure. *Qual. Quant. 42*, 417–426. https://doi.org/10.1007/s11135-006-9055-1

Mekanik, F., Imteaz, M.A., Gato-Trinidad, S., and *Elmahdi, A.,* 2013: Multiple regression and Artificial neural network for long-term rainfall forecasting using large scale climate modes. *J. Hydrol. 503*, 11–21. https://doi.org/10.1016/j.jhydrol.2013.08.035

Muslehuddin, M., and *Faisal, N.,* 2006: Long range forecast of Sindh monsoon. *Pak. J. Meteorol. 3*, 35–44.

Mahmood, A., Khan, T.M.A., and *Faisal, N.,* 2006: Relationship between El Nino and summer monsoon rainfall over Pakistan. *Pak. J. Marine Sci. 15*, 161–178.

Menke, W., and *Menke, J.,* 2009: Environmental data analysis with MATLAB. Elsevier, London.

Maier, H.R., and *Dandy, G.C.,* 2000: Neural networks for the prediction and forecasting of water resources variables: A review of modelling issues and applications. *Environ. Model. Softw. 15*, 101–124. https://doi.org/10.1016/S1364-8152(99)00007-9

Muslehuddin, M., Mir, H., and *Faisal, N.,* 2005: Sindh Summer (June-september) Monsoon Rainfall Prediction. *Pak. J. Meteorol. 2*, 91–108.

Rehman, A., Jingdong, L., Shahzad, B., Chandio, A.A., Hussain, I., Nabi, G., Iqbal, M.S., 2015: Economic perspectives of major field crops of Pakistan: An empirical study. Pacific Sci. Rev. B: Humanit. Soci. Sci. 1, 145–158. https://doi.org/10.1016/j.psrb.2016.09.002

Rasul, G., Afzal, M., Zahid, M., and *Bukhari, S.A.A.,* 2012: Climate Change in Pakistan Focused on Sindh Province, Technical Report PMD 25/2012 55. Pakistan Meteorological Department, Islamabad, Pakistan, 2012, https://doi.org/10.13140/2.1.2170.6560

Rashid, A., 2004: Mpact of El-Nino on summer monsoon rainfall of Pakistan. *Pak. J. Meteorol. 1*, 35–43.

Solomon, S., 2019: Understanding the impacts of climate change on water access and the lives of women in Tharparkar District, Sindh Province, Pakistan: A Literature Review 1990-2018.

Sarfaraz., 2007: Monsoon dynamics: Its behavioral impact in Pakistan's perspective. *Pak. J. Meteorol. 4*, 55–73.

Shukla, R.P., Tripathi, K.C., Pandey, A.C., and *Das, I.M.L.,* 2011: Prediction of Indian summer monsoon rainfall using Niño indices: A neural network approach. *Atmos. Res. 102*, 99–109. https://doi.org/10.1016/j.atmosres.2011.06.013

SWP, 2021: Climate of Sindh. https://sindhweatherportal.wordpress.com/climate-of-sindh/. 1 January 2021.

DOI:10.28974/idojaras.2023.3.5

IDŐJÁRÁS

Quarterly Journal of the Hungarian Meteorological Service
Vol. 127, No. 3, July – September, 2023, pp. 347–377

Considerations regarding the evolution of extreme temperatures in the Banat Plain in the last six decades

Mihai Dudaş* and **Petru Urdea**

West University of Timişoara
Department of Geography
Bulevardul Vasile Pârvan 4, Timișoara 300223, Romania

**Corresponding author E-mail: mihai.dudas74@e-uvt.ro*

(Manuscript received in final form November 7, 2022)

Abstract— During cold winter nights we often hear the question "where is the global warming, should it not be warmer?". Low temperatures that can still be recorded in the Banat Plain during winter or media reports of cold waves affecting various regions worldwide seem to the common man to be in total contradiction with the concerns of the scientific community about global warming. With this article we are trying to follow the evolution of some meteorological parameters that can affect the population in one way or another, namely number of tropical days, number of winter days, number of tropical nights, number of frosty nights, absolute maximum and minimum temperatures. Thus, the data obtained from the three national meteorological services (Romanian, Hungarian, and Serbian) operating on the territory of the Banat Plain were grouped in a common database and analyzed both in Excel and with the help of the non-parametric Mann-Kendall test, obtaining a series of conclusions on the evolution of the abovementioned parameters, as well as on the way how the increase in the risk of high temperatures is compensated (or not) by the decrease in the risk of low temperatures.

Key-words: tropical days, winter days, tropical nights, frosty nights, absolute maximum and minimum temperatures, Mann-Kendall test, Banat Plain

1. Introduction

Although climate change, including global warming, are normal phenomena caused by natural factors that climate scientists have been concerned about since the 19th century, the extent of these changes or the increasing global temperatures in the past decades and their increasing impact on human society have intensified the concerns of the international scientific community about the role of human society in amplifying climate change, its extent and evolution, the prevention or at least mitigation of its effects, etc. With this article, part of a larger, not yet completed work (*Dudaş* and *Urdea*, 2021), we want to contribute to the study of climate change over the last six decades and its effects at local level, focusing on the evolution of extreme temperatures, temperatures that can affect in one way or another the smooth running of human society. Numerous studies, taken not only at global level, but also at regional or local level (*Bartholy* and *Pongrácz*, 2007; *Gocić* and *Trajković*, 2012; *Cheval et al.*, 2014; *Gavrilov et al.*, 2016; *Lakatos et al.*, 2016; *Janković et al.*, 2019; *Papić et al.*, 2020*; Şmuleac et al.*, 2021; *Bačević et al.*, 2021; *Milentijević et al.*, 2022, etc), show us an increase in average temperatures in recent decades, which can also be observed from the data we have for the lowland Banat region (*Table 1*). Without denying the indirect effects of global warming on the area under investigation, we want to see how some of the climatic parameters that directly affect the population have evolved over the last six decades, namely those parameters related to high and low temperatures, and to see if it can be said that the increase in intensity of the hazards caused by high temperatures is compensated by the decrease in intensity of the hazards caused by low temperatures.

Table 1. Weather stations (operated by the Centrul Meteorologic Regional Banat-Crișana, Republički Hidrometeorološki Zavod Srbije, RHMZ, and Országos Meteorológiai Szolgálat, OMSZ), years of observation, and mean annual air temperatures used in the study

No.	Station name	Years of observation available	Mean annual air temperature (1961–1990) (°C)	Mean annual air temperature (1991–2020) (°C)
1.	Timișoara	1961–2020	10.6	11.7
2.	Arad	1961–2020	10.4	11.3
3.	Caransebeș	1961–2020	10.1	11.1
4.	Szeged	1901–2020	10.5	11.4
5.	Kikinda	1961–1985, 1991–2020	10.8	11.9
6.	Zrenjanin	1961–1985, 1991–2020	10.9	12.1
7.	Vršac	1961–1985, 1991–2020	11.4	12.4

In a historical sense, the Banat region can be defined as the region bounded on the north by the river Mureş, on the south by the Danube, on the west by the Tisza, which extends east to the border with Transylvania and Wallachia, being currently divided between 3 states: Romania, Serbia, and Hungary (*Fig. 1*). Located in the southeastern part of the Pannonian Plain (Nagyalföld or Alföld), the Banat Plain occupies the western part of the Banat region, in the east, the boundary to the Banat Hills and Mountains being approximately given by the contour lines ranging from 160 m to 200 m, on a sinuous line between Lipova and the area where the Nera flows into the Danube (*Posea*, 1997) (*Fig. 1*). The altitudinal distribution of the Banat Plain brings out the existence of a higher level, near the hills and mountains and a lower level, with young and less developed landforms, the boundary between the two types of plain generally following the contour line of 100 m (*Ianoş et al.*, 1997) (*Fig. 1*).

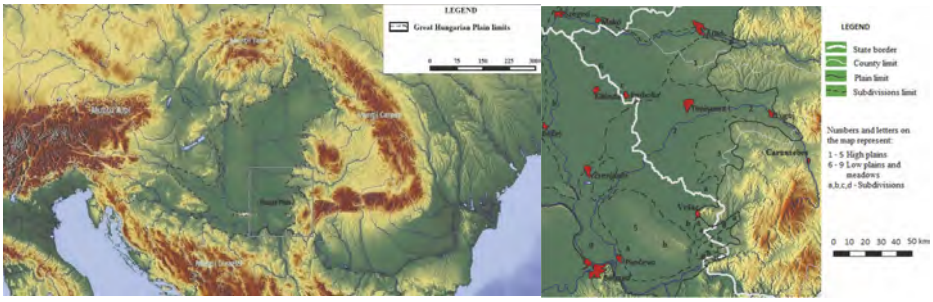

Fig. 1. The location of the Banat Plain within the Pannonian Basin, boundaries and subdivisions (adaptation after various sources).

The geographic location of the Banat Plain, along with the general movement of the atmosphere, determines the existence of a moderate temperate continental climate. Even if we can talk about a certain homogeneity of the main climatic elements all across the studied area, there are small differences with regard to the micro- and topoclimate, differences caused by the natural environment elements or anthropic influence. Calculated for the last 60 years (1961–2020), the multiannual mean temperature value in the Banat Plain is in the range of 10.5–12 °C, increasing by about one degree in the second half of the period (*Table 1*), while the average annual rainfall in the Banat Plain for the same period is generally between 500–700 mm (Centrul Meteorologic Regional Banat - Crişana, Republički Hidrometeorološki Zavod Srbije, RHMZ, Országos Meteorológiai Szolgálat, OMSZ).

2. Database and methodology

The first known meteorological measurements were made in the Banat Plain between 1780 and 1803 by Carl Josef Klapka in Timișoara (*Réthly*, 1918, 1970). Although measurements were made during the entire 19th century in various localities in the lowland Banat, the sporadic nature of these measurements, as well as their accuracy according to current standards, led us not to mention them during this work. The lack of meteorological parameters or the incomplete data strings we have from different meteorological stations for the 20th century have also limited our options quite a lot regarding the period and the meteorological stations investigated. Finally, we chose seven meteorological stations, Timișoara, Kikinda, Zrenjanin, and Vršac being located within the limits of the Banat Plain, while Arad, Szeged, and Caransebeș are located slightly outside the limits of the investigated area, north of the river Mureș, respectively, west of the Tisza or in the Caransebeș depression, an extension of the plain within the mountainous area (*Fig. 1*).

For the years 1986–1990 we are still missing data from Kikinda, Zrenjanin, and Vršac, but we consider that these missings do not affect the image of the evolution trends and the final conclusions.

Given that the aim of this work is to follow the evolution of temperature-related hazards, the following six parameters were chosen:

- number of tropical days (Td) or number of hot days – days when the maximum temperature is ≥ 30 °C;
- number of winter days (Wd) or ice days – days when the maximum temperature is ≤ 0° C;
- number of tropical nights (Tn) – days with a minimum temperature ≥ 20 °C;
- number of frosty nights (Fn) or number of severe cold days – days with a minimum temperature ≤ -10 °C;
- absolute highs – the highest temperature in a month/year;
- absolute lows – the lowest temperature in a month/year.

Even if not all six parameters fall entirely into the category of phenomena defined as hazards (potentially damaging phenomena), it cannot be denied the discomfort they create and the expense of reducing this discomfort.

The completion of this article involved several stages:

a. Collecting the necessary data and creating a small database in Excel. Data for the Romanian meteorological stations were purchased from the Regional Meteorological Center of Banat – Crișana (Centrul Meteorologic Regional Banat – Crișana), data for the Szeged weather station are available online at the Hungarian Meteorological Service (Országos Meteorológiai Szolgálat) website (https://www.met.hu), while data for Serbian weather stations were

taken from the Meteorological Yearbooks of the Federal Hydrometeorological Institute of Yugoslavia/Republican Hydrometeorological Service of Serbia (Republički Hidrometeorološki Zavod Srbije), also available online (https://www.hidmet.gov.rs/index.php).

b. Observing and verifying the data to avoid discrepancies between the data from a given station and the data from other stations for a given parameter in a given year or between different parameters from the same weather station for a given year; obtaining average values for the Banat Plain for all parameters.

c. Making graphs and obtaining the trend equation using linear regression for all parameters, both for monthly and annual trends. Trend equation was calculated by Excel with the formula $y = ax+b$, where y represents the parameter in a given year, a is the slope, x is the time in years, and b is the parameter at the beginning of the period. Easy to perform and interpret, there are three possible scenarios: if $a \geq 0$, the trend is positive, increasing, if $a = 0$, there is no trend, and if $a \leq 0$ the trend is negative, decreasing (*Gavrilov et al.*, 2016).

d. Applying the Mann-Kendall non-parametric test for all parameters to confirm the presence of trends in both monthly and annual values. Under MK test, two hypotheses have been tested: the null hypothesis, H_o, indicating no trend in the time series; and the alternative hypothesis, H_a, indicating that there is a significant trend in the time series for a given level of significance. The probability, p, has been calculated in percents to determine the level of confidence in the hypothesis. When the p value calculated is less than the assumed significance level a (e.g., a=5%), the H_o hypothesis has to be rejected (no trend) and the Ha (there is a significant trend) should be accepted. If p is higher than significance level a, the H_o hypothesis (no trend) cannot be rejected (*Gavrilov et al.*, 2016).
XLSTAT software (http://www.xlstat.com/en) has been used to calculate the probability and hypothesis testing.

e. Performing arithmetic operations between existing parameters, from the evolution of the resulting parameters (Td+Wd, Tn+Fn, Td-Wd, Tn-Fn, absolute thermal amplitudes) being able to better observe the increasing or decreasing trends of the thermal risk, as well as the climate evolution trends.

3. Results

As mentioned earlier, we will paint an image of the evolution trends for extreme temperatures in the Banat Plain through several climate parameters.

3.1. Tropical days

Tropical days (Td) may occur in the Banat Plain starting from April until October, their average for the interval 1961–2020 is 32 days/year, with higher values at Timişoara, Zrenjanin, Arad, Vršac, or Kikinda and lower in Szeged and Caransebeş. The lowest average value was recorded in 1978, 5.7 days/year, and the highest in 2012, 72.3 days/year, and in terms of the absolute minimum, it was recorded in 1977 at Caransebeş, 2 days/year, and the absolute maximum in 2012 at Zrenjanin, 78 days/year (*Table 2*).

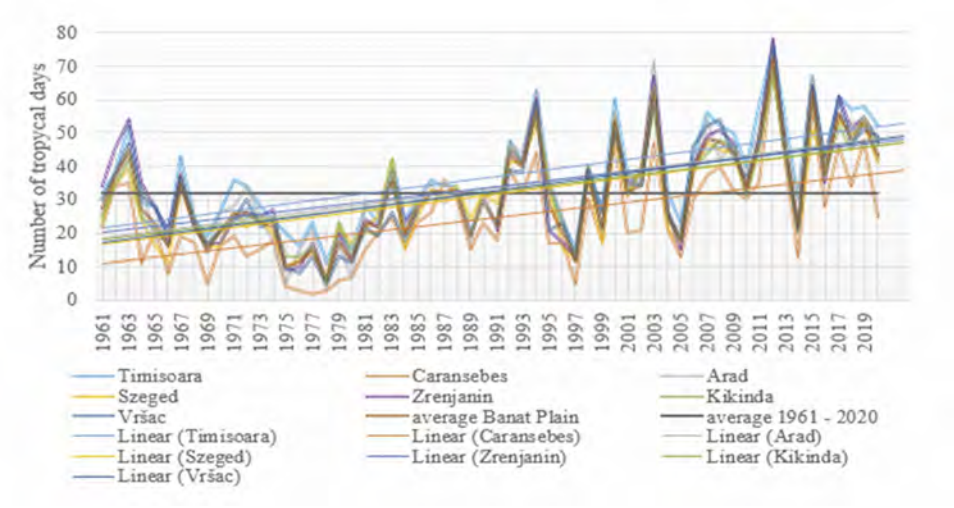

Fig. 2. Evolution of the annual number of tropical days at the analyzed meteorological stations.

Table 2. Evolution of the annual number of tropical days in the Banat Plain analyzed by Mann-Kendall trend tests

Station name	Trend equation	Min.	Max.	Mean	Std. deviation	Kendall 's tau	p-value	Sen's slope
Timişoara	y=0.5127x+20.996	11	76	36.633	15.362	0.379	<0.0001	0.500
Caransebeş	y=0.4592x+10.462	2	70	24.467	14.509	0.377	<0.0001	0.455
Arad	y=0.5078x+18.012	3	71	33.500	15.534	0.401	<0.0001	0.488
Szeged	y=0.4980x+16.077	7	71	31.267	14.483	0.418	<0.0001	0.529
Zrenjanin	y=0.4538x+19.838	6	78	33.782	16.566	0.313	0.001	0.457
Kikinda	y=0.4727x+17.731	5	68	32.255	14.513	0.367	<0.0001	0.455
Vršac	y=0.5142x+16.854	5	76	32.655	16.198	0.362	0.000	0.500
average Banat Plain	y=0.4884x+17.056	5.714	72.286	31.953	14.723	0.376	<0.0001	0.479

An evolution over time of this indicator for the last 6 decades (*Fig. 2*) reveals us values generally below average for the first three decades, with small exceedances of the average values during seven years in the 1960s and 1980s and values below average in 23 years, the longest period with below average values being between 1968 and 1982. In the last three decades, there is a predominance of above-average values, values that exceed by 50% the multiannual average being registered in 1994, 2000, 2003, 2007, 2012, 2015, and 2017–2019. Over the decades, there is a decrease in values in the 1970s, compared to the 1960s, followed by a steady increase to the present day.

The Mann-Kendal trend test confirms the general growth trend of this parameter, both at the level of the Banat Plain and at the level of each analyzed meteorological station (*Table 2*).

Concerning the monthly distribution of this parameter (*Fig. 3*), in the Banat Plain there can be tropical days starting from April, but their number is very low, with a total of 21 cases, all in the last 3 decades and with a peak in 2013, when there were 1–2 cases for each weather station analyzed. The Mann-Kendal trend test confirms the existence of a trend, but the Sen's slope is 0 (*Table 3*). In May, the average number of tropical days for the whole Banat Plain has been 1.18 days/month for the last six decades, with relatively uniformly distributed values, except for the 8th decade of the last century, with 0.5 days/month and the 1st decade of our century, with 2.6 days, giving the slightly increasing trend of this parameter. In 22 years there have been no tropical days at all in the Banat Plain in May. Half of the cases were recorded in the last two decades of the interval, while the maximum number of tropical days, 9.9, was recorded in 2003. The Mann-Kendal trend test confirms the existence of a trend, but with a very small slope (*Table 3*).

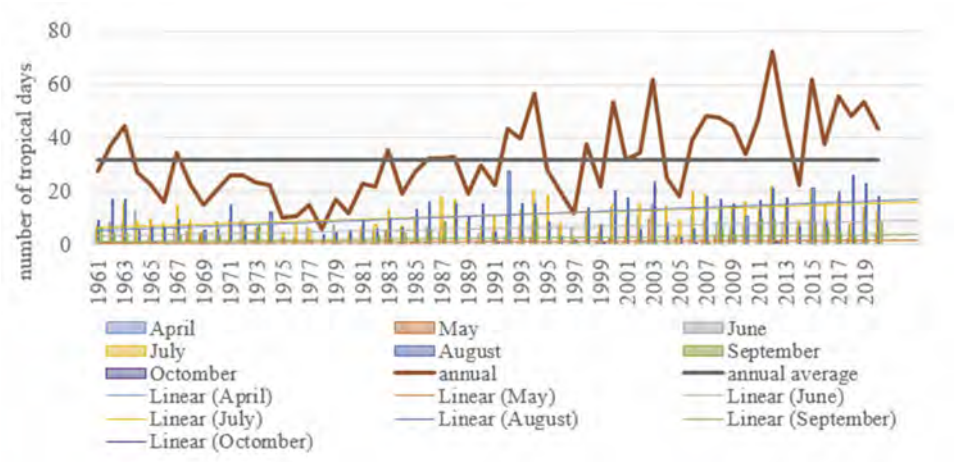

Fig. 3. Evolution of the monthly number of tropical days in the Banat Plain.

Table 3. Evolution of the monthly number of tropical days in the Banat Plain analyzed by Mann-Kendall trend tests

Month	Trend equation	Min.	Max.	Mean	Std. deviation	Kendall's tau	p-value	Sen's slope
April	y=0.0035x-0.0571	0	1.429	0.050	0.210	0.297	0.005	0
May	y=0.0178x+0.6393	0	9.857	1.182	1.766	0.191	0.040	0.006
June	y=0.0965x+3.0554	0	15.429	5.998	4.057	0.277	0.002	0.099
July	y=0.1456x+6.5737	1.857	21.857	11.013	4.913	0.343	<0.0001	0.143
August	y=0.1876x+5.4510	0	27.714	11.171	6.908	0.339	<0.0001	0.199
September	y=0.0372x+1.3539	0	10.429	2.488	2.987	0.089	0.326	0.011
Octomber	y=0.0003x+0.0395	0	1	0.050	0.197	0.059	0.584	0

For June, the average of 6 tropical days/month is exceeded in the early 1960s growing steadily since the second half of the 1990s. Zero tropical days were recorded in June 1978, 1988, and 1989, and the maximum, 15.4 tropical days, in June 2003. The Mann-Kendal trend test confirms the existence of a trend, with a significant slope (*Table 3*). For July, the average of 11 tropical days/month is exceeded twice in the 1960s and three times in the 1980s, then consistently since 1990, with the maximum number of tropical days in July being 21.9 days in 2012 and the minimum 1.9 days in 1978. A very large difference also occurs between the number of tropical days recorded in July in the 8th decade of the last century, 59.7, and the number of tropical days recorded in the last decade, 146.6. The Mann-Kendal trend test confirms the existence of a trend, with a significant slope (*Table 3*). August shows the strongest upward trend in the number of tropical days, exceeding the number of tropical days in July in the second part of the period. This trend is best illustrated by the difference between the number of tropical days recorded in the 8th decade of the last century, 5.94/month, and the number of days recorded in the last decade, 17.91/month. The average is 11.2 tropical days/month, but the values vary widely, from 0 days in 1968 or 1976 to 27.7 days in 1992. The Mann-Kendal trend test confirms the existence of a trend, with a significant slope (*Table 3*).

For the month of September, the average of 2.5 tropical days/month is exceeded especially in the last decade, when the average was 5.3, with this decade actually dictating the upward trend of this indicator. However, the record number of tropical days in September was recorded in 1994, 10.4, while months with no tropical days were in 13 cases. The Mann-Kendal trend test does not confirm the existence of a trend (*Table 3*). In October, as in April, we have a number of 21 cases registered in the Banat Plain in the last 60 years, most of them in 1965 and 2012, then in 2006, 1991, and 1999; these are missing from Szeged, where the last tropical day in October was recorded in 1942. Same as for September, the Mann-Kendal trend test does not confirm the existence of a trend (*Table 3*).

3.2. Winter days

The average number of winter days (Wd) for the Banat Plain over the last six decades has been 19.72 days/year, higher in Szeged, Arad, and Kikinda and lower in Zrenjanin, Caransebeș, Timișoara, and Vršac. The graph of the evolution over time of this indicator in the Banat Plain (*Fig. 4*) shows several periods with a high number of winter days between 1962 and 1969, with a maximum of 47.1 days/year in the Banat Plain and an absolute maximum of 57 winter days/year in Szeged, both in 1963, then 1985–1993, 2002–2005, and 2009–2012, alternating with periods when the number is below average, such as 1972–1975, with a minimum of 3 winter days/year in the Banat Plain and an absolute minimum of 2 days/year in Timișoara, Caransebeș, and Vršac, both in 1974, then in 2006–2008, and 2013–2020.

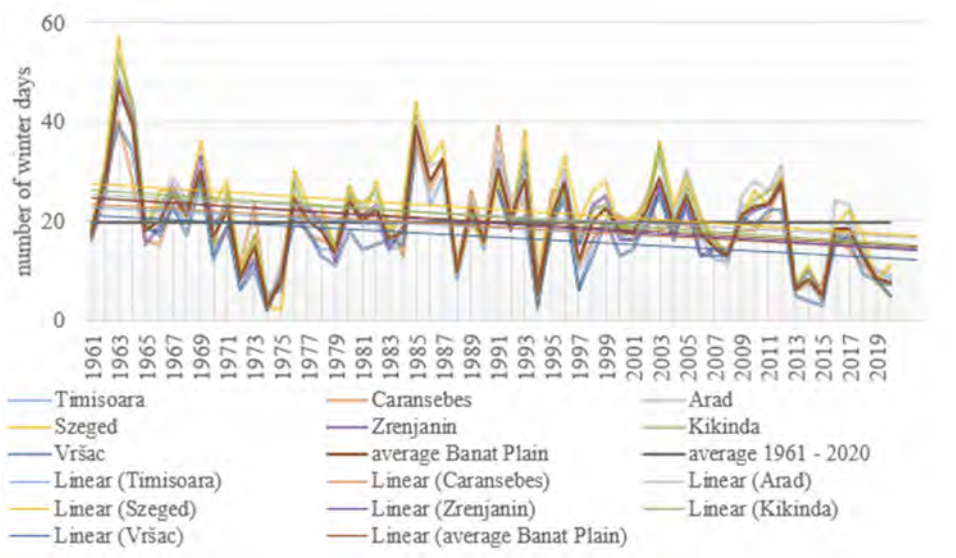

Fig. 4. Evolution of the annual number of winter days at the analyzed meteorological stations.

If we analyze this parameter by decades, we notice a very high number of winter days in the 1960s, 26.4/year, followed by a low number of winter days in the 1970s, 15.6/year, again a high number of winter days in the 1980s, 22.3/year, decreasing until the last decade, when an average of 13.5 winter days/year are recorded. The very high number of cases in the 1960s, correlated with the low number of winter days recorded in the last decade, determines the downward trend of this parameter at all meteorological station analyzed (*Fig. 4*).

The Mann-Kendal trend test confirms the decreasing trend of this parameter for the Banat Plain and also for Caransebeș, Szeged, Zrenjanin, Kikinda, and Vršac, while for Timișoara and Arad the existence of a trend is not confirmed (*Table 4*).

Table 4. Evolution of the annual number of winter days in the Banat Plain analyzed by Mann-Kendall trend tests

Station name	Trend equation	Min.	Max.	Mean	Std. deviation	Kendall's tau	p-value	Sen's slope
Timişoara	y=-0.1358x+22.609	2	44	18.467	8.771	-0.141	0.117	-0.104
Caransebeş	y=-0.1533x+23.527	2	40	18.850	8.038	-0.235	0.009	-0.157
Arad	y=-0.1404x+25.383	2	49	21.100	9.628	-0.113	0.206	-0.108
Szeged	y=-0.1721x+27.667	2	57	22.417	10.187	-0.187	0.037	-0.158
Zrenjanin	y=-0.1730x+24.605	5	48	19.291	8.954	-0.233	0.013	-0.174
Kikinda	y=-0.1814x+26.264	4	53	20.691	9.739	-0.229	0.015	-0.163
Vršac	y=-0.1461x+21.072	2	39	16.582	8.078	-0.189	0.045	-0.125
average Banat Plain	y=-0.1589x+24.575	3	47.143	19.728	8.731	-0.186	0.036	-0.138

Winter days may occur in the Banat Plain from November until March. In November, the average number of winter days for the Banat Plain ranges from 0 days in most years to 4 – 5 days in 1978, 1988, and 1993, the average for the whole range being 0.6 winter days/month. The trend is slightly downward, with low values in the first and last two decades analyzed and higher values in the 8th - 10th decades, with a maximum of 1.2 days in the last decade of the 20th century and a minimum of 0.1 days in the first decade of the 21st century (*Fig. 5*). The Mann-Kendal trend test does not confirm the existence of a trend (*Table 5*). In December, we have a maximum number of winter days in the 1960s, 8.1, followed by a decrease in the number of days in the 1970s, when, although the absolute maximum of 16.4 days is reached in 1977, the average for the whole decade is 4.9 days, thenit is followed by an increase to 7 days/month in the first decade of the 21st century, and again a decrease to 3.3 days in the last decade. The average of this parameter for the whole interval is 5.8 winter days/month, with a downward trend. The minimum of 0.14 days/month is reached in 1979, 1985, and 2020, years in which only one winter day was recorded at one of the stations analyzed (in 1979 at Caransebeș, in 1985 and 2020 at Szeged) (*Fig. 5*). The Mann-Kendal trend test does not confirm the existence of a trend (*Table 5*).

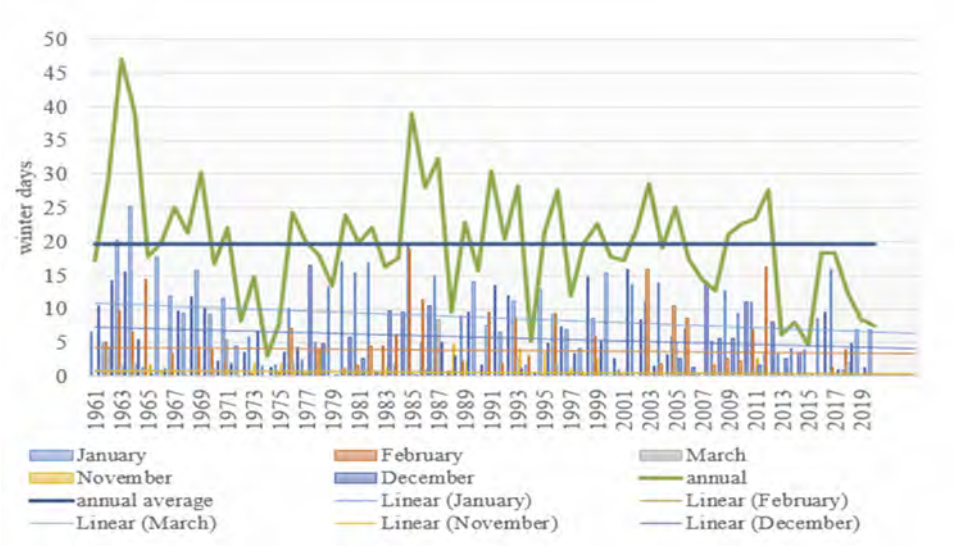

Fig. 5. Evolution of the monthly number of winter days in the Banat Plain.

Table 5. Evolution of the monthly number of winter days in the Banat Plain analyzed by Mann-Kendall trend tests

Month	Trend equation	Min.	Max.	Mean	Std. deviation	Kendall's tau	p-value	Sen's slope
January	y=-0.0717x+10.913	0.429	25.286	8.724	5.808	-0.129	0.146	-0.064
February	y=-0.0172x+4.309	0	18.857	3.866	4.659	-0.094	0.297	-0.011
March	y=-0.0129x+1.0583	0	8.500	0.665	1.587	-0.123	0.221	0
November	y=-0.0066x+0.8288	0	4.750	0.627	1.165	-0.089	0.363	0
December	y=-0.0505x+7.3853	0.143	16.429	5.846	4.746	-0.124	0.164	-0.039

In January, the month with the most winter days, the evolution over the last 6 decades is very similar to the annual evolution of this parameter, with the most winter days recorded in the first decade of observation, 12.2 days, and the fewest in the last, 6.6 days, with the absolute maximum in 1964 and the absolute minimum in 1983 and 2007. Although the graph shows a downward trend, the Mann-Kendal trend test does not confirm the existence of a trend (*Table 5*). In February, this parameter oscillates between above-average values in decades 9, 7, 1, and 10 and below-average values in decades 8 and 2, with the maximum number of winter days in the 1980s, 5.4 days, and the fewest in the 1970s, 1.6,

with the absolute maximum reached in 1985 and the absolute minimum of 0 days reached in 10 of the 60 years (*Fig. 5*). The Mann-Kendal trend test does not confirm the existence of a trend (*Table 5*). In March, although there were no winter days in most years, the average for the whole interval is 0.7 days/month, with a predominance in the first half of the interval, a maximum of 1 day/month in the 1980s and a minimum of 0.3 days/month in the last decade, an absolute maximum in March 1987, and a downward trend (*Fig. 5*). The Mann-Kendal trend test does not confirm the existence of a trend (*Table 5*).

A representation of the two climatic parameters, tropical days (Td) and winter days (Wd), on the same graph (*Fig. 6*) can lead us to a few intermediate conclusions on the evolution of climate risks over the last 6 decades in the Banat Plain:

The decrease in the sum and consequently in the average (Td+Wd and (Td+Wd)/2) in the 1970s compared to the 1960s and then the steady increase of these two indicators until today shows a decrease in extreme temperature risk in the 1970s, a decade that has been the safest in terms of extreme temperature risk for the past 60 years, and then a steady increase until today, with the last decade being the most exposed to extreme temperature risk, with a total of 62.2 days/year, compared to 32.4 days/year in the 1970s; the absolute minimum of 18 days/year in total was in 1975 and the absolute maximum of 100 days was in 2012. The Mann-Kendal trend test confirms the existence of an increasing trend (*Table 6*).

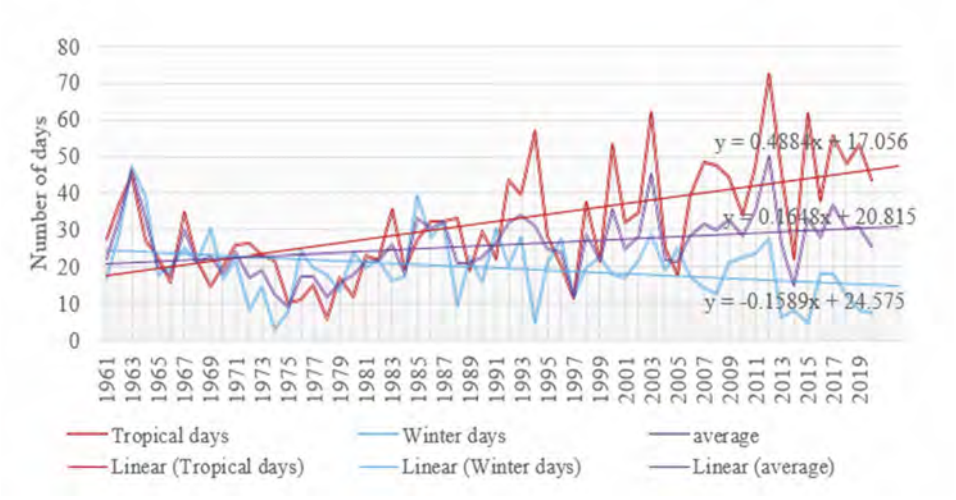

Fig. 6. Evolution of the annual number of tropical and winter days in the Banat Plain.

Table 6. Evolution of the annual number of tropical and winter days in the Banat Plain analyzed by Mann-Kendall trend tests

Parameter	Min.	Max.	Mean	Std. deviation	Kendall's tau	p-value	Sen's slope
Tropical days Td	5.714	72.286	31.953	14.723	0.376	<0.0001	0.479
Winter days Wd	3	47.143	19.728	8.731	-0.186	0.036	-0.138
average (Td+Wd)/2	9	50	25.840	8.282	0.273	0.002	0.185
sum Td+Wd	18	100	51.681	16.564	0.273	0.002	0.370
diference Td-Wd	-15.429	57	12.225	17.653	0.433	<0.0001	0.617

The increase in the average difference between the number of tropical days and the number of winter days (Td-Wd), from 0.3 days/year in the 1960s to 35.2 days/year in the last decade, and the decrease in the number of years with negative values of this parameter, from 3 to 4 years/decade in the last century to only one year in the last two decades, indicate a pronounced increase in the risk of high temperatures compared to the risk of low temperatures. The Mann-Kendal trend test also confirms the existence of an increasing trend (*Table 6*).

3.3. Tropical nights

The average number of tropical nights (Tn) for the Banat Plain over the last six decades has been 4.4 days/year, higher in Vršac and Zrenjanin and lower in Kikinda, Timişoara, Arad, Caransebeş and Szeged; the weather station of Vršac stands out in particular, with values well above the annual average of the Banat Plain in all 60 years, values below the multiannual average being recorded only in 5 years, in the first half of the interval (*Fig. 7*). An evolution over time of this indicator at the level of the entire Banat Plain shows values below average in 27 of the 30 years in the first half of the interval, the only years in which more than 4.4 tropical nights/year were recorded are 1963, 1987, and 1988, and values are shown above average in 24 of the 30 years in the second half of the interval; the highest value was recorded in 2015, 16.4 tropical nights on average for the Banat Plain. Also, if we relate these values to decades, we observe a decrease in the number of tropical nights in the 70s, compared to the 60s, then there is a constant increase until today, when, in the last decade, 8.4 tropical nights/year were recorded. The trend, clearly increasing, shows different values for the analyzed stations, being more accentuated in Zrenjanin and Vršac and less accentuated in Szeged and Caransebeș. The Mann-Kendal trend test confirms the general growth trend of this parameter, both at the level of the Banat Plain and at the level of each analyzed meteorological station (*Table 7*).

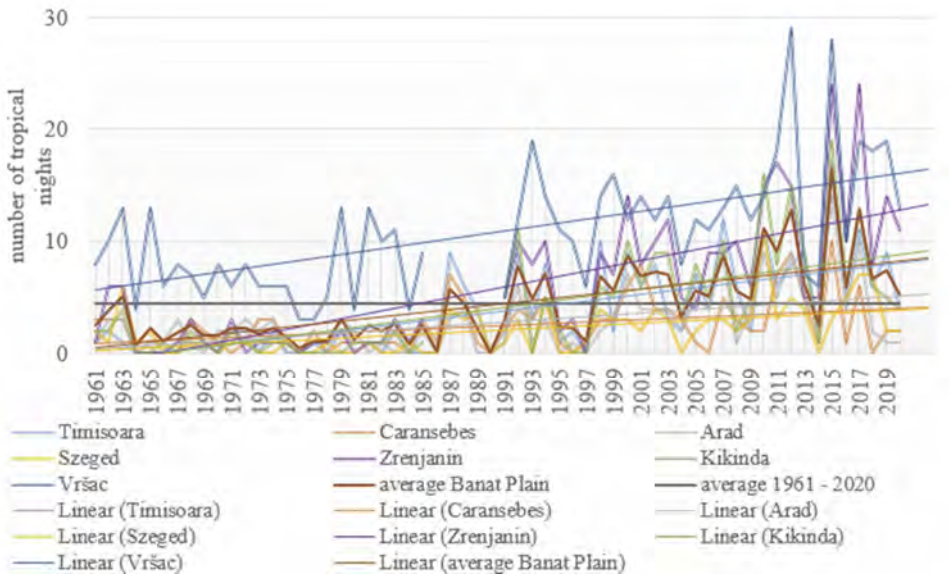

Fig. 7. Evolution of the annual number of tropical nights at the analyzed meteorological stations.

Table 7. Evolution of the annual number of tropical nights in the Banat Plain analyzed by Mann-Kendall trend tests

Station name	Trend equation	Min.	Max.	Mean	Std. deviation	Kendall's tau	p-value	Sen's slope
Timişoara	y=0.1492x-0.8508	0	17	3.700	3.959	0.491	<0.0001	0.114
Caransebeş	y=0.0531x+0.8814	0	10	2.500	2.397	0.257	0.0060	0.034
Arad	y=0.0817x+0.2910	0	14	2.783	2.865	0.338	0	0.055
Szeged	y=0.0621x+0.1384	0	11	2.033	2.224	0.344	0	0.048
Zrenjanin	y=0.2368x-1.3475	0	24	5.927	5.912	0.576	<0.0001	0.200
Kikinda	y=0.1638x-0.9228	0	19	4.109	4.609	0.454	<0.0001	0.121
Vršac	y=0.1767x+5.4784	3	29	10.909	5.545	0.398	<0.0001	0.160
average Banat Plain	y=0.1329x+0.3533	0	16.429	4.408	3.441	0.469	<0.0001	0.109

Although, theoretically, tropical nights can occur in the Banat Plain from April onwards, in the last 60 years they have been accidental, with only 2 cases recorded, both in Vršac, in 1975 and 2018. In May, the average number of tropical nights of the last 6 decades for the entire Banat Plain was 0.13 days per month, 84% of the cases being recorded in Vršac, 9% in Caransebeş, 5% in Zrenjanin and

one case in Timișoara, with higher values in the 7th and 10th decades of the 20th century and the 1st decade of the 21st century and lower values in the 8th and 9th decades of the last century, as well as in the last decade. In 29 years there were no tropical days recorded at all in the Banat Plain in May, while the maximum number of tropical nights, 6 cases/7 stations, was recorded in 1968. The Mann-Kendal trend test does not confirm the existence of a trend in these two months (*Table 8*).

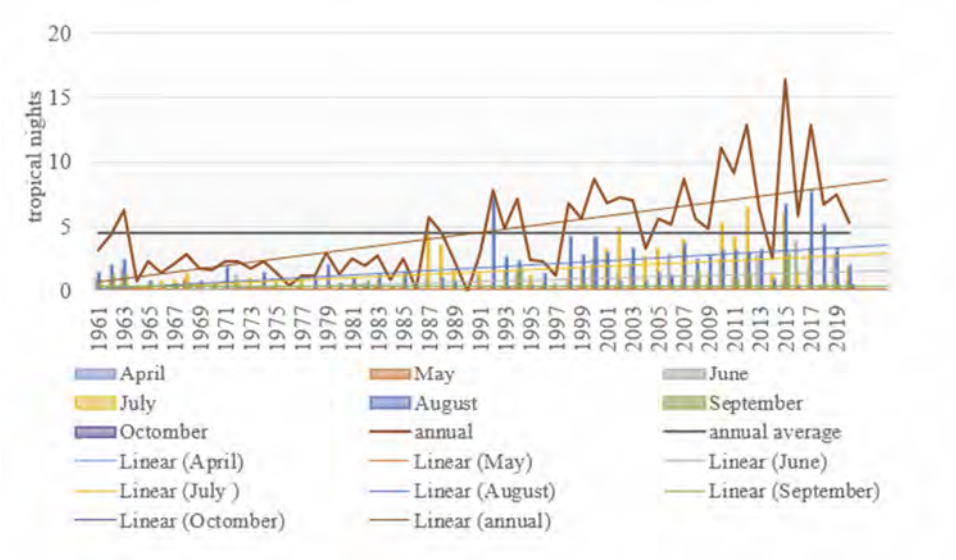

Fig. 8. Evolution of the monthly number of tropical nights in the Banat Plain.

Table 8. Evolution of the monthly number of tropical nights in the Banat Plain analyzed by Mann-Kendall trend tests

Month	Trend equation	Min.	Max.	Mean	Std. deviation	Kendall's tau	p-value	Sen's slope
April	y=0.0001x+0.0019	0	0.143	0.005	0.026	0.053	0.621	0
May	y=-0.0005x+0.1488	0	0.857	0.133	0.174	0.025	0.804	0
June	y=0.0258x-0.0493	0	3.857	0.738	0.880	0.356	0	0.015
July	y=0.0456x+0.0683	0	6.429	1.460	1.591	0.369	<0.0001	0.029
August	y=0.0550x+0.06410	0	7.714	1.740	1.794	0.377	<0.0001	0.042
September	y=0.0016x+0.3165	0	2.857	0.365	0.528	-0.100	0.290	0
October	y=0.0006x-0.00008	0	0.429	0.019	0.072	0.057	0.593	0

The number of tropical nights in June, continuously increasing since the 1980s, went from 0.2 nights/month in the 8th-9th decades to 1.6 nights/month in the last decade, the average over the last 6 decades was 0.7 nights/month; the maximum was recorded in 2016, 3.86 nights/month, while 0 cases were recorded 10 times. For July, the average of 1.5 tropical nights/month is exceeded for the first time in 1987 growing steadily since 1998, reaching 2.7 tropical nights/month in the first decade of the 21st century, with a slight decrease in the second decade; 0 days were recorded in four years, and the maximum occurred in 2012. August has the maximum number of tropical nights per month, an average of 1.7, with lower and decreasing values in the first 3 decades, a minimum in the 1980s, when the number of tropical nights is higher (double) in July, there is a pronounced increase in the 1990s, when the number of tropical nights in August is double compared to July, a further decrease and predominance of tropical nights in July occur for the first decade of the current century and an increase in the last decade. The Mann-Kendal trend test confirms the existence of an upward trend in these three months (*Fig. 8, Table 8*).

In September, we have an average of 0.36 tropical nights/month, with the highest values occurring in the first and last of the 6 decades observed, and the lowest in the 1970s and 1980s, September being the only month in which the trend of this parameter is not increasing; the high number of tropical nights in the last decade is mainly due to the high number of tropical nights recorded in 2015, 7 in Vršac, 6 in Zrenjanin, 4 in Caransebeş, and 1 in Timişoara, Arad, and Kikinda. For the month of October, it is more unusual to record tropical nights, in the last 60 years there have been 8 cases in 5 years, 7 cases in Vršac and one in Zrenjanin, with a peak in 2020, when there were two cases in Vršac and one in Zrenjanin. The Mann-Kendal trend test does not confirm the existence of a trend in these two months (*Table 8*).

3.4. Frosty nights

The average number of frosty nights (Fn) over the last six decades for the Banat Plain has been 9 nights/year, higher in Arad, Szeged, or Vršac and lower in Timişoara, Kikinda, Caransebeș, and Zrenjanin. The time evolution graph (*Fig. 9*) shows an alternation of periods with a high number of frosty nights with periods in which the number of frosty nights is much below average, with a maximum in the 1960s, when the average number at the Banat Plain level was 14 nights/year, followed by a decrease to 7.3 nights/year in the 1970s and again an increase to 10.7 nights/year in the 1980s. In the last 3 decades, although this alternation continues, the annual average of frosty nights is lower than the average for the last 6 decades, the trend of evolution of this parameter being visibly decreasing; in the last decade there was an average of 5.2 frosty nights/year in the Banat Plain. Minimum annual values of this parameter were recorded in 1974, when only Vršac recorded one frosty night, and 2007, when Szeged recorded one frosty night, the average on the Banat Plain in both cases was 0.14, while maximum annual values were in 1985, with 31.9 frosty nights and 1963, with 30.1. The Mann-Kendal trend test confirms the general

decreasing trend of this parameter, both at the level of the Banat Plain and at the level of each analyzed meteorological station (*Table 9*).

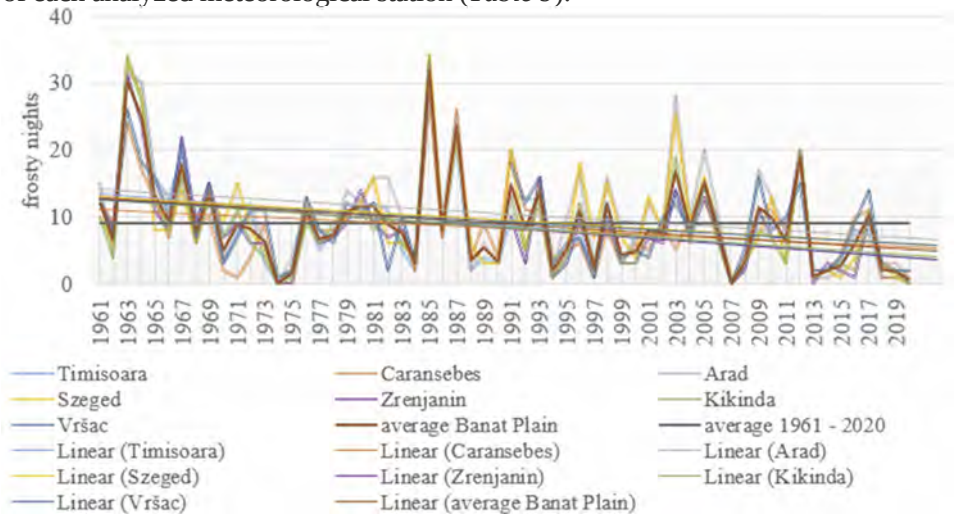

Fig. 9. Evolution of the annual number of frosty nights at the analyzed meteorological stations.

Table 9. Evolution of the annual number of frosty nights in the Banat Plain analyzed by Mann-Kendall trend tests

Station name	Trend equation	Min.	Max.	Mean	Std. deviation	Kendall's tau	p-value	Sen's slope
Timişoara	y=-0.1612x+13.584	0	32	8.667	7.201	-0.293	0.001	-0.125
Caransebeş	y=-0.0957x+11.269	0	28	8.350	6.257	-0.191	0.035	-0.098
Arad	y=-0.1232x+14.275	0	32	10.517	7.769	-0.197	0.029	-0.106
Szeged	y=-0.1193x+13.072	0	34	9.433	7.758	-0.220	0.015	-0.111
Zrenjanin	y=-0.1519x+13.013	0	33	8.345	7.170	-0.293	0.002	-0.13
Kikinda	y=-0.1375x+12.644	0	34	8.418	7.440	-0.275	0.004	-0.114
Vršac	y=-0.1133x+12.737	0	32	9.255	6.513	-0.221	0.020	-0.100
average Banat Plain	y=-0.1294x+12.948	0.143	31.857	9.001	6.813	-0.236	0.008	-0.118

Frosty nights can be expected in the Banat Plain from November until March. In November, the average number of days with frosty nights for the Banat Plain ranges from 0 days in the majority of years to 2.6 days in 1983, the average for the whole period is 0.2 frosty nights/month. The trend is slightly downward,

most of the frosty nights were recorded in the first half of the interval, then three years with frosty nights in the interval 1993–1995, and there is only one record for the last 2 decades, in 2005, in Arad. In December, we have an average of 2 days with frosty nights/month, highlighting the period between 1998–2002, when the absolute maximum is recorded, 10.8 frosty nights/month in 1998, followed by the years 2003–2008 and 2013–2020, with values well below average, reaching 0 frosty nights/month in 2003, 2004, 2013, 2017, 2019 and 2020, the latter determining the downward trend of the entire interval. The Mann-Kendal trend test confirms the existence of a trend only for November, but with a zero slope (*Fig. 10, Table 10*).

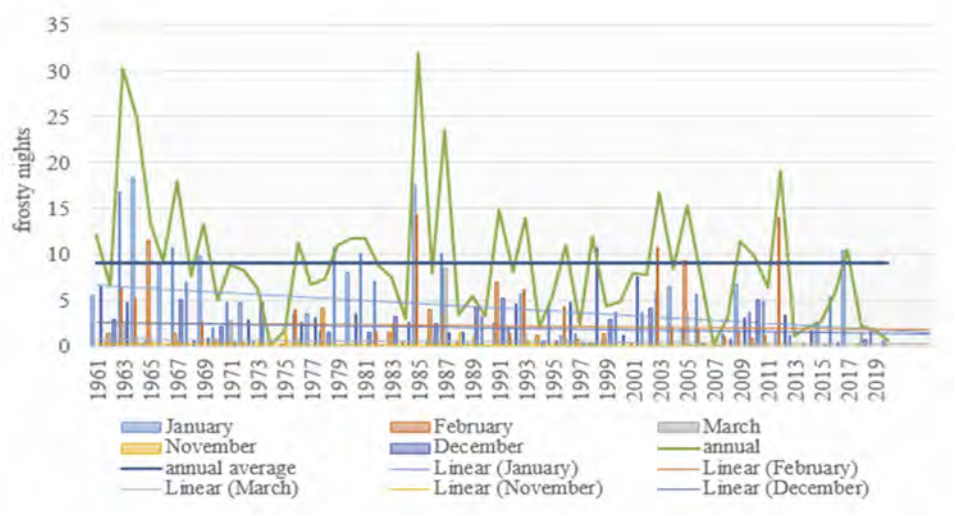

Fig. 10. Evolution of the monthly number of frosty nights in the Banat Plain.

Table 10. Evolution of the monthly number of frosty nights in the Banat Plain analyzed by Mann-Kendall trend tests

Month	Trend equation	Min.	Max.	Mean	Std. deviation	Kendall's tau	p-value	Sen's slope
January	y=-0.0827x+6.7469	0	18.286	4.226	4.498	-0.158	0.077	-0.044
February	y=-0.0129x+2.5658	0	14.286	2.174	3.495	-0.105	0.255	0
March	y=-0.0081x+0.7076	0	8.500	0.461	1.275	-0.163	0.100	0
November	y=-0.0055x+0.3400	0	2.571	0.173	0.444	-0.237	0.020	0

December	y=-0.0203x+2.5877	0	10.714	1.967	2.278	-0.155	0.089	-0.012

In January, the month with the most frosty nights, the evolution over the last 6 decades is similar to the annual evolution of this parameter, with the most frosty nights recorded in the first decade of observation, 8, except that the fewest frosty nights, 2.2, were recorded in the 1990s; the absolute maximum was in 1964 and the absolute minimum in 1975, 1983, 1984, 1988, 2001, 2007, and 2011, with 0 days. The strongly decreasing trend visible on the graph is not confirmed by the Mann-Kendal trend test (*Fig. 10, Table 10*).

In February, this parameter oscillates between values above the average of 2.2 frosty nights in the 7th, 1st, and 9th decades, 2.2 frosty nights in the 10th decade and values below this average in the 8th and 2nd decades, with the highest number of frosty nights in the 1960s, 3 nights on average, and the fewest in the 1970s, 0. 9, with the absolute maximum reached in 1985, 14.3 frosty nights, and the absolute minimum of 0 frosty nights reached in 20 of these 60 years. The trend, which is not very downward, leads to December being overtaken by February for this parameter, although in the first half of the period analyzed, the situation was the opposite. In March, although in most years there were no frosty nights, the average for the whole interval is 0.5 days/month, with 1987 standing out with 8.5 frosty nights and with a downward trend. The Mann-Kendal trend test does not confirm the existence of a trend in these two months (*Table 10*).

Combining again two opposite parameters, tropical nights (Tn) and frosty nights (Fn), on the same graph (*Fig. 11*), we can find some intermediate conclusions about the evolution of climate risks in the last 6 decades in the Banat Plain:

The sharp decrease in the sum and mean (Tn+Fn and (Tn+Fn)/2) from maximum values in the 1960s to minimum values in the 1970s, then a slow increase until a decade ago, and again a decrease in the last decade are mainly due to the evolution of the number of cold nights. The decrease in the last decade was unable to be compensated by the increase in the number of tropical nights. Again, the 1970s can be considered the safest in terms of extreme temperature risk for the past 60 years, with an average Tn+Fn sum of 9 days/year and a minimum sum of 2.4 days in 1974. The 1960s were the most exposed to extreme temperature risk with an average Tn+Fn sum of 16.3 days/year and a maximum of 35.3 days in 1963 (*Fig. 11, Table 11*). The Mann-Kendal trend test does not confirm the existence of a trend for any of the two parameters (*Table 11*).

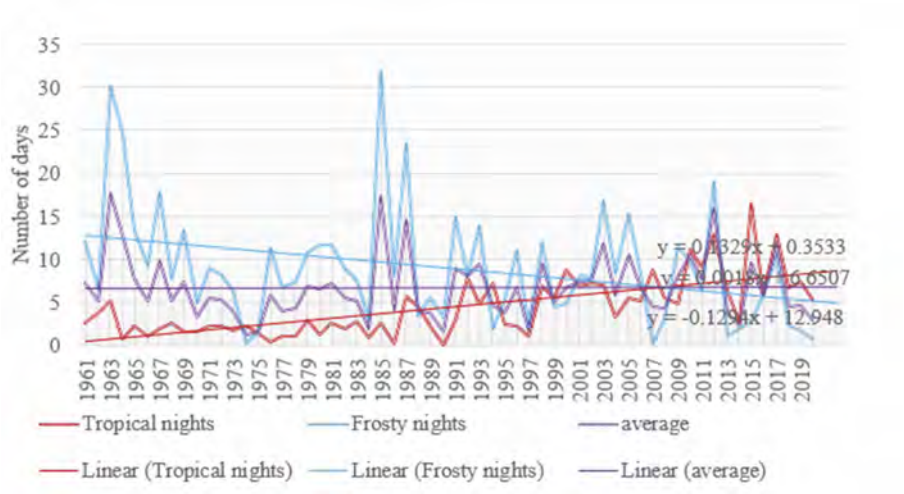

Fig. 11. Evolution of the annual number of tropical and frosty nights in the Banat Plain.

Table 11. Evolution of the annual number of tropical and frosty nights in the Banat Plain analyzed by Mann-Kendall trend tests

Parameter	Min.	Max.	Mean	Std. deviation	Kendall's tau	p-value	Sen's slope
Tropical nights Tn	0	16.429	4.408	3.441	0.469	<0.0001	0.109
Frosty nights Fn	0.143	31.857	9.001	6.813	-0.236	0.008	-0.118
average (Tn+Fn)/2	1.214	17.643	6.704	3.725	0.019	0.833	0.008
sum Tn+Fn	2.429	35.286	13.408	7.450	0.019	0.833	0.017
diference Tn-Fn	-29.286	13.714	-4.593	7.811	0.440	<0.0001	0.238

The difference between the two parameters (Tn-Fn) also decreases very quickly in the 1970s (-5.6 nights/year) compared to the 1960s (-11.6 nights/year), increases in the 1980s due to the increase in the number of frosty nights, then decreases again until today, when it reaches positive values (3.3 nights/year); the minimum of -29.3 is recorded in 1985, and the maximum of 13.7 in 2015. It is also worth mentioning that while in the first half of the period, this parameter had positive values only in two years, 1974 and 1988, in the last decade only one negative value was recorded, in 2012. The Mann-Kendal trend test also confirms the existence of an increasing trend (*Table 11*).

3.5. Absolute maximum temperature

The absolute maximum temperature measured in the Banat Plain for the period 1961–2020 was 42.9 °C, recorded on July 24, 2007 in Zrenjanin, at the same date as the absolute maximums measured were for Vršac, 42.2 °C, Timișoara, 41.1 °C, Caransebeș, 40.3 °C, and Kikinda, 40 °C, after the absolute maximum temperature of 39.8 °C had been recorded two days earlier for Szeged; in Arad, the absolute maximum of 40.8 °C was recorded on July 23, 2017. From the data available to us, we can state that 2007 and 2017 were the only years out of the last 60 in which temperatures above 40 °C were recorded, with the average annual maximum for the Banat Plain exceeding 40 °C in 2007; annual maximums above 39 °C were also recorded in 2000, 2012, 1988, and 1961. As for the lower values of the annual maximums in the Banat Plain, it can be seen that an annual maximum below 35 °C has not been recorded since 1997, while such values were recorded quite frequently in the 7th–8th decades. The trends in the evolution of maximum temperatures are positive, the graph shows a more marked increase for the weather station of Szeged, the only station where the absolute maximum for the last 60 years does not reach 40 °C, and a more moderate increase for Timișoara, the station with the highest average annual maximum, and for Caransebeș, the station with the lowest average annual maximum. The Mann-Kendal trend test confirms the existence of an increasing trend for all weather stations except Caransebeș (*Fig. 12, Table 12*).

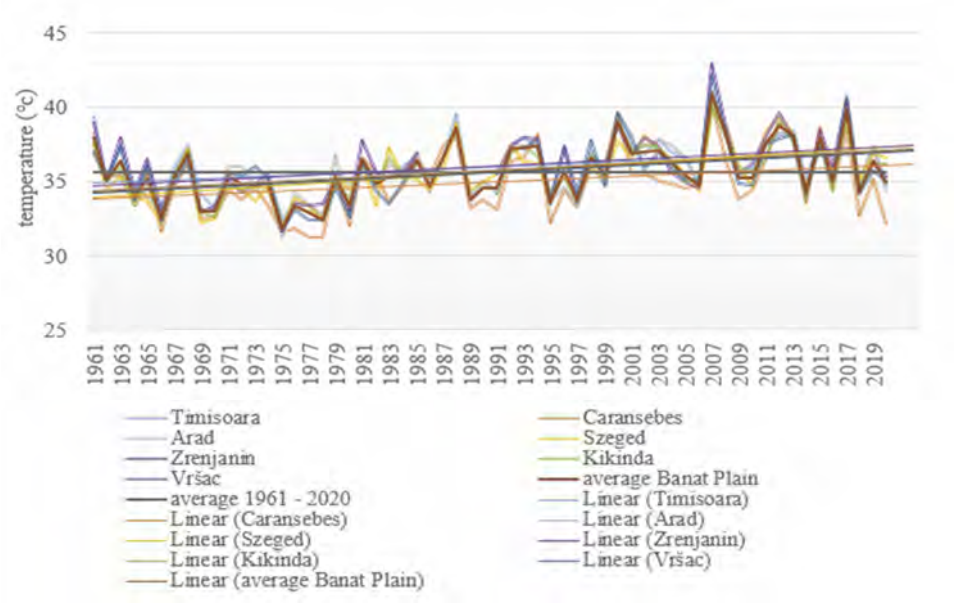

Fig. 12. Evolution of the annual maximum temperatures at the analyzed meteorological stations.

Table 12. Evolution of the annual maximum temperatures in the Banat Plain analyzed by Mann-Kendall trend tests

Station name	Trend equation	Min.	Max.	Mean	Std. deviation	Kendall's tau	p-value	Sen's slope
Timișoara	y=0.0372x+34.862	32.4	41.1	35.997	1.908	0.227	0.011	0.040
Caransebeș	y=0.0375x+33.812	31.2	40.3	34.957	2.165	0.166	0.062	0.031
Arad	y=0.0467x+34.345	31.2	40.8	35.768	2.004	0.272	0.002	0.047
Szeged	y=0.0587x+33.798	31.7	39.8	35.588	1.912	0.375	<0.0001	0.058
Zrenjanin	y=0.0457x+34.593	31.6	42.9	35.996	2.152	0.265	0.005	0.042
Kikinda	y=0.0483x+34.099	32.1	40.0	35.584	1.859	0.308	0.001	0.050
Vršac	y=0.0465x+34.188	31.7	42.2	35.617	2.149	0.229	0.015	0.042

3.6. Absolute minimum temperature

The absolute minimum temperature measured in the Banat Plain for the period 1961–2020 was -35.3 °C recorded on January 24, 1963 in Timișoara. On the same day being recorded the absolute minimums were -32.6 °C, for Vršac, -30.4 °C in Zrenjanin, -29.8 °C in Kikinda, and -29.8 °C Arad, while the next day was recorded the absolute minimum for Caransebeș, -26.8 °C; in Szeged the absolute minimum of -27.8 °C was recorded on January 31, 1987. From the data available to us, we can state that 1963 was the only year in the last 60 in which temperatures below -30 °C were recorded and the only year when the average annual minimum for the Banat Plain reached -30 °C; annual average minimum below -25 °C was also recorded in 1987. The only years when average lows did not fall below -10 °C were 1974, 2007, and 2020. The evolution trends of minimum temperatures are positive, the graph showing a more pronounced increase for the weather stations of Timișoara and Vršac, the latter being the station with the lowest average annual minimum, but the Mann-Kendal trend test does not confirm the existence of any trend for any of the studied weather stations (*Fig. 13, Table 13*).

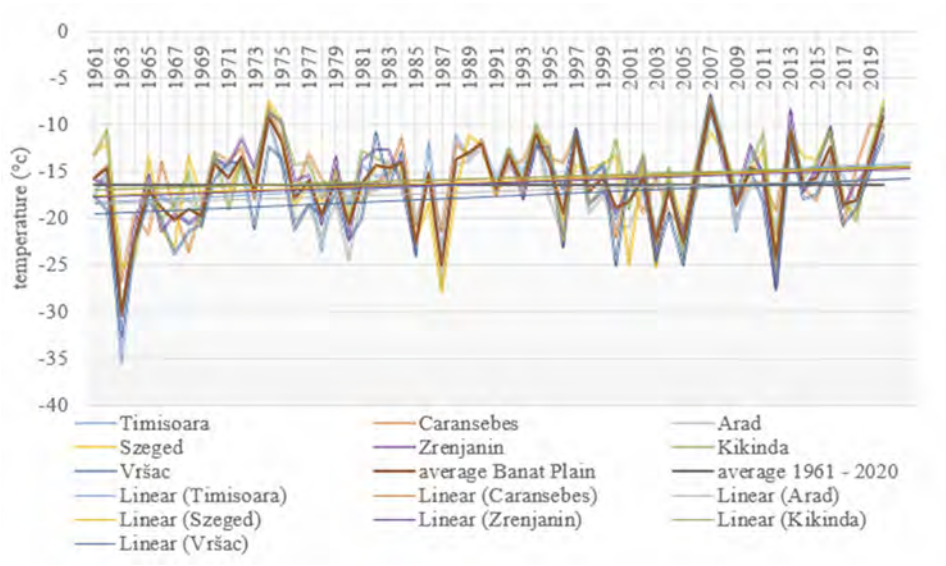

Fig. 13. Evolution of the annual minimum temperatures at the analyzed meteorological stations.

Table 13. Evolution of the annual minimum temperatures in the Banat Plain analyzed by Mann-Kendall trend tests

Station name	Trend equation	Min.	Max.	Mean	Std. deviation	Kendall's tau	p-value	Sen's slope
Timişoara	y=0.0696x-18.357	-35.3	-6.7	-16.233	4.555	0.132	0.139	0.048
Caransebeş	y=0.0384x-16.995	-26.8	-7.7	-15.823	3.865	0.095	0.284	0.034
Arad	y=0.0445x-18.523	-29.8	-7.7	-17.165	4.383	0.103	0.248	0.035
Szeged	y=0.0485x-17.569	-27.8	-7.5	-16.090	4.515	0.146	0.101	0.053
Zrenjanin	y=0.0488x-17.714	-30.4	-6.9	-16.215	4.780	0.124	0.182	0.054
Kikinda	y=0.0430x-17.041	-29.8	-7.2	-15.720	4.697	0.118	0.206	0.047
Vršac	y=0.0617x-19.638	-32.6	-8.6	-17.743	4.682	0.165	0.078	0.064

The monthly absolute maximum (*Fig. 14*) and minimum (*Fig. 15*) temperatures show an upward trend, with more pronounced increases in general in the winter and summer months and more moderate in the spring and autumn months. These trends are generally in line with the general evolution of temperatures in the Banat Plain. The Mann-Kendal trend test confirms the existence of an increasing trend for monthly maximum temperatures in February, June, July, August, and December, as well as for monthly minimum temperatures in July, August, September, and December (*Table 14*).

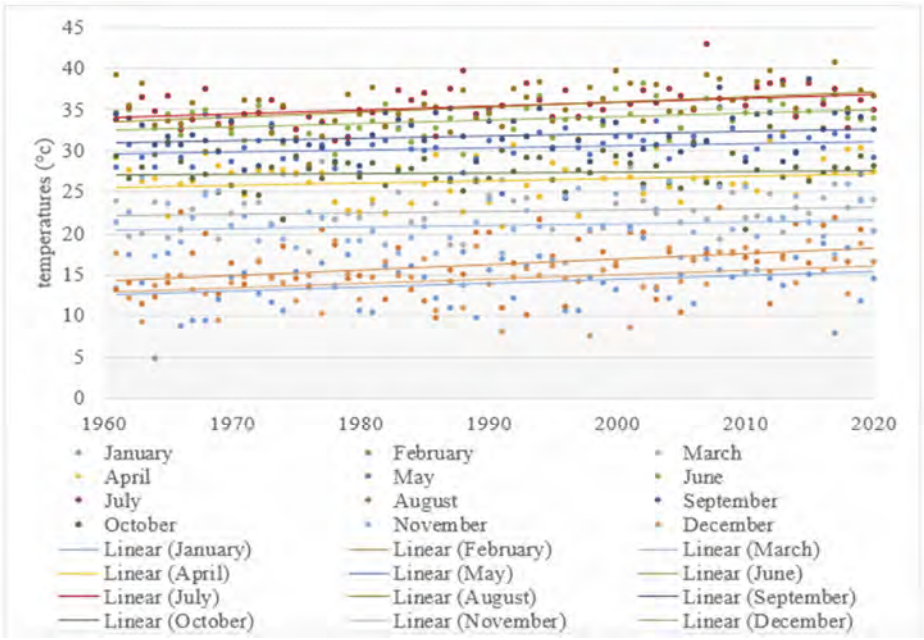

Fig. 14. Evolution of the monthly absolute maximum temperatures in the Banat Plain.

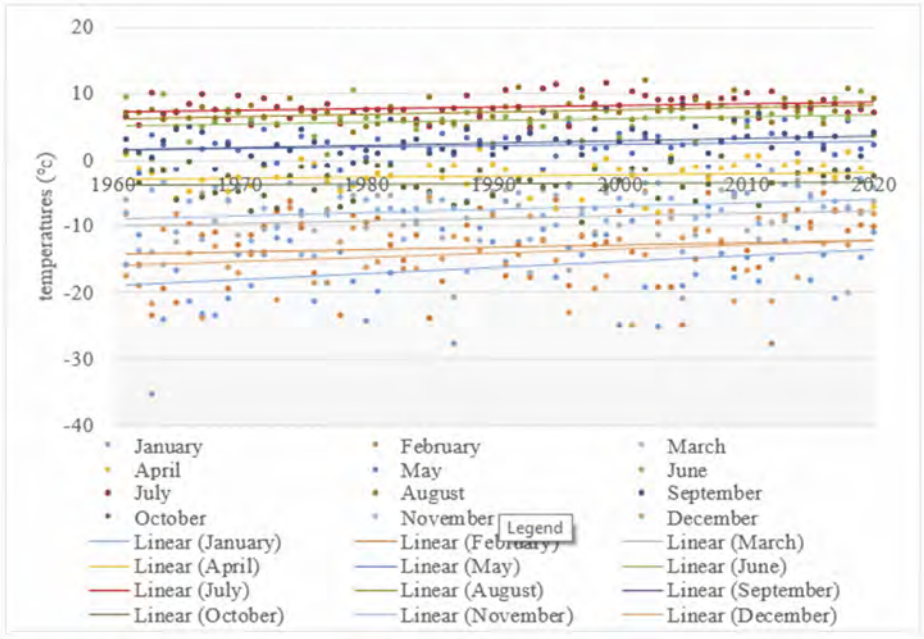

Fig. 15. Evolution of the monthly absolute minimum temperatures in the Banat Plain.

Table 14. Evolution of the monthly absolute maximum and minimum temperatures in the Banat Plain analyzed by Mann-Kendall trend tests

Month	Max/ min	Trend equation	Min	Max	Mean	Std. deviation	Kendall's tau	p-value	Sen's slope
January	max	y=0.0467x-78.985	4.8	20.7	13.99	3.093	0.163	0.068	0.050
	min	y=0.0878x-190.87	-35.3	-6.6	-16.19	5.754	0.151	0.09	0.084
February	max	y=0.0653x-113.66	9.6	23.1	16.28	3.52	0.227	0.011	0.072
	min	y=0.0376x-88.079	-27.7	-4.9	-13.19	5.593	0.083	0.352	0.039
March	max	y=0.0166x-10.435	16.2	28.6	22.68	2.544	0.103	0.246	0.021
	min	y=0.0377x-84.005	-21.0	-2.3	-8.92	4.540	0.155	0.082	0.052
April	max	y=0.0279x-29.044	20.7	32.2	26.44	2.551	0.087	0.329	0.024
	min	y=0.0188x-40.015	-8.1	1.6	-2.58	2.274	0.143	0.109	0.030
May	max	y=0.0239x-17.281	24.8	35.2	30.36	2.028	0.165	0.065	0.028
	min	y=0.0201x-37.801	-2.3	6.0	2.22	2.025	0.112	0.209	0.016
June	max	y=0.0413x-48.564	28.6	38.1	33.70	2.048	0.247	0.006	0.042
	min	y=0.0258x-45.413	0	10.5	6.03	2.163	0.130	0.146	0.019
July	max	y=0.0481x-60.311	31.1	42.9	35.53	2.173	0.281	0.002	0.047
	min	y=0.0262x-44.177	4.6	11.5	8.00	1.661	0.182	0.042	0.027
August	max	y=0.0620x-87.977	28.3	40.8	35.35	2.605	0.292	0.001	0.065
	min	y=0.0340x-60.398	4.3	11.8	7.22	1.610	0.252	0.005	0.033
September	max	y=0.0268x-21.450	24.1	38.6	31.8	2.541	0.098	0.272	0.02
	min	y=0.0366x-70.220	-4.2	8.5	2.59	2.364	0.176	0.048	0.038
October	max	y=0.0075x+12.482	20.4	32.8	27.36	2.058	0.039	0.664	0.006
	min	y=0.0059x-15.568	-9.5	1.2	-3.74	2.314	0.059	0.511	0.013
November	max	y=0.0189x-16.652	13.4	26.8	20.99	3.007	0.069	0.436	0.018
	min	y=0.0496x-106.29	-17.0	-1.8	-7.55	3.353	0.158	0.075	0.047
December	max	y=0.0534x-91.853	7.5	19.1	14.50	2.769	0.250	0.005	0.059
	min	y=0.0627x-138.72	-24.9	-5.7	-13.99	4.607	0.186	0.036	0.080

The absolute annual thermal amplitudes, for the Banat Plain as well as for the analyzed meteorological stations (*Fig.16*), show important oscillations from one year to another, with values above average especially in the 1960s and 2000s and below average in the 1970s, 1980s, and 1990s, but we cannot speak about the existence of a trend, which is also visible from the Mann-Kendall trend test (*Table 15*).

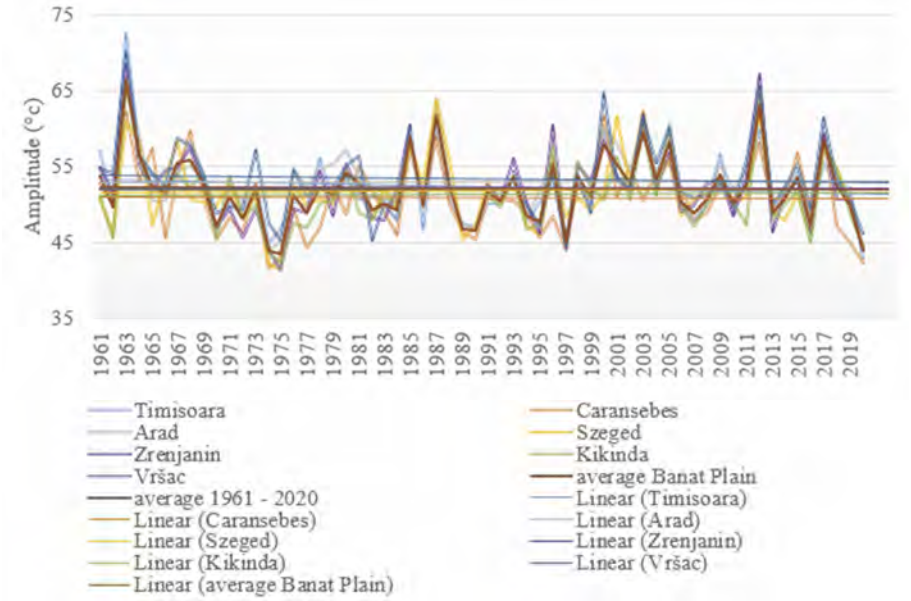

Fig. 16. Evolution of the annual absolute thermal amplitude at the analyzed meteorological stations.

Table 15. Evolution of the annual absolute thermal amplitude in the Banat Plain analyzed by Mann-Kendall trend tests

Station name	Trend equation	Min	Max	Mean	Std. deviation	Kendall's tau	p-value	Sen's slope
Timişoara	y=-0.0324x+53.219	42.9	72.6	52.23	4.851	-0.041	0.646	-0.014
Caransebeş	y=-0.0009x+50.806	41.6	62.2	50.78	4.744	0.004	0.964	0.001
Arad	y=0.0021x+52.868	43.8	65.2	52.933	4.719	0	1	0
Szeged	y=0.0102x+51.368	41.4	63.7	51.678	4.768	0.008	0.929	0.003
Zrenjanin	y=-0.0031x+52.307	41.3	68.4	52.211	5.340	-0.027	0.771	-0.017
Kikinda	y=0.0053x+51.140	42.1	65.8	51.304	4.875	-0.016	0.867	-0.007
Vršac	y=-0.0152x+53.826	44.6	70.0	53.359	5.157	-0.071	0.451	-0.026

Also, the values of the monthly absolute thermal amplitudes oscillate quite a lot from one year to another (*Fig. 17*), the amplitude of the oscillations is greater in the months of January-March and November-December, months for which there is generally a very slight downward trend in these values, a trend that cannot be confirmed by the result of the Mann-Kendall trend test, which does not confirm the existence of a trend for any month (*Table 16*).

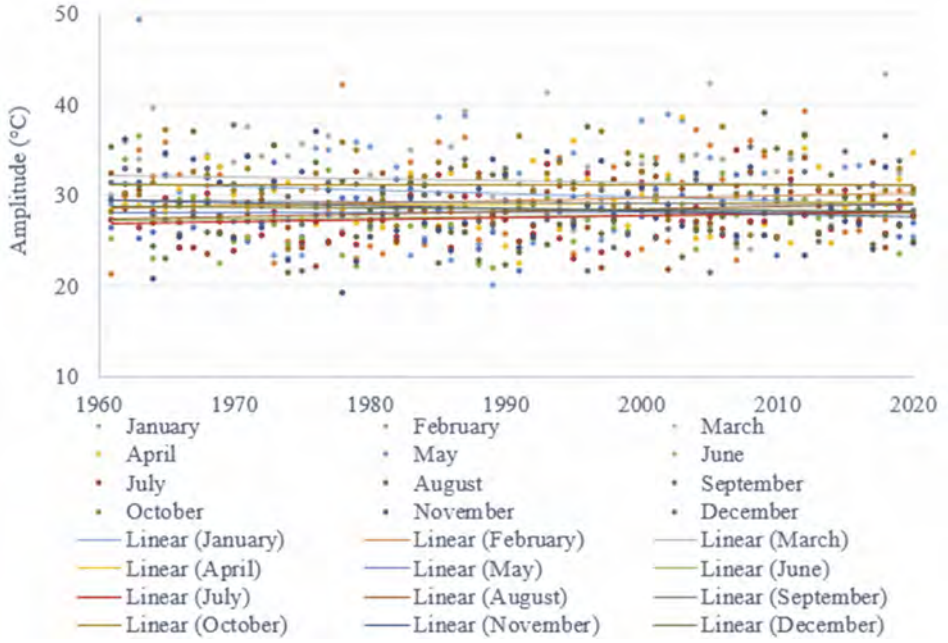

Fig. 17. Evolution of the monthly absolute thermal amplitudes in the Banat Plain.

Table 16. Evolution of the monthly absolute thermal amplitudes in the Banat Plain analyzed by Mann-Kendall trend tests

Month	Trend equation	Min	Max	Mean	Std. deviation	Kendall's tau	p-value	Sen's slope
January	y=-0.0410x+111.890	20.0	49.3	30.190	5.290	-0.053	0.549	-0.025
February	y=0.0277x-25.580	21.3	42.1	29.478	4.593	0.088	0.323	0.033
March	y=-0.0211x+73.570	23.9	43.3	31.603	4.329	-0.076	0.393	-0.028
April	y=0.0091x+10.971	22.4	38.5	29.023	3.202	-0.016	0.853	-0.004
May	y=0.0038x+20.519	21.6	33.7	28.135	2.664	0.064	0.471	0.016
June	y=0.0155x-3.1504	21.9	36.4	27.667	3.112	0.110	0.216	0.029
July	y=0.0219x-16.134	22.9	34.9	27.503	2.633	0.080	0.368	0.018
August	y=0.0280x-27.579	21.7	34.0	28.132	2.920	0.107	0.23	0.027
September	y=-0.0098x+48.770	21.4	37.7	29.213	3.344	-0.044	0.619	-0.012
October	y=0.0015x+28.050	24.0	37.5	31.108	3.144	0.014	0.878	0.004
November	y=-0.0307x+89.635	19.2	37.0	28.548	3.883	-0.096	0.281	-0.034
December	y=-0.0092x+46.869	21.4	39.0	28.507	4.287	-0.042	0.637	-0.015

4. Discussion and conclusion

The comparative analysis of all the parameters used is a good opportunity to find out the trends of the climatic evolution in the Banat Plain in the last six decades.

Tropical days (Td) are on average 32/year in the Banat Plain, the highest value is on average, 36.6 in Timișoara, the lowest is 24.5 in Caransebeș. The number of Td/year decreases in the 1970s compared to the 1960s, then increases steadily until nowadays, the increasing trend being confirmed even by the Mann-Kendall test, for all weather stations. The fewest Td occurred in the 1970s, the most in the 2010s. Of the monthly distribution we see significant increases in August, followed by July and June, increases confirmed also by the Mann-Kendall test.

Winter days (Wd) are on average 19.7/year in the Banat Plain, the highest value is on average, 22.4 in Szeged, the lowest is 16.6 in Vršac. The number of Wd/year decreases in the 1970s compared to the 1960s, then increases in the 1980s and decreases again until today, in the last decade the number of Wd is lower than in the 1970s. The fewest Wd occurred in the 2010s, the most in the 1960s. The Mann-Kendall test confirms the existence of a negative trend for this parameter at the level of the Banat Plain and most of the stations, except for Timișoara and Arad. However, the Mann-Kendall test does not confirm the existence of a trend in the monthly values of this parameter.

If we consider Td and Wd as potential climatic risk phenomena with a lower impact on the population, we can say that, from this point of view, the lowest risk in the Banat Plain was in the 1970s followed by a constant increase of this risk until nowadays, when the sum Td+Wd has the highest values. The increase observed for this parameter (Td+Wd) with a decreasing number of Wd, as well as a constant increase of the Td-Wd difference in the latest decades, which indicates a constant increase of the risk of high temperatures. The level of this increase exceeds the level of the decrease of the risk of low temperatures. The Mann-Kendall test confirms the existence of a positive trend for the two parameters, Td+Wd and Td-Wd.

Tropical nights (Tn) are on average 4.4/year in the Banat Plain, the highest value is on average, 10.9 in Vršac, the lowest is 2/year in Szeged. The number of Tn/year decreases in the 1970s compared to the 1960s, then steadily increases until nowadays, the increasing trend is confirmed also by the Mann-Kendall test for all weather stations. Identical to Td, the fewest Tn occurred in the 1970s, the most in the 2010s. From the monthly distribution we observe significant increases in August, followed by those in July and June. These increases are confirmed also by the Mann-Kendall test.

Frosty nights (Fn) are on average 9/year in the Banat Plain, the highest value is on average, 10.5 in Arad, the lowest is 8.3 in Zrenjanin and Caransebeș. The number of Fn/year decreases in the 1970s compared to the 1960s, then increases in the 1980s, decreases in the 1990s, increases in the 2000s, and decreases again

until today. The fewest Fn occured in the 2010s, the most in the 1960s. The Mann-Kendall test confirms the existence of a negative trend for this parameter both at the Banat Plain level and for all meteorological stations, but does not confirm the existence of a trend in the monthly values of this parameter, only for the month of November, when the slope (Sen's slope) is 0.

Considering Tn and Fn as potential climatic risk phenomena with a medium impact on the population, we can again say that, from this point of view, the lowest risk at the Banat Plain level was in the 1970s, when the sum of Tn+Fn recorded minimum values, followed by an oscillating increase of this risk until nowadays. These oscillations are determined by the oscillation of the number of Fn, the slight increase of this parameter is also determined by the evolution of the number of Fn. The most risk remains in the 7th decade of the 20th century, with values of this parameter that have not been reached since then. Regarding the Tn-Fn difference, this also generally oscillates in line with the Fn number oscillations, the latter is much higher than the Tn in the 1960s, this difference is diminishing over time and finally, in the last decade, the Tn number exceeds the Fn number. The Mann-Kendall test confirms the existence of a positive trend in the difference between Td and Wd, but does not confirm the existence of a trend in the sum of Td+Wd.

Annual absolute maximum temperatures range from values below 35 °C, common in the 1960s and 1970s, to values above 40 °C, recorded in 2007 and 2017. A slight increase can be observed at all weather stations, which is confirmed by the Mann-Kendall test for all stations except Caransebeș. The same test also confirms the positive evolution of monthly absolute maximum temperatures at the Banat Plain level, but only for February, June, July, August, and December.

The absolute annual minimum temperatures are generally between -10 °C and -25 °C at all stations in the Banat Plain, with lows below -25 °C only in 2003, 2012, 1987, and 1963. In 1963 the temperature dropped to -35.3 °C. A slight increase can be observed at all meteorological stations, but this is not confirmed by the Mann-Kendall test at any station. However, the same test confirms the positive evolution of monthly absolute minimum temperatures at the Banat Plain level for July, August, September, and December.

Given that absolute maximum and minimum temperatures should be considered as climate hazards with a rather high impact on human society, we consider that an indicator in this respect could be the difference between them, namely the absolute annual amplitude. This shows the highest values of the last 6 decades in the 1960s and the lowest in the 1970s, continued by a slight increase in the 1980s, a decrease in the 1990s, and again an increase in the last 20 years, but not reaching the level of the 1960s. For this parameter we cannot speak of the existence of a trend, neither for annual nor for monthly amplitudes.

As a final conclusion, we can say that due to the general climatic warming that is also felt in the Banat Plain, the risk of high temperatures increases, while the risk of low temperatures does not decrease to the same extent. As for very high

temperatures, although the risk of their occurrence is increasing, it is somewhat offset by the decrease in the risk of very low temperatures. The most affected decade of the last 6 decades is the 7th decade of the last century, and the least affected is the 8th decade. However, looking at the trends of these parameters over time, we can conclude that in the near future things may change, and we will no longer be able to say that in terms of temperature-related hazards, the situation is better than in the 1960s.

References

Bačević, N. R., Milentijević, N. M., Valjarević, A., Gicić, A., Kićović, D., Radaković, M.G., Nikolić, M., and *Pantelić, M.,* 2021: Spatiotemporal variability of air temperatures in Central Serbia from 1949 to 2018. *Időjárás 125*, 229–253. https://doi.org/10.28974/idojaras.2021.2.4

Bartholy, J. and *Pongrácz, R.*, 2007: Regional analysis of extreme temperature and precipitation indices for the Carpathian Basin from 1946 to 2001. *Glob. Planet. Change 57*, 83–95. https://doi.org/10.1016/j.gloplacha.2006.11.002

Cheval, S., Birsan, M. V., and *Dumitrescu, A.,* 2014: Climate variability in the Carpathian Mountains Region over 1961–2010. *Glob. Planet. Change 118*, 85–96. http://dx.doi.org/10.1016/j.gloplacha.2014.04.005

Dudaş, M. and *Urdea, P.*, 2021: Meteorological hazards in the Banat plain mentioned in ancient and medieval writings. *RHGT 16*(31–32), 61–76.

Gavrilov, M.B., Tosić, I., Marković, S.B., Unkasević, M., and *Petrović, P.*, 2016: The analysis of annual and seasonal temperature trends using Mann Kendall test in Vojvodina, Serbia. *Időjárás 120*, 183–198.

Gocić, M. and *Trajković, S.*, 2012: Analysis of changes in meteorological variables using Mann-Kendall and Sen's slope estimator statistical tests in Serbia, *Glob. Planet Change 100*, 172–182. http://dx.doi.org/10.1016/j.gloplacha.2012.10.014

Hungarian Meteorological Service (Országos Meteorológiai Szolgálat), 2022: Climate – Climate of Hungary – Climate Data Series 1901–2020 – Szeged – Data. https://www.met.hu/ (accessed 8 February 2022).

Ianoş, G., Puşcă, I., and *Goian, M.*, 1997: Solurile Banatului. Condiţii naturale şi fertilitate, Edit. Mirton, Timişoara. (In Romanian)

Janković, A., Podraščanin, Z., and *Djurdjevic, V.*, 2019: Future climate change impacts on residential heating and cooling degree days in Serbia. *Időjárás 123*, 351–370. https://doi.org/10.28974/idojaras.2019.3.6

Lakatos, M., Bihari, Z., Szentimrey, T., Spinoni, J., and *Szalai, S.*, 2016: Analyses of temperature extremes in the Carpathian Region in the period 1961-2010. *Időjárás 120*, 41–51.

Milentijević, N.M., Valjarević, A., Bačević, N.R., Ristić, D., Kalkan, K., Cimbaljević, M., Dragojlović, J., Savić, S., and *Pantelić, M.*, 2022: Assessment of observed and projected climate changes in Bačka (Serbia) using trend analysis and climate modeling. *Időjárás 126*, 47–68. https://doi.org/10.28974/idojaras.2022.1.3

Papić, D., Baćevič, N. R., Valjarević, A., Milentijević, N., Gavrilov, M. B., Živković, M., and *Marković, S. B.*, 2020: Assessment of air temperature trend in South and Southeast Bosnia and Herzegovina from 1961 to 2017. *Időjárás 124*, 381–399. https://doi.org/10.28974/idojaras.2020.3.5

Posea, G., 1997: Câmpia de Vest a României (Câmpia Banato – Crişană), Edit. Fundaţiei România de Mâine, Bucureşti, (In Romanian)

Republic Hydrometeorological Service of Serbia (Republički hidrometeorološki zavod Srbije Srbije RHMZ), 1961–2020: Meteorological Yearbook – Climatological Data. (accessed 26 December 2021). http://www.hidmet.gov.rs/

Réthly, A., 1918: Temesvár régi hőmérsékleti megfigyelései 1780. Szeptember – 1803. December, *Természettudományi Füzetek. A Délmagyarországi Természettudományi Társulat Közlönye 42*, 27–43. (In Hungarian)

Réthly, A., 1970: *Időjárási események és elemi csapások Magyarországon 1701–1800-ig*, Akadémiai Kiadó, Budapest. (In Hungarian)

Timişoara Weather Bureau (Centrul Meteorologic Regional Banat - Crişana), 2022: meteorological data

Şmuleac, L., Rujescu, C., Şmuleac, A., Imbrea, F., Radulov, I., Manea, D., Ienciu, A., Adamov, T., and *Paşcălău, R.*, 2020: Impact of Climate Change in the Banat Plain, Western Romania, on the Accessibility of Water for Crop Production in Agriculture, *Agriculture 10*(10): 437. https://doi.org/10.3390/agriculture10100437

DOI:10.28974/idojaras.2023.3.6

IDŐJÁRÁS

Quarterly Journal of the Hungarian Meteorological Service
Vol. 127, No. 3, July – September, 2023, pp. 379–399

Contribution to the study of climate change in Serbia using continentality, oceanity, and aridity indices

Dragan Burić [1,*], **Jovan Mihajlović** [2], **Vladan Ducić** [2], **Milan Milenković** [3], and **Goran Anđelković**[2]

[1]*Department of Geography*
Faculty of Philosophy
University of Montenegro
Danila Bojovica bb, 81400 Niksic, Montenegro

[2]*Faculty of Geography*
University of Belgrade
Studentski trg 3/3, 11000 Belgrade, Serbia

[3]*Geographical Institute "Jovan Cvijić" SASA*
Djure Jakšića 9, 11000 Belgrade, Serbia

**Corresponding author E–mail: draganburic33@gmail.com*

(Manuscript received in final form November 10, 2022)

Abstract— The aim of the study is to present some specific climatic conditions on the territory of the Republic of Serbia based on the analysis of four climate indices, which can help in understanding contemporary climate changes. Temperature and precipitation data from 31 meteorological stations for the period 1951–2010 were used. The relative homogeneity of the data series was done using the MASH v3.02 method. The indices used are: Johansson Continentality Index, Kerner Oceanity Index, De Martonne Aridity Index, and Pinna Combinative Index. Geospatial analysis of the distribution of the values of the four mentioned indices was done using the QGIS package 2.8.1. The results of the research show that the continentality effect is present in most of Serbia, while oceanity is observed locally, mainly in the western and southwestern parts of the country. The further analysis showed that there is no dry and semi–dry Mediterranean climate in Serbia. Considering that it is dry in the warmest part of the year (July–September), when the need for water is increased, which is clearly shown by the Walter climate diagram, as well as the fact that an increase in temperature and a decrease in precipitation during the vegetation period were observed in the second 30–year period (1981–2010), it can be concluded that in Serbia there is a tendency towards arid climate. The results presented in this paper can help decision makers to plan certain climate change adaptation measures.

Key-words: climate indices, continentality, oceanity, aridity, QGIS, Serbia

1. Introduction

Based on the analysis of monthly, seasonal, or annual values of temperature and precipitation, a general picture of the climate of a given area can be obtained. But, very often, it is necessary to determine some specifics of the climate. Then the analysis of additional climate indicators obtained with the help of climate indices, which complexly represent the climate of a place, is approached. Thus, climate indices show some specifics of climate, such as the degree of continentality, oceanity, aridity, or they are used to consider the influence of weather types on the human body. A more detailed spatial distribution and variation of climate indices has been done for the northern parts of Greece (*Baltas,* 2007) and Italy (*Nistor,* 2016), as well as for the area of Turkey (*Deniz et al.,* 2011) and Pakistan (*Gadiwala et al.,* 2013). There are also other analyses in numerous studies (*Sjögersten* and *Wookey,* 2004; *Filatov et al.,* 2005; *Croitoru et al.,* 2013; *Blanka et al.,* 2013; *Andrade* and *Corte-Real,* 2015; *Araghi et al.,* 2018; *Jahangir* and *Danehkar,* 2022). There are a lot of research papers dealing with climate indices in Serbia and other countries of the Balkan Peninsula (*Vujević,* 1961; *Maćejka,* 2003; *Malinović-Milićević,* 2013; *Pecelj et al.,* 2013, 2017; *Basarin et al*., 2014, 2017; *Stojićević et al*., 2016; *Burić et al.,* 2018, 2019; *Milentijević et al.,* 2018). Climate indices have found their application in many industries, especially in forecasting agricultural production and opportunities for the development of certain types of tourism (*Dalezios et al.,* 2001; *Deniz et al.,* 2011; *Moral et al.,* 2016; *Ren et al.,* 2017; *Kamyar et al.,* 2020; *Gudko et al.,* 2021).

In the reports of the Intergovernmental Panel on Climate Change (*IPCC,* 2021) it is pointed out that Europe has warmed significantly in the last 5–6 decades. The area of Southern Europe and the Mediterranean also registers a significant trend of rising temperatures, while regional differences are observed in precipitation, but many studies indicate the presence of a negative trend and more frequent and prolonged droughts (*Komuscu,* 2001; *Gao* and *Giorgi,* 2008; *Feyen* and *Dankers,* 2009; *Koutroulis et al.,* 2010; *Tsanis et al.,* 2011; *Kjellström et al.,* 2011; *Hoerling et al.,* 2012; *IPCC,* 2014; *Karabulut,* 2015). In the Western Balkans, the region to which Serbia belongs, there is also a significant trend of rising temperatures, while annual precipitation in general had a slight negative trend (*Kurnik et al.,* 2017). Climate projections suggest that the Western Balkans could face significant climate change in the future, as the region is very vulnerable in relation to the most part of the European continent (*Lung* and *Hilden,* 2017; *IPCC,* 2021). As a result of climate change, i.e., the anthropogenic greenhouse effect, the results of projections for Serbia (*Kržič et al.,* 2011; *Djurdjevic et al.,* 2019) and the neighboring Montenegro (*Burić* and *Doderović,* 2020; *Doderović et al*., 2020; *Burić* and *Doderović,* 2021) show that in the future we can expect a reduction in precipitation and a significantly warmer climate, with more frequent extreme weather and climate events (more frequent and prolonged droughts, heavy rains, floods, etc.). Yet,

Burić and *Stanojević*, (2020) point out that changes in cloudiness over Montenegro, and thus fluctuations in precipitation, can be largely attributed to variations in teleconnections (atmospheric and oceanic).

In the era of contemporary climate change, there is no doubt that climate indices will have an increasingly important application not only in agriculture, tourism, and other sectors of the economy, but may indicate the need for more rational water use, especially in areas where precipitation trends are registered and projected. Therefore, the aim of this paper is a more complex presentation of climatic conditions in Serbia, using geospatial analysis of the distribution and variation of four climate indices: Johansson Continentality Index (*Johansson*, 1926; *Conrad* and *Pollak*, 1951), Kerner Oceanity Index (*Kerner*, 1905; *Retuerto* and *Carballeira*, 1992; *Gavilan*, 2005; *Baltas*, 2007), De Martonne Aridity Index (*De Martonne*, 1926), and Pinna Combinative Index (*Zambakas*, 1992). For the purposes of this paper, the period 1951–2010 was used, and the indices were calculated on the basis of average monthly and annual values of temperature and precipitation from the 31 meteorological stations in Serbia. A Walter climate diagram was made, using as an example a typical representative of the climate of Serbia, and in order to see if there is a dry period in the year, based on the monthly values of temperature and precipitation. In order to determine the aridization trend, monthly data were also used to make polar diagrams for two 30-year periods (1951–1980 and 1981–2010). Thus, by applying the climate indices of continentality and oceanity, numerical differentiation is given, and the degree of influence of the mainland and neighboring sea and ocean basins (Adriatic, Mediterranean, Atlantic) on the climate of Serbia in the observed 60-year period is indicated.

The conceptual model used in this paper is that the influences of sea surfaces on continental masses are important, and their influence rate on the weather and climate of the surrounding geographical areas depends on the distance and relief characteristics. The relationship between oceanic and land surfaces is one of the most important in the Earth's climate system. It can be said that oceanity is the degree of influence of the ocean and sea surfaces on the neighboring land, which is the opposite in the case of continentality. In fact, these influences are mostly predisposed to synoptic situations during the year, i.e., they relate to the trajectories and position of cyclones and weather fronts coming from the sea, in general. In that sense, the results presented in this paper represent a kind of "synoptic" classification of climate indices in Serbia in the mesoscale.

2. Databases and methodology

2.1. Area of interest

The field of research is Serbia, a country in Southeast Europe and the Balkan Peninsula. It is a landlocked country (no access to the sea), with an area of 88361 km². The air distance between the capital (Belgrade) and the Adriatic and Aegean Sea is about 350 km, or about 500 km, while the Black Sea is about 620 km, and the Atlantic coast is over 1300 km away. The relief is lowland in the north (part of the Pannonian lowland), and in the rest of the country it has a hilly–mountainous character. The lowest point is in the east (28 m above sea level) – at the confluence of the Timok River and the Danube (tripoint of Serbia, Bulgaria, and Romania), while the mountain peaks in the south reach a height of just over 2500 m. Serbia is located almost in the middle of the northern hemisphere, i.e. between the coordinates $41^{0}53'$ and $46^{0}11'$N (*Fig. 1*). Latitude, relief characteristics, distance from the sea, and variations of upper air currents are the main factors that shape the climate of this country. In general, according to the Köppen climate classification, moderately warm (*C*) and moderately cold or boreal (*D*) climates are present in Serbia. Lower terrains have the characteristics of *C* climate, while mountainous areas above 1000 m above sea level are characterized by *D* climate.

Fig. 1. Locations and altitude of meteorological stations used in the analysis.

2.2. Data

For the purposes of this research, monthly/annual data of temperature and precipitation from the 31 meteorological stations (MS), obtained from the Republic Hydrometeorological Service of Serbia, were used. Time series, for the observed 60-year period (1951–2010), were complete for 20 MS, while for 5 MS a negligible percentage of data was missing (up to 0.5%). The other 6 MS, located in southern Serbia, lacked up to 15% of the data in series (MS: Kosovska Mitrovica, Pristina, Prizren, Dragas, and Pec), mainly for the period after 2000. After visual inspection, the relative homogeneity of data sets from all MS was examined. For these purposes, the Multiple Analysis of Series for Homogenization (MASH) method, developed by the Hungarian Meteorological Service, was used (*Szentimrey*, 1999, 2003). Using MASH methods, parts of time series that did not meet the conditions of homogeneity (which were inhomogeneous) were excluded from further analysis (0.1–0.9% of data, depending on the time series). For the purposes of this paper, version MASHv3.02 was used (*Szentimrey*, 2007), which is used not only for data quality control, but also for estimating missing (and removed inhomogeneous) data in arrays. In this way, time series (data series) of temperature and precipitation for 31 MS were completed. The hypsometry of MS is as follows: 24 MS are up to 500 m above sea level (77.4%), two are at altitudes between 500 and 1000 m (6.5%), and 5 MS are at altitudes above 1000 m (16.1%).

2.3. The used methods

Based on the mean monthly values of temperature and precipitation, and the data on the latitude of the MS included in the analysis, calculations were made for the Johansson Continentality Index, Kerner Oceanity Index, De Martonne Aridity Index, and Pinna Combinative Index. The spatial distribution of the obtained results was done using the Quantum Geographic Information System (QGIS), and in order to make the maps as clear as possible, raster GIS was used.

Johansson Continentality Index (CCI). *Conrad* and *Pollak* (1951) suggested a modification of *Johansson* (1926) equation of climate classification, because the continentality index tends to infinity when tends to zero. The modified equation has the following form (climatic categories according to Conrad and Pollak are given in *Table 1*):

$$CCI = 1.7\ T_{ata} / \sin(\phi + 10) - 14.0 \qquad (1)$$

where T_{ata} is the annual temperature amplitude and φ is the station latitude in degrees.

Table 1. Climate classification according to *Conrad* and *Pollak* (1950)

Climate type	CCI
hyper–oceanic	$-20 \leq$ **CCI** < 20
oceanic/maritime	$20 \leq$ **CCI** < 50
sub–continental	$50 \leq$ **CCI** < 60
continental	$60 \leq$ **CCI** < 80
extreme/hyper–continental	$80 \leq$ **CCI** ≤ 120

Kerner Oceanity Index (KOI). Assuming that in a maritime climate, autumn is a little warmer than spring, *Retuerto* and *Carballeira* (1992), *Gavilan* (2005), and *Baltas* (2007) define the Kerner Oceanity Index by the following formula (categorization of climate according to KOI values is given in *Table 2*):

$$KOI = 100\ (T_{oct} - T_{apr})/T_{ata}, \tag{2}$$

where T_{oct} and T_{apr} are the average monthly temperature in October and April, respectively.

Table 2. Climate classification according to *Kerner* (1905)

Climate type	KOI
hyper–continental	**KOI** ≤ -10
continental	$-10 <$ **KOI** ≤ 0
sub–continental	$0 <$ **KOI** ≤ 10
oceanic	$10 <$ **KOI** ≤ 20
hyper–oceanic	$20 <$ **KOI** ≤ 50

De Martonne Aridity Index (I_{DM}). There are several aridity indices used in climatology, the most famous being the De Martonne Aridity Index (*De Martonne*, 1926), which was also applied in this research. De Martonne's climate

classification is based on the duration of drought during the year, and this aridity-humidity index is defined as the ratio of average annual precipitation (*R*) and temperature (*T*) values increased by 10 °C (the climate classification according to De Martonne is given in *Table 3*):

$$I_{DM} = R/(T + 10)\ . \tag{3}$$

Table 3. Climate classification according to the De Martonne Aridity Index

Climate type	I_{DM}	Annual precipitation (mm)
dry	$I_{DM} < 10$	$R < 200$
semi–dry	$10 \leq I_{DM} < 20$	$200 \leq R < 400$
Mediterranean	$20 \leq I_{DM} < 24$	$400 \leq R < 500$
Semi–humid	$24 \leq I_{DM} < 28$	$500 \leq R < 600$
humid	$28 \leq I_{DM} < 35$	$600 \leq R < 700$
very humid	a) $35 \leq I_{DM} \leq 55$ b) $I_{DM} > 55$	a) $700 \leq R < 800$ b) $R > 800$

Pinna Combinative Index (Ip). Pinna has developed a combinative index (*Zambakas*, 1992; *Baltas*, 2007; *Deniz et al*., 2011), which has the following form:

$$I_P = 1/2/(I_{DM} + 12R_d/T_d + 10)\ , \tag{4}$$

where R_d and T_d are the mean values of precipitation and temperature of the driest month and *Ip* is used to indicate drought-prone regions that need irrigation. The modified climate classification according to the Pinna Combinative Index is shown in *Table 4*. The modification was performed by the author in order to adapt the climate classification categories to the temperate climate in which Serbia is located.

Table 4. Modified climate classification according to the Pinna Combinative Index by the author

Climate type	I_P	Type of vegetation
arid	$Ip < 10$	not specified
semiarid Mediterranean	$10 \leq Ip \leq 20$	formal Mediterranean
modified Mediterranean	$20 < Ip \leq 30$	sub Mediterranean
humid continental	$30 < Ip \leq 44$	mixed forests and steppes
perhumid continental A	$44 < Ip \leq 80$	coniferous forests
perhumid continental B	$Ip > 80$	coniferous forests and tundra

2.3.1. Procedure of creating raster maps using QGIS 2.8.1.

The spatial distribution of the obtained results was done using the Quantum Geographic Information System, version 2.8.1 (*QGIS 2.8.1*). In order to make the maps as clear as possible, raster GIS was used. Data from 31 weather stations were used to create the raster. Latitude (φ), longitude (λ), and altitude (h) of MS were used as a predictor variable to create a regression model based on which the interpolation of temperature/precipitation was done. Further, based on the *Shuttle Radar Topography Mission (SRTM)* and *Digital Elevation Model (DEM),* at a resolution of 30x30 m, the mean and standard deviation of slope and terrain exposure were calculated from circular zones with a diameter of 10 km that were formed around the stations. Due to the later phases of the work, two auxiliary rasters were formed for φ and λ. The choice of predictors was made based on the significance they have in the regression model. It turned out that in the case of precipitation, the highest percentage of variance affects combinations λ, h, and the mean values of the slope of the terrain around the station. Considering the temperature, the highest percentage of the variance covers h and φ.

The next step was to divide the dataset into a subset for interpolation (27 stations) and a subset for testing the accuracy of modeled temperature and precipitation values (4 stations, mostly evenly distributed from north to south: Vrsac, Cuprija, Leskovac, Smederevo). In the subset for interpolation, new values of temperature and precipitation were formed by multiplying the coefficients from the regression model with the values of the selected predictors for each station and subtracting the values thus obtained from the observed ones. A separate layer was made out of these new values of temperature and precipitation, using simple kriging, which was then transferred to a raster shape. Multiplying the coefficients from the regression model by the corresponding rasters (*DEM*, auxiliary rasters for φ and λ) and by adding to the previously formed temperature and precipitation rasters, raster maps were obtained.

The accuracy of the applied approach was verified by comparing the temperature/precipitation values, with the cells from the subset for testing and the

pixel values in which the stations are located. The difference between such modeled and observed values is expressed through *mean absolute error (MAE)* and *root mean square error (RMSE)*, and the obtained results are shown in *Table 5*.

Table 5. Mean absolute error (MAE) and root mean square error (RMSE) of the modeled air temperature and precipitation values for all three series (1951–1980, 1981–2010, and 1951–2010)

	Error	Jan	Feb	Mar	Apr	May	Jun	Jul	Aug	Sep	Oct	Nov	Dec	Annual
Temperature														
1951–1980	RMSE	0.6	0.3	0.5	0.5	0.6	0.6	0.6	0.6	0.6	0.6	0.6	0.6	0.6
	MAE	0.5	0.3	0.4	0.5	0.6	0.5	0.5	0.5	0.5	0.4	0.5	0.5	0.5
1981–2010	RMSE	0.6	0.5	0.5	0.5	0.5	0.3	0.5	0.4	0.5	0.7	0.9	0.5	0.5
	MAE	0.5	0.4	0.4	0.3	0.3	0.2	0.3	0.4	0.4	0.5	0.7	0.5	0.4
1951–2010	RMSE	0.9	0.5	0.5	0.5	0.4	0.3	0.3	0.4	0.5	0.6	0.7	0.9	0.5
	MAE	0.8	0.4	0.4	0.4	0.3	0.3	0.3	0.3	0.4	0.4	0.4	0.7	0.4
Precipitation														
1951–1980	RMSE	6.1	8.6	7.8	4	3.6	4.1	6.7	5.9	6.7	7.5	3.9	6.4	55.4
	MAE	5.8	7.8	6.5	2.9	3.2	3.3	6.3	5.4	6.6	7.2	3.6	5.5	49.9
1981–2010	RMSE	7.9	6.6	7.8	6.4	2.6	6.9	2.9	3.1	3.8	7.6	7.7	5.1	56.6
	MAE	6.9	5.3	7.8	4.1	2.0	5.9	2.3	2.7	3.2	7.3	7.1	4.9	56.3
1951–2010	RMSE	6.0	5.6	7.0	3.8	2.5	4.4	3.7	3.4	4.9	6.6	5.8	5.7	54.4
	MAE	5.8	5.5	6.9	2.9	2.2	3.5	3.1	3.3	4.7	5.7	5.5	5.4	53.0

The whole procedure was performed in *QGIS 2.8.1*, while the softwares *R* and *STATISTICA 8* were used to form the regression model and calculate the errors. Only the *Inverse Distance Weighted (IDW)* geostatistical interpolation method was used to create maps of the Pinna Combinative Index and Johansson Continentality Index. This geostatistical interpolation method was used due to the complexity of the Pinna Combinative Index (Johansson Continentality Index) formula, which takes into account precipitation and temperature of the driest month, and the driest month is not the same at each meteorological station in Serbia.

3. Results and discussion

The first part of the results provides an analysis of the spatial distribution of precipitation and temperature in Serbia. The second part will present the results of the considered climate indices.

3.1. Spatial distribution of average annual precipitation and temperature in Serbia

The average annual rainfall in Serbia, calculated for the period 1951–2010, varies a lot. The highest amount of precipitation is registered in the southwestern and western parts of the country (827.4–1134.1 mm), and the lowest in the northeastern and northern parts (520–600 mm). In the average year, the difference in precipitation between the wettest and the driest place is 613.4 mm. In general, it can be concluded that precipitation is decreasing from the southwest and west to the northeast and east of the country (*Fig. 2a*). Differences in the amount of precipitation in Serbia are due to relief dissection and the influence of cyclonic circulation. Namely, the southwestern and western parts of Serbia (areas richest in precipitation) are much more often affected by the periphery of cyclone activity from the south (when the center of the cyclone is above the Adriatic or when the so-called Genoa cyclones are active), while the northern parts remain out of reach. When it comes to temperature, the average annual values for the period 1951–2010, range from 1.0 °C in the higher mountain areas to 11.7 °C in the plains and valleys of Serbia (*Fig. 2b*). In general, the temperature decreases from lowland areas in the north to the mountainous areas in the south.

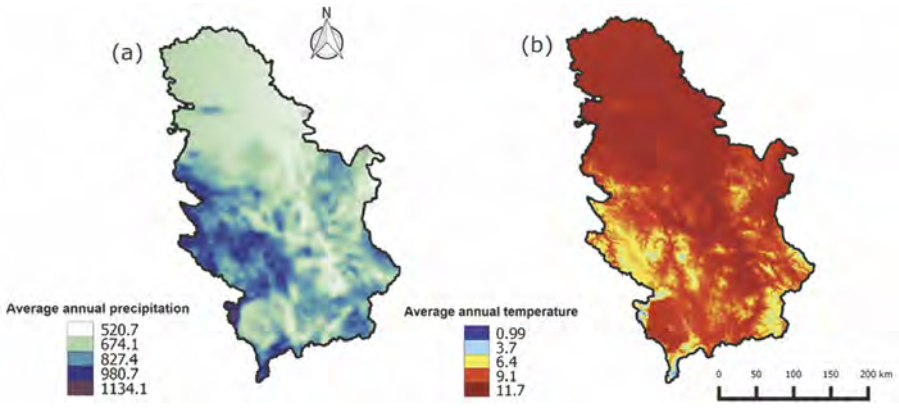

Fig. 2. Average annual values of precipitation (a) and temperature (b) in Serbia for the period 1951–2010.

3.2. Spatial distribution of climate indices

Analysis of the Johansson Continentality Index (*CCI*), which indicates the degree of continentality, showed that its values range from 23.1 (MS Kopaonik) to 34.8 (MS Negotin). Thus, the absolute difference of *CCI* in Serbia, for the period 1951–2010, is 11.7, which speaks in favor of how the climate under the influence of general synoptic schemes above Serbia is diversified in a relatively small area. The lowest values of this index are distributed mainly on the stations in western and southwestern Serbia, which are more influenced by maritime air masses. Moreover, all categories of climate types according to the *CCI* index in Serbia (*Fig. 3a*) belong to the oceanic/maritime climate with varying degrees of this effect. The minimum values of the *CCI* index occur at mountain stations at higher altitudes, which is in line with the laws of general synoptic schemes over Serbia. The maximum values of the *CCI* index indicate the more continental parts of Serbia, namely the northeastern and northern parts (the edge of the Pannonian Plain). The average value of *CCI* for the entire territory of Serbia is 30.7 and indicates that the climate of this country is oceanic/maritime, in general.

However, the values of the Kerner Oceanity Index (*KOI*) indicate that both continental and oceanic climates are present in Serbia. This is in line with the geographical position, the influence of relief elements, and variations in synoptic conditions over Serbia. The values of this index vary from -2.5 (MSNegotin) to 17.6 (MSKopaonik). According to the values of *KOI*, MSs in the northeast and north (Negotin, Zajecar, Sremska Mitrovica, Sombor, and Palic), i.e., parts of the country that are less influenced by maritime air masses from the Adriatic and Mediterranean, have the highest degree of continentality in Serbia. On the other hand, MSs located in higher mountain areas in the southwest and south, i.e., parts of Serbia that are closer to the Adriatic and Mediterranean, have the highest amounts of precipitation in the country and the highest values of *KOI* (*Fig. 3b*). In support of the fact that maritime and continental influences intertwine in Serbia is the average value for the entire territory of the country, which is 1.75.

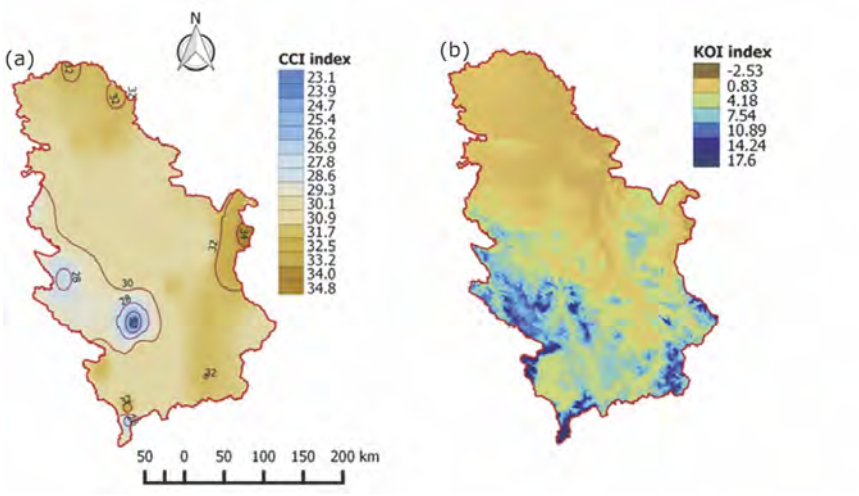

Fig. 3. Spatial distribution of the Johansson Continentality Index according to *Conrad* and *Pollak* (1951) (a) and the Kerner Oceanity Index (b) for the period 1951–2010.

The values of the two previous indices (*CCI* and *KOI*) largely correspond, which shows a statistically significant correlation and coefficient of determination, which is $r^2 = 0.69$ (*Fig. 4*). However, if the results of *CCI* and *KOI* were to be evaluated, it would be concluded that the Kerner Oceanity Index (*KOI*) is more appropriate for the territory of Serbia, regardless of the fact that the classification distinguishes only two categories (continental and maritime climates).

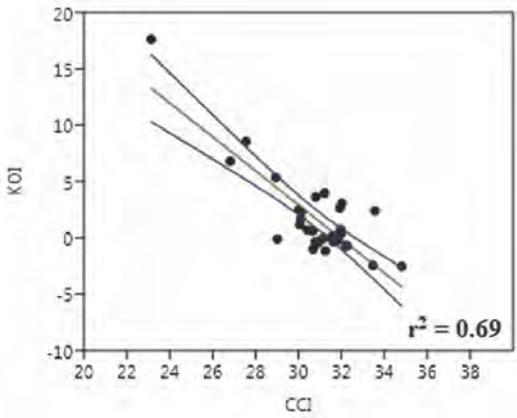

Fig. 4. Statistical analysis between the *CCI* index and the *KOI* index for the period 1951–2010 (blue lines indicate a 95% confidence interval).

One of the most frequently used indicators of aridity is the De Martonne Aridity Index (I_{DM}). For the period 1951–2010, I_{DM} ranges from semi-humid values in the northern part of the country (min. 26.7) to a very humid climate in the southern part of Serbia (max. 72.8). Therefore, the values of this index are gradually increasing from the northern, northeastern, and eastern parts of Serbia to the western, southwestern, and southern parts (*Fig. 5*), which is in line with the spatial distribution of precipitation. In other words, on the annual level, the degree of aridity increases from the southwest and west to the northeast and north of Serbia. When observing the entire period (1951–2010), the average value of the aridity index for the territory of Serbia is 34.7, i.e., it is on the border of the semi-humid and humid climates.

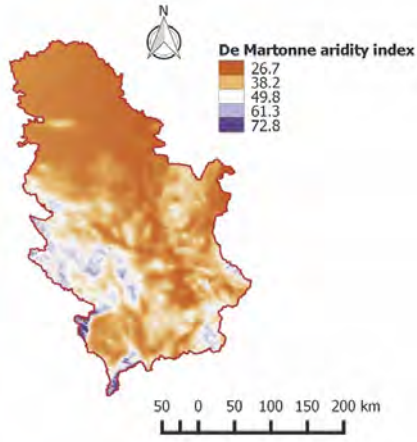

Fig. 5. De Martonne Aridity Index in Serbia for the period 1951–2010.

According to climate models, in the conditions of contemporary climate change in the area of Southeast Europe, i.e., the Balkan Peninsula, and thus in Serbia, an increase in aridity should be expected. To verify this, the years were categorized according to the I_{DM} values for the two subperiods 1951–1980 and 1981–2010. The results showed that the frequency of years belonging to the classes very humid and humid did not change significantly during the two observed periods. However, the frequency of years with semi-humid characteristics in the first 30-year period (1951–1980) was 3 years (10%), and in the second period (1981–2010) it was doubled (20%). This means that the climate of Serbia in the second 30-year period, observed on an annual basis, has become more arid (*Table 6*), which is a consequence of a significant trend of increasing average annual temperatures, because no significant changes are observed in precipitation. In any case, the previous analysis clearly identified the signal of climate change in Serbia, which can be linked to global warming and the problem of aridity in Southeast Europe in general.

Table 6. Annual frequency according to the De Martonne Aridity Index (I_{DM}) climate classification for the periods 1951–1980 and 1981–2010

Climate type	I_{DM} s	1951–1980		1981–2010	
		Frequency	Frequency (%)	Frequency	Frequency (%)
dry	$I_{DM} < 10$	0	0	0	0
semi-dry	$10 \leq I_{DM} < 20$	0	0	0	0
Mediterranean	$20 \leq I_{DM} < 24$	0	0	0	0
semi-humid	$24 \leq I_{DM} < 28$	3	10	6	20
humid	$2 \leq I_{DM} < 35$	18	60	16	53.3
very humid	$35 \leq I_{DM}$	9	30	8	26.7

In order to determine in more detail the climatic characteristics in Serbia, the Pinna Combinative Index (*Ip*) for the period 1951–2010 was calculated (*Fig. 6*). At all meteorological stations included in the analysis, the values of this index ranged over 20, which means that the climate is humid, in general. Therefore, according to the values of Ip, the arid and semiarid Mediterranean climate is not present in Serbia, which is in line with the geographical position of Serbia and the dominant physical-geographical factors.

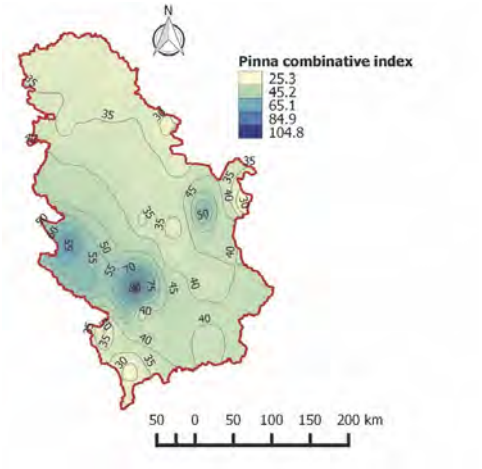

Fig. 6. Pinna Combinative Index in Serbia for the period 1951–2010.

The obtained value of *Ip* (25.3–26) belonged to the class of modified Mediterranean climate (semiarid climate) only for two MSs (Negotin and Prizren), and this can be related to smaller annual precipitation amounts and pluviometric regime. In the higher mountain areas, i.e. in the places that register the highest precipitation, *Ip* values go up to 104.8 (MS Kopaonik), so that the

western and southwestern parts of Serbia have the characteristics of perhumid continental A and B climate. The average value of *Ip* for the entire territory of Serbia is 39.8, which corresponds to the humid continental climate in which mixed forest and steppe vegetation dominate.

In any case, the territory of Serbia is outside the Mediterranean (semiarid) climate, but it should be noted that the two mentioned localities are close to this type. The influence of the Mediterranean reaches the southern parts of the country (MS Prizren – parts of the country closest to the Adriatic and Aegean Sea), while in the northeast (MS Negotin), there is less rainfall, as well as in northern Serbia, but these areas cannot be meteorologically linked to the Mediterranean climate in climatic-vegetation sense.

The spatial distribution and variation of I_p and I_{DM} in Serbia is quite similar, which is confirmed by the high value of the coefficient of determination of r^2 = 0.78 (*Fig. 7*). The limit value of the De Martonne Aridity Index of 28 (humid climate) coincides with the Pinna Combinative Index greater than 20 (all values > 20 indicate the humidity of the climate). However, when it comes to isolating the arid or humid climate of MS included in the analysis, evaluating the results of these two indices, we believe that I_{DM} can be preferred over I_p.

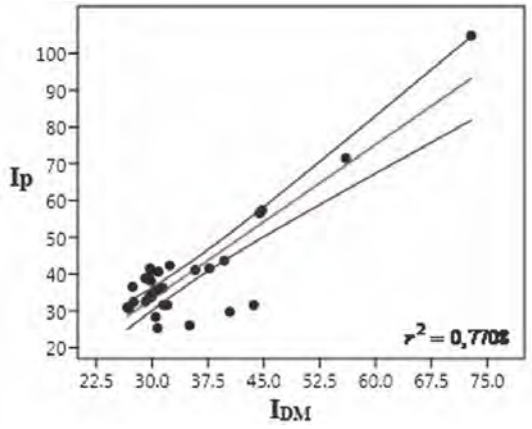

Fig. 7. Statistical analysis between the De Martonne Aridity Index (I_{DM}) and the Pinna Combinative Index (I_p) for the period 1951–2010 (blue lines indicate a 95% confidence interval).

3.3. Climate analysis on a monthly basis

In order to conduct an analysis on a monthly basis and to be efficient, one MS was chosen as a typical representative of the dominant climate in Serbia. The decision

that it should be MS Kragujevac is due to the fact that it is located almost in the geographical center of Serbia and at an altitude of less than 500 m (about 65% of the territory of Serbia has an altitude of up to 500 m). We first constructed a Walter climatic diagram, specificity of which is that the curves of temperature and precipitation are in a certain ratio (1:2, 1:3, and 1:10), in order to highlight dry and/or rainy periods. (*Walter et al.*, 1975). In Kragujevac, in general and in most of Serbia, during the colder part of the year (October–March), the amount of precipitation is lower than in the warmer half (April–September). The month, in which the ratio of precipitation (R) and temperature (T) is 1:2 ($R < 2T$) on the diagram is dry, and semi-dry when the ratio is $2T < R < 3T$. The graph clearly shows that the dry season lasts from July to September, in general (*Fig. 8*).

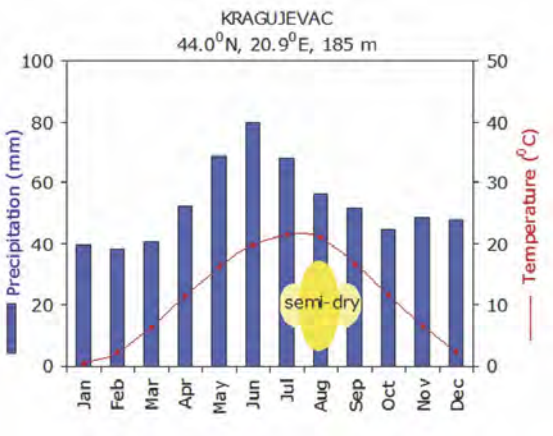

Fig. 8. Climate diagram of temperature and precipitation for MS Kragujevac (1951–2010).

The polar diagrams show the average monthly values of precipitation (*Fig. 9a*) and temperature (*Fig. 9b*). When it comes to precipitation, it is noticed that the monthly amounts range from 40 mm (February) to 80 mm (June). Comparing two simultaneous periods (1951–1980 and 1981–2010), it can be concluded that in the second 30–year period there was a decrease in precipitation in the period when water is most needed by vegetation (May–June–July) and an increase in temperature, especially in the warmer part of the year (May–August). The facts that the dry season lasts from July to September (Walter climate diagram), i.e., in the warmer part of the year when the need for water is higher, and that in the second 30–year period there was an increase in temperature and a decrease in precipitation during the vegetation period, clearly indicate the tendency towards more arid conditions in Serbia.

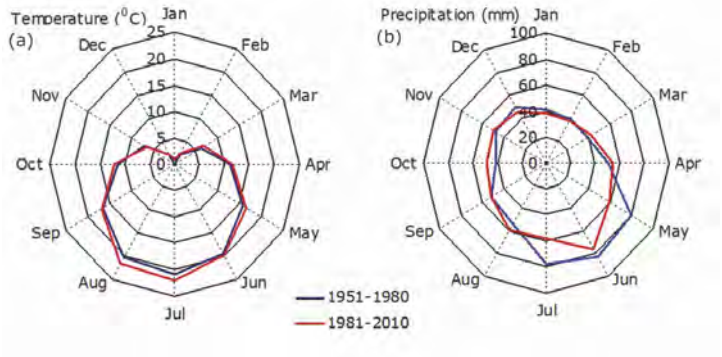

Fig. 9. Polar diagram of precipitation (a) and temperature (b) for MS Kragujevac, for the periods 1951–1980 and 1981–2010.

4. Conclusion

In order to define the climate in more detail, i.e., the degree of continentality and oceanity, the paper presents the spatial distribution of climate indices on the territory of Serbia, and the results are presented in the form of appropriate thematic maps. Based on data from 31 MSs for the period 1951–2010, the classification of climate continentality using the *CCI* index is in line with the climate classification based on the *KOI* index. This is confirmed by the high correlation between the mentioned indices of continentality and oceanity, i.e., similar spatial distribution and variation. The effect of continentality was discovered on most MS in Serbia, while the effect of oceanity was discovered on the MS located in the southwestern and western hilly and mountainous part of Serbia. This can be attributed to general synoptic patterns over Serbia during a multi-year period.

Climate classification according to the De Martonne Aridity Index (I_{DM}) and the Pinna Combinative Index (I_p) has been made also, and the results obtained are largely compatible. This is also shown by the conducted statistical analysis of the coefficients of determination, which were high and indicated a similar spatial distribution and variation. However, a more precise classification of Serbia's climate is provided by the I_{DM}. According to the results obtained by I_p, it is evident, that there is no arid and semiarid Mediterranean climate on the territory of Serbia, which is in line with the geographical position and physical-geographical conditions prevailing in this country (primarily synoptic conditions and relief characteristics). According to the results of the I_{DM}, there are no dry and semi-dry Mediterranean climate zones on the territory of Serbia. The range of I_{DM} climate categories varies from semi-humid to very humid climates. The Walter climate diagram indicates that it is dry in the warmest, and arguably the most unfavorable part of the year. This circumstance (dry period in the warmest part of the year, when the need for water is increased), as well as the fact that in the second 30–

year period (1981–2010), higher temperatures and lower precipitation are registered, as it is shown by polar diagrams for Kragujevac, a typical representative of the climate of Serbia, indicate that the climate of this country is becoming more arid, in general. The results of this study could be of application significance in many areas of human activity, especially in the applied branches of agriculture, tourism, and water management.

References

Andrade, C. and *Corte-Real, J.*, 2015: Spatial distribution of climate indices in the Iberian Peninsula. AIP Conference Proceedings, 1648(1), 110006. https://doi.org/10.1063/1.4912413

Araghi, A., Martinez, C.J., Adamowski, J., and *Olesen J.E.*, 2018: Spatiotemporal variations of aridity in Iran using high-resolution gridded data. *Int. J. Climatol., 38*(6), 2701–2717. https://doi.org/10.1002/joc.5454

Baltas, E., 2007: Spatial distribution of climatic indices in northern Greece. *Meteorol. Appl. 14*, 69–78. https://doi.org/10.1002/met.7

Basarin, B., Kržič, A., Lazić, L., Lukić, T., Đorđević, J., Petrović Janićijević, B., Ćopić, S., Matić, D., Hrnjak, I., and *Matzarakis, A.*, 2014: Evaluation of bioclimate conditions in two Special Nature Reserves in Vojvodina (Northern Serbia). *Carpathian J. Earth Environ. Sci. 9*(4), 93–108. https://www.urbanclimate.net/matzarakis/papers/Basarin_et_al_2014.pdf

Basarin, B., Lukić, T., Mesaroš, M., Pavić, D., Đorđević, J., and *Matzarakis, A.*, 2017: Spatial and temporal analysis of extreme bioclimate conditions in Vojvodina, Northern Serbia. *Int J. Climatol., 38*(1), 142–157. https://doi.org/10.1002/joc.5166

Blanka, V., Mezősi, G., and *Meyer, B.*, 2013: Projected changes in the drought hazard in Hungary due to climate change. *Időjárás 117*, 219–237. https://www.researchgate.net/publication/261870735

Burić, D., Ivanović, R., and *Milenković, M.*, 2018: Indicator of specificity of climate: the example of Podgorica (Montenegro). *J. Geograp. Inst. "Jovan Cvijić" SASA 68*(3), 399–403. https://doi.org/10.2298/IJGI180423009B

Burić, D., Milenković, M., and *Ducić, V.*, 2019: The specifities of the climate of Danilovgrad (Montenegro). *Bull. Serbian Geograph. Soc. 99*(1), 19–28. https://doi.org/10.2298/GSGD1901019B

Burić, D. and *Doderović, M.*, 2020: Projected temperature changes in Kolašin (Montenegro) up to 2100 according to EBU-POM and ALADIN regional climate models. *Időjárás 124*, 427–445. http://doi.org/10.28974/idojaras.2020.4.1

Burić, D. and *Stanojević, G.*, 2020: Trends and possible causes of cloudiness variability in Montenegro in the period 1961–2017. *Climate Res. 81*, 187–205. https://doi.org/10.3354/cr01615

Burić, D. and *Doderović, M*, 2021: Changes in temperature and precipitation in the instrumental period (1951-2018) and projections up to 2100 in Podgorica (Montenegro). *Int. J. Climatol., 41*(S1), E133–E149. https://doi.org/10.1002/joc.6671

Conrad, V.A. and *Pollak, L.W.*, 1951: Methods in climatology, 2nd edition. Harvard university press, Cambridge, Massachusetts, pp. 459. *Amer. J. Physics 19*(1), 64–65. https://doi.org/10.1119/1.1932708

Croitoru, A.E., Piticar, A., Imbroane, A.M., and *Burada, D.C.*, 2013: Spatiotemporal distribution of aridity indices based on temperature and precipitation in the extra-Carpathian regions of Romania. *Theor. Appl. Climatol., 112*(3-4), 597–607. https://doi.org/10.1007/s00704-012-0755-2

Dalezios, N, Domenikiotis, X, Loukas, A, Tzortzis, ST, and *Kalaitzidis, C*, 2001: Cotton yield estimation based on NOAA/AVHRR produced NDVI. *Phys. Chemist. Earth, Part B: Hydrol. Oceans and Atmosphere 26*(3), 247–251. https://doi.org/10.1016/S1464-1909(00)00247-1

De Martonne, E., 1926: Une nouvelle fonction climatologique: l'indice d'aridite [A New Climatological Function: The Aridity Index]. *La Meteorologie 2*, 449–458. https://ci.nii.ac.jp/naid/10027359266

Deniz, A., Toros, H., and *Incecik, S*., 2011: Spatial variations of climate indices in Turkey. *Int. J. Climatol. 31*(3), 394–403. https://doi.org/10.1002/joc.2081

Doderović, M., Burić, D., Ducić, V., and *Mijanović, I.*, 2020: Recent and Future Air Temperature and Precipitation Changes in the mountainous nort of Montenegro. *J. Geograph. Inst. "Jovan Cvijić" Serbian Acad. SASA 70*(3), 189-201. https://doi.org/10.2298/IJGI2003189D

Djurdjevic, V., Trbić, G., Krzic, A., and *Bozanic, D.*, 2019: Projected changes in multi-day extreme precipitation over the Western Balkan region. In (eds. *Leal Filho W, Trbic G, Filipovic D*.). Climate change adaptation in Eastern Europe, Climate Change Management, Springer, Cham, 15–28. https://doi.org/10.1007/978-3-030-03383-5_2

Feyen, L., and *Dankers, R.*, 2009: Impact of global warming on streamflow drought in Europe. *J. Geophysi. Res.: Atmospheres, 114*(D17), D17116. https://doi.org/10.1029/2008JD011438

Filatov, N., Salo, Y., and *Nazarova, L.*, 2005: Effect of climate variabilityon natural water bodies in Northwest Russia. 15th International Northern Research Basins Symposium and Workshop, Luleå to Kvikkjokk, Sweden,31–41. https://www.diva-portal.org/smash/get/diva2:1001653/FULLTEXT01.pdf

Gadiwala, M.S., Usman, A., Akhtar, M., and *Jamil, K.*, 2013: Empirical models for the estimation of global solar radiation with sunshine hours on horizontal surfaces in various cities of Pakistan. *Pakistan J Meteorol 9*(18), 43–49. https://agris.fao.org/agris-search/search.do?recordID=PK2014000141

Gao, X., and *Giorgi, F.*, 2008: Increased aridity in the Mediterranean region under greenhouse gas forcing estimated from high resolution simulations with a regional climate model. *Glob.Plane. Change 62*(3–4), 195–209. https://doi.org/10.1016/j.gloplacha.2008.02.002

Gavilan, R.G., 2005: The use of climatic parameters and indices invegetation distribution. A case study in the Spanish Sistema Central. *Int J of Biometeorol. 50*(2), 111–120. https://doi.org/10.1007/s00484-005-0271-5

Gudko, V., Usatov, A., Ioshpa, A., Denisenko Y., Shevtsova V., and *Azarin, K.*, 2021: Agro–climatic conditions of the Southern Federal District of Russia in the context of climate change. *Theor. Appl. Climatol. 145*, 989–1006. https://doi.org/10.1007/s00704-021-03677-y

Hoerling, M., Eischeid, J., Perlwitz, J., Quan, X., Zhang, T., and *Pegion, P.*, 2012: On the Increased Frequency of Mediterranean Drought. *J Climate, 25*(6), 2146–2161. https://doi.org/10.1175/JCLI-D-11-00296.1

IPCC, 2014: Climate change 2014. Synthesis report. In: Pachauri, R.K. and Meyer, L.A. (Eds.), Contribution of Working Groups I, II and III to the Fifth Assessment Report of the Intergovernmental Panel on Climate Change Core Writing Team, Geneva, Switzerland. IPCC.

IPCC, 2021: Summary for Policymakers. In: Climate Change 2021. The Physical Science Basis, Contribution of Working Group I to the Sixth Assessment Report of the Intergovernmental Panel on Climate Change [(eds.)*Masson-Delmotte, V., P. Zhai, A. Pirani, S. L. Connors, C. Péan, S. Berger, N. Caud, Y. Chen, L. Goldfarb, M. I. Gomis, M. Huang, K. Leitzell, E. Lonnoy, J.B.R. Matthews, T. K. Maycock, T. Waterfield, O. Yelekçi, R. Yu and B. Zhou*]. Cambridge University Press. In Press.

Jahangir, M.H., and *Danehkar, S.*, 2022: A comparative drought assessment in Gilan, Iran using Pálfai drought index, de Martonne aridity index, and Pinna combinative index. *Arab J Geosci., 15*, 90. https://doi.org/10.1007/s12517-021-09107-7

Johansson, O.V., 1926: Über die Asymmetrie der meteorologischen Schwankungen. In: *Soc. Sci. Fennica, Commentationes Phys. Math. 3*, Iff. Google Scholar

Kamyar, A., Yazdanpanah, H., Movahedi, S., and *Morimoto, D.*, 2020: Assessment of the impacts of climate change on agro-climatic indices in Iran. *Theor. Appl. Climatol. 142*, 1359–1367. https://doi.org/10.1007/s00704-020-03385-z

Karabulut, M., 2015: Drought analysis in Antakya-Kahramanmaraş Graben, Turkey. *J. Arid Land. 7*, 741–754. https://doi.org/10.1007/s40333-015-0011-6

Kerner, F.V., 1905: Thermoisodromen. Versuch einer kartographischen Darstellung des jahrlichen Ganges der Lufttemperatur. *Abh. Geogr. Ges.Wien, Bd. VI*, H. 3. (In German)

Kjellström, E., Nikulin, G., Hansson, U., Strandberg, G., and *Ullerstig, A.*, 2011: 21st century changes in the European climate: uncertainties derived from an ensemble of regional climate model simulations. *Tellus A: Dynam. Meteorol. Oceanograph. 63*(1), 24–40. https://doi.org/10.1111/j.1600-0870.2010.00475.x

Kurnik, B., Füssel, H.M., van der Linden, P., and *Simmons, A.*, 2017: Changes in the climate system, Section 3.2: Atmosphere. Climate change, impacts and vulnerability in Europe 2016. An indicator-based report. EEA Report, Number: 1/2017, 69–88. https://www.yumpu.com/en/document/read/56771568/climate-change-impacts-and-vulnerability-in-europe-2016

Komuscu, A.U., 2001: An Analysis of Recent Drought Conditions in Turkey in Relation to Circulation Patterns. *Drought Network News 13*, 4–6. https://digitalcommons.unl.edu/droughtnetnews/22/

Koutroulis, A.G., Vrochidou, A., and *Tsanis, I.K.*, 2010: Spatiotemporal characteristics of meteorological drought for the Island of Crete. *J Hydrometeor. 12*(2), 206–226. https://doi.org/10.1175/2010JHM1252.1

Kržić, A., Tošić, I., Djurdjević, V., Veljović, K., and *Rajković, B.*, 2011: Changes in climate indices for Serbia according to the SRES-A1B and SRES-A2 scenarios. *Clim Res. 49*, 73–86. https://doi.org/10.3354/cr01008

Lung, T., and *Hilden, M.*, 2017: Multi-sectoral vulnerability and risks, Section 6.2: multi-sectoral impacts and vulnerabilities across Europe. Climate Change, Impacts and Vulnerability in Europe 2016. An Indicator-based Report. EEA Report, Number: 1/2017, 273–281.

Maćejka, M., 2003: Klima i njen zdravstveni značaj u banjama Srbije. Srpsko geografsko društvo, b.str. 1-190. (eng. *Climate and its health significance in the spas of Serbia.* Serbian Geographical Society, pp 190). ark:/13960/t46q8tc1c (In Serbian)

Malinović–Milićević, S., 2013: Bioclimatic Characteristic of Banat. *J. Geograph.l Inst. "Jovan Cvijic" SASA, 63*(1), 11–20. https://doi.org/10.2298/IJGI1301011M

Milentijević, N., Dragojlović, J., Cimbaljević, M., Ristić, D., Kalkan, K., and *Burić., D.*, 2018: Analysis equivalent temperature - case of Kragujevac city. *Bull. Serbian Geograph. Soc. 98*(1), 61–77. https://doi.org/10.2298/GSGD180225003M

Moral, F.J., Rebollo, F.J., Paniagua, L.L., García, A., and *Honorio, F.*, 2016: Integration of climatic indices in an objective probabilistic model for establishing and mapping viticultural climatic zones in a region. *Theor. Appl. Climatol. 124*, 1033–1043. https://doi.org/10.1007/s00704-015-1484-0

Nistor, M.M., 2016: Spatial distribution of climate indices in the Emilia-Romagna region. *Meteorol. Appl. 23*(2), 304–313. https://doi.org/10.1002/met.1555

Pecelj, M., Krajić, A., Trbić, G., Stevanović, V., and *Golijanin, J.*, 2013: Bioclimatic Characteristics of the City of Novi Sad Based on Human Heat Balance. Proc. 6th International Conference on Climate Change, Global Warming and Biological Problems, Recent Advances in Environmental Science, Cyprus, 244–249. https://scholar.google.com/scholar?cluster=17733867487233207995&hl

Pecelj, M., Đorđević, A., Pecelj, M.R., Pecelj–Purković, J., Filipović, D., and *Šećerov, V.*, 2017: Biothermal conditions on Mt. Zlatibor based on thermophysiological indices. *Arch. Biol. Sci. 69*(3), 455–461. https://doi.org/10.2298/ABS151223120P

Ren, W., Wang, Y., Li, J., Feng, P., and *Smith, R.J.*, 2017: Drought forecasting in Luanhe River basin involving climatic indices. *Theor. Appl. Climatol. 130*, 1133–1148. https://doi.org/10.1007/s00704-016-1952-1

Retuerto, R., and *Carballeira A.*, 1992: Use of direct gradient analysis to study the climate-vegetation relationships in Galicia, Spain. *Vegetatio 101*(2), 183–194. https://doi.org/10.1007/BF00033201

Stojićević, G., Basarin, B., and *Lukić, T.*, 2016: Detailed Bioclimate Analysis of Banja Koviljača (Serbia). *Geographica Pannonica, 20*(3), 127–135. doi: 10.18421/GP20.03-01

Szentimrey, T., 1999: Multiple analysis of series for homogenization (MASH). Proceedings of the Second Seminar for Homogenization of Surface Climatological Data, Budapest, Hungary: WMO, WCDMP-Number: 41. 27–46.

Szentimrey, T., 2003: Multiple analysis of series for homogenization (MASH); Verification procedure for homogenized time series. Fourth seminar for homogenization and quality control in climatological databases. Budapest, Hungary. WMO-TD. Number: 1236, WCDMP Number: 56. 193–201.

Szentimrey, T., 2007: Manual of Homogenization Software MASHv3.02. Hungarian Meteorological Service.

Sjögersten, S., and *Wookey, P.A.*, 2004: Decomposition of mountain birch leaflitter at the forest-tundra ecotone in the Fennoscandian mountains inrelation to climate and soil conditions. *Plant Soil 262*, 215–227. https://www.jstor.org/stable/42951528

Tsanis, I.K., Koutroulis, A.G., Daliakopoulos, I.N., and *Jacob, D.*, 2011: Severe climateinduced water shortage and extremes in Crete. *Clim Change, 106*(4), 667–677. https://doi.org/10.1007/s10584-011-0048-2

Vujević, P., 1961: Prilozi za bioklimatologiju oblasti Kopaonika. *Zbornik radova Institut „J. Cvijić“ 18*, 1-91. (eng.: Contributions to the bioclimatology of the Kopaonik area. *J. Geograph Inst. "Jovan Cvijić" SASA 18*, 1–91. (In Serbian)

Walter, H., Harnickell, E., and *Mueller–Dombois, D.*, 1975: Climate-diagram Maps of the Individual Continents and the Ecological Climatic Regions of the Earth. Springer–Verlag, BerlinI, 1–36. https://www.researchgate.net/publication/245669481

Zambakas, J., 1992: General Climatology. Department of Geology, National and Kapodistrian University of Athens, Athens. Google Scholar

DOI:10.28974/idojaras.2023.3.7

IDŐJÁRÁS

Quarterly Journal of the Hungarian Meteorological Service
Vol. 127, No. 3, July – September, 2023, pp. 401–420

Evaluation of wind comfort with computational fluid dynamics simulations for pedestrian sidewalks around buildings

Alper Aydemir*, **Fikriye Ezgi Karahüseyin**, and **Yaşar Can Yılmaz**

Nuh Naci Yazgan University, Engineering Faculty
Civil Engineering Department
Nuh Naci Yazgan University Campus Kocasinan,
38050 Kayseri, Turkey

**Corresponding author E-mail: aydemir@nny.edu.tr*

(Manuscript received in final form November 23, 2022)

Abstract— Wind power could be one of the most clean and powerful renewable resources for electrical energy production, but on the other hand, uncontrolled wind flow especially in urban places could cause undesired situations as damage to buildings, decrease in pedestrian comfort, environmental damage, or even life loss. Construction of high-rise buildings, widely spread structures within cities, and environmental changes forces, engineers to find quick, reliable, and also economically viable solutions during design stages, but wind comfort of sidewalks generally not considered enough even if they are located in crowded areas. The web-based computer aided engineering (CAE) program named Simscale which runs on the basis of sophisticated graphical interface was used as computational fluid dynamics (CFD) software to determine wind speeds under influence of buildings in the Nuh Naci Yazgan University campus. Also, field measurements carried out in campus area for a short term period were compared with long term hourly wind speed data obtained from the Turkish State Meteorological Service (MGM) station located in Kayseri to identify most optimal wind speed data for the research area. Results of analysis showed that wind speed increased in the mostly used paths of campus, which means that the layout of buildings negatively affected the wind comfort. CFD analysis softwares could be used to determine the possible consquences of wind with less economic investment in a short time, and they could be used in accordance with comfort criterias as well as safety regulations.

Key-words: wind, pedestrian wind comfort, wind analysis, computational fluid dynamics

1. Introduction

Wind is defined as a weather event that is determined in relation to the earth, generally it develops horizontally and has environmental effects (MGM, 2021). Wind direction and speed stand out as important determining criteria. Measurements related to wind gain importance, especially when investigating its effect on different surfaces. Although earth winds can be measured at different heights, measurements made 10 meters above the earth are used as reference data.

Wind power could be one of the most clean and powerful renewable resources for electricity production, but uncontrolled wind flows around urban places could cause undesired situations such as damage to buildings, pedestrian comfort loss, environmental damage, or even life loss. Also, effects of wind around sidewalks generally not considered enough by engineers, so pedestrian wind comfort is one of the important subjects especially for the last years. The computational fluid dynamics programs, experimental studies generally made in wind tunnels, and field measurements are most common solutions to overcome this wind effect problem.

The wind tunnel testing, the techniques of computational fluid dynamics (CFD) have also been increasingly exploited by academic researchers and industrial practitioners in various ways (*Hu* and *Wang*, 2005). Buildings or obstacles around buildings could be well modeled with CFD, as well as parts or elements of structures could be modeled in the same manner. For example, wind loads on solar photovoltaic collectors can be modeled by using both CFD and wind tunnel experiments with smoke visualization observations (*Meroney* and *Neff*, 2010). Obstacles such as trees around pedestrian roads were also examined, and numerical results with field measurements of wind velocity and turbulent energy around trees were compared (*Mochida et al*., 2008). There are many studies in literature for both experimental and CFD analyses, while comparison studies show good correlation, so in some cases solely CFD analysis could be used to define wind analysis. The Architectural Institute of Japan (AIJ) conducted experiments on high-rise buildings and compared findings with CFD results obtained by the ANSYS Fluent software, and results that show the simulation by all two-equation turbulence models have good agreement with experimental results (*Behrouzi et al*., 2013). However, the complexity of the investigated problem effects the accuracy of results. For example, results of a study showed that the CFD model underestimated the pollutant concentrations on the leeward (also overestimated on windward) walls inside the street canyon in the presence of trees, while the simulated pattern and magnitude of pollutant dispersion were similar to those in the wind-tunnel measurements (*Kang et al*., 2017). Another study focused on the influence of an upstream building on a downstream target building. When the interfering building is located downstream of the target building, it may strengthen the leeward reverse flow of the target building, which

may induce higher pollutants re-enter ration on the leeward side of the target building (*Cui et al.*, 2016).

Main constraints for wind studies especially for the one such as pedestrian comfort are high-cost of analysis and time-consuming wind flow analysis processes. Developments in technology lead new solutions for wind-based researches. Computational fluid dynamics (CFD) analysis programs are the most suitable ways for wind flow simulations, because they are relatively low-cost compared to wind tunnel experiments and need less time depending on computational hardware. Technological developments lead to faster computers as well as to online based CFD softwares running on online servers, which allow users to reach projects from all over the world by using internet. Investigations of the urban flow in a complex morphological street network that is coincidentally similar to the ancient Algeria city Ghardaïa were investigated, and a CFD model was suggested to simulate the air flow behavior in this urban area (*Houda et al.*, 2012). High wind speed condition simulations with 3D steady RANS and the realizable k–ε model for 12 wind directions with surface roughness parameterization and specification were performed. The simulation results of mean wind speed and wind direction are generally within 10–20% of the corresponding measurement values (*Blocken et. al.*, 2015). Wind studies about pedestrian comfort include three aspects: (1) statistical meteorological data, (2) aerodynamic information, and (3) a comfort criterion (*Blocken* and *Persoon*, 2009). Another study investigated turbulent flow fields over two typical urban elements, a row of trees with low packing density and an isolated building with high packing density with a modified k - ε model and a large eddy simulation (LES) model (*Qi* and *Ishihara*, 2018).

Urban areas should be designed to ensure the comfort, health, and safety for inhabitants and users around them, so this makes wind comfort and wind safety for pedestrians as an important requirement for urban areas (*Blocken et al*., 2012). This comfort could be arranged with detailed engineering studies based on regulations for pedestrian wind comfort criteria. Changes in urban areas such as construction of higher buildings, city plans without wind analysis, changes in wind speeds, and climate change effects influence the wind flows. Higher height buildings resulted changes for wind flows around urban blocks. These changes could be simulated with CFD and also by experimental using of wind tunnel experiments in a turbulent boundary layer *(Yoshie et al*., 2006). Effects of high-rise buildings on pedestrian level wind (PLW) comfort could be reduced with using some obstacles in the wind flow way. For example, a canopy or a podium can significantly reduce the area-averaged PLW speed (up to 29%) and the maximum PLW speed (up to 36%) around the high-rise building (*Van Druenen et al*., 2019). Studies of wind comfort and wind safety involve combining statistical meteorological data, aerodynamic information, wind comfort, and safety criteria (*Blocken et al*., 2012). Changes in wind speeds should be very variable depending on the measurement period. Seasonal wind changes and

topography are main reasons of this variation. The semi-closed U-type street canyon has been widely used in the high-density trans-oriented development of urban design for providing private space. However, U-type canyon exhibits a lower wind speed at the pedestrian level than that of the parallel canyon both inside and in the vicinity of the street canyons, especially under parallel wind direction (*Cui et al*., 2019). Many countries publish written regulations about wind safety or wind comfort. In the Netherlands, the wind code is not another legal building requirement, but a helping hand to include wind comfort in a building program, and it explicitly regulates the technical procedures and quality control (*Willemsen* and *Wisse*, 2007). Statistical analysis using long time period data could help researchers to find required wind speeds for studies, but if there are safety regulations, these restrictions force researchers to find different solutions. Also, it could be suggested to measure field data for a long time period before the planning stage and to use it during the design stage, but in most cases, it could not be possible because of tight construction schedule of civil engineering projects or the high economic investment costs for these kinds of measurements could be high.

Complex problems including wind loads on structures could be solved both with wind tunnels and CFD. These methods could be well used in extraordinary shaped buildings such as telescopes (*Mamou et al*., 2008). There are basically two types of parameters that act as sources of error in CFD results. First, there are modeling errors that arise from the turbulence models used and the physical boundary conditions applied. The other errors stem from the numerical modeling (*Franke et al.*, 2004). Most of the studies about wind conditions in passages between parallel side-by-side buildings focus on pedestrian-level winds. Two main categories can be distinguished: (1) Fundamental studies, which are typically conducted for simple, generic building configurations to obtain insight in the flow behavior, to study the influence of different building dimensions and passage widths, and to provide input for knowledge-based expert systems (KBES) and/or for model validation. (2) Applied studies, which provide knowledge of the wind environmental conditions in specific and often much more complex case studies (*Blocken et al*., 2007). *Du* and *Mak* made a research about Hong Kong, and their results indicated that the lift-up design can improve the wind comfort in building surroundings, and its influence is highly dependent on the incident wind direction (*Du* and *Mak*, 2017). Studies involved with wind flow simulation require detailed examination even if it is wind tunnel experiment or CFD. Accuracy of these methods mostly changeable depending on many factors. There are some uncertainties inherent in wind tunnel experiments (such as measuring instrument errors, incidental errors, errors in the position where the sensor is installed, etc.), but there are no such uncertainties in CFD, and furthermore, it is very difficult to have an arbitrary approach flow in the wind tunnel, while this can be freely done in CFD (*Yoshie et al*., 2007). In single building models, which are considered to give the highest accuracy in the experiment, the CFD analysis results were

consistent with experimental results within an accuracy about 10% in the strong wind region *(Yoshie et al*., 2007). The results of pedestrian wind comfort analysis could be well applied to different projects such as autonomous control systems. Assessment of wind around passages for Silvertop Towers in Antwerp showed that traditional remedial studies gave unsatisfactory results, so an automatic control system has been designed and analyzed to modify the wind climate in the passages. The measurements are performed in upper through-passages above the passage canopies and the control system is estimated to leave doors open for about 50% to 70% of the time (*Blocken et al*., 2004).

In this study, pedestrian wind comfort analysis has been performed with Simscale CFD software by using wind flow data obtained from the Turkish State Meteorological Service (MGM). Section 2 describes statistical analysis of wind data and information used in CFD software about the university campus. Results of the wind comfort analysis given in Section 3, and Section 4 comprises conclusion of the whole investigation with suggestions to guide future studies in the subject of the pedestrian wind comfort.

2. Material and method

2.1. Material

Nuh Naci Yazgan University (NNY University) is a non-profit private university supported by industry and charity, and it has active collaboration with industry that leads to high quality in both local and international student placements (NNY, 2021). NNY University is officially founded by the Kayseri Higher Education and Social Aid Foundation (KHESAF) in 2009. Location of university is in the northwestern side of Kayseri province in Turkey. This makes the university campus buildings, roads, and sidewalks vulnerable for high-speed winds coming from south direction. Situation plan and general view of university campus are given in *Figs. 1* and *2*, respectively. The terrain of surroundings near the university campus is given in *Fig. 3*, where a red circle indicates the campus. It can be seen that the north side of the area is surrounded by relatively high hills from the north direction, while fully open field from the south direction.

Fig. 1. Nuh Naci Yazgan University Campus situation plan.

Fig. 2. General view of university campus.

Fig. 3. Terrain around campus area.

2.2. Wind data

Measurements of wind speeds are carried out by the Turkish State Meteorological Service (MGM) in Turkey. In this study wind speeds have been obtained from the Kayseri Regional Directorate of MGM. While Nuh Naci Yazgan University located in the Erkilet district, the closest wind measurement station is located in the city center. Distribution of wind speeds change in seasonal, monthly, daily, and even hourly periods. Hourly wind speeds including direction for long time period (2009–2018) obtained from MGM was used in this study. Wind flow direction changes in very short periods because of various reasons, nevertheless, prevailing wind direction is vital for wind flow based studies. Distributions of wind events for the observation period are given in *Fig. 4*.

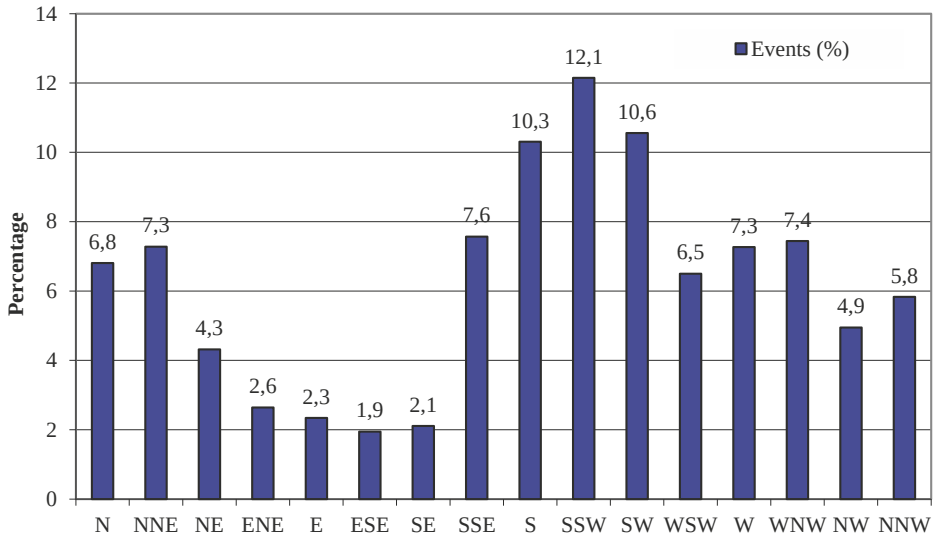

Fig. 4. Distribution of wind directions.

Besides wind directions, it is also important to define wind speeds. Changes in wind speeds must be definitely considered during the analysis because turbulence, obstacles (such as buildings), and pressure differences obligate changes in both wind direction and speed. Wind speeds grouped in 6 speed classes, and the distribution based on these classes are given in *Fig. 5*.

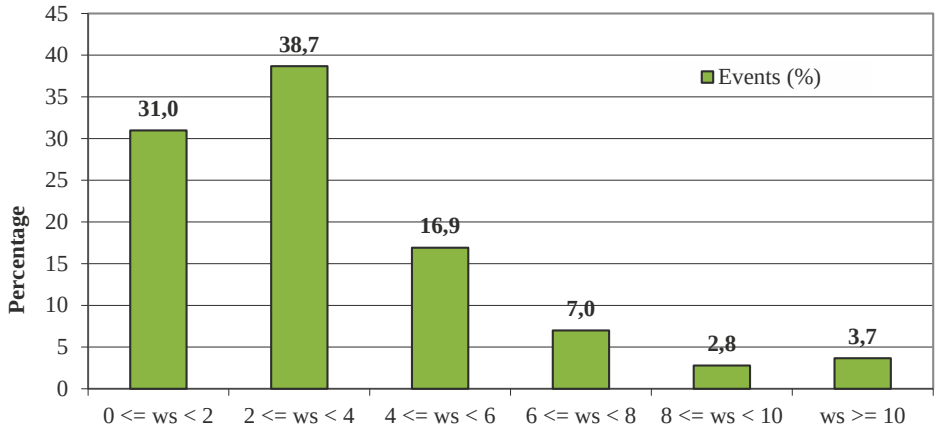

Fig. 5. Wind speed class distribution.

Wind roses are used to find the prevailing direction and also wind speed distribution for a specific area. The wind rose for Kayseri is given in *Fig. 6*, and it could be concluded that the prevailing wind direction is south-southwest (SSW).

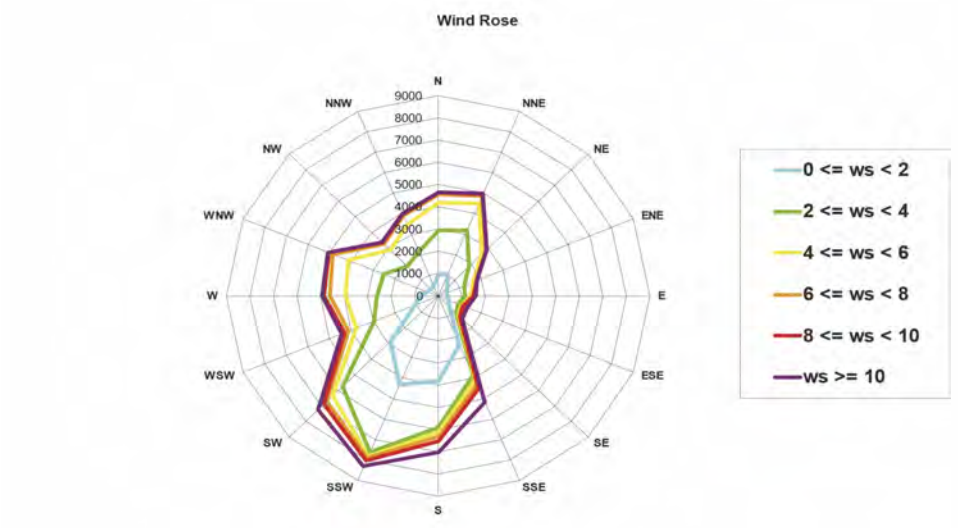

Fig. 6. Wind rose drawn with Kayseri long-term wind speed data.

Distribution of winds based on classes could give a clue about the consequences of wind effects around the investigated buildings, but for a detailed CFD analysis it is important to select and use the most suitable wind speed according to the special requirements of the project. In this study, average wind speeds according to the frequency analysis are selected to reflect a normal daily life situation. Number of wind events and average speeds sorted with the EnviroComp Consulting Wind Tool are given in *Table 1* (*Enviroware*, 2018).

Table 1. Frequency analysis of wind speed data

Direction	0≤ws<2	2≤ws<4	4≤ws<6	6≤ws<8	8≤ws<10	ws≥10	Average speed (m/s)	Number of events	Events (%)
N	951	2004	1233	379	71	11	4.9	4649	6.8
NNE	1076	2122	1285	378	90	20	5.9	4971	7.3
NE	559	1303	748	250	67	21	5.0	2948	4.3
ENE	375	841	404	123	34	26	3.6	1803	2.6
E	409	741	252	97	42	57	3.1	1598	2.3
ESE	458	445	142	64	52	167	3.6	1328	1.9
SE	672	419	94	70	67	117	3.6	1439	2.1
SSE	2393	1484	225	202	209	657	2.9	5170	7.6
S	3824	2063	239	204	186	522	3.2	7038	10.3
SSW	4294	3301	198	110	120	273	3.1	8296	12.1
SW	2863	2882	609	330	216	311	2.5	7211	10.6
WSW	1074	1887	807	356	202	114	1.9	4440	6.5
W	777	1827	1347	674	220	120	2.0	4965	7.3
WNW	516	1999	1636	690	178	64	3.3	5083	7.4
NW	419	1434	1040	393	80	13	3.7	3379	4.9
NNW	496	1659	1296	452	69	12	4.9	3984	5.8

Number of events	21156	26411	11555	4772	1903	2505
Events (%)	31.0	38.7	16.9	7.0	2.8	3.7

Wind speed could be measured in many different time scales. The MGM wind data of Kayseri province has been statistically investigated as given previous sections of this study. For wind comfort modeling, it is crucial to find wind speeds

in the examination area for realistic results. Mini weather stations are widely used in small regions to measure and record weather events. A mini weather station funded from the TUBITAK (The Scientific and Technological Research Council of Turkey) project was placed in the campus area to find hourly wind speeds. A selected sample for wind speeds measured with mini weather station located near Engineering Faculty of Nuh Naci Yazgan University are given in *Fig. 7*.

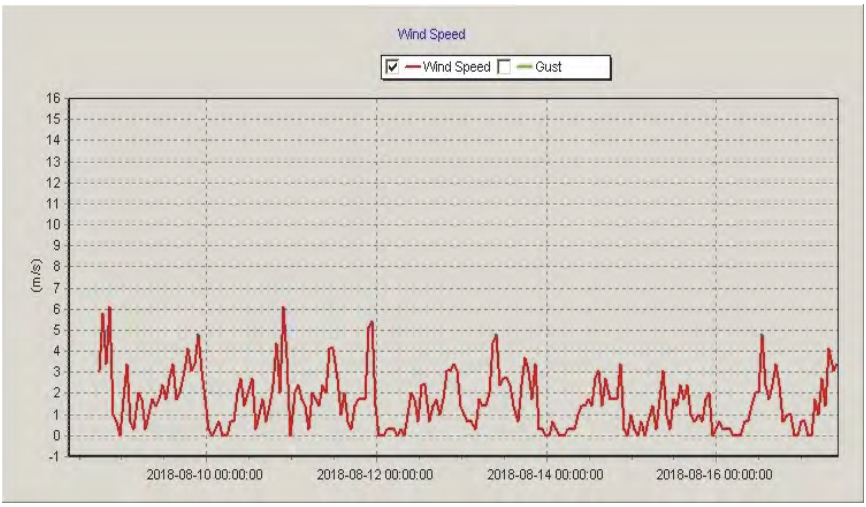

Fig. 7. A sample of wind speed data obtained from field measurements.

Measurements of wind speeds in the campus area data were recorded in a very short period when compared with MGM data, but it was seen that wind speeds were very variable, especially in the hourly periods, during night-day changes which was reasonably expected. It was also found that the measured wind speed values in the campus area are close but always a little bit lower than the MGM values in the same month's same day, and so MGM values are selected as primary wind data in this study.

Measurements of wind speeds are taken at 10 m height from the ground surface as a standard in worldwide. Nevertheless, the pedestrian level wind comfort analysis needs to be made in a proper height. This height should be a suitable height in meters for every person in public. In this pedestrian wind comfort study, the university campus was selected as case study, and the investigations showed that the proper height value which is suitable for most students was around 1.5 meters, and so authors decided to use this value as reference point. The main obstacle during wind speed calculations is the wind

speed profile which is in a logarithmic form. There are many studies about the wind speed variation with height, but the main conflict about the subject is the surface roughness of the investigation area. From those wind profile models, the most convenient one was selected as power law profile, because it is a widely used model, and it would allow to find the vertical wind speed profile. The power law profile in a basic form is given as:

$$\frac{U_{(z)}}{U_{(z_r)}} = \left(\frac{z}{z_r}\right)^{\alpha} \quad (1)$$

where $U_{(z)}$ is the velocity of wind in desired height, $U_{(zr)}$ is the reference wind speed at height z_r, z is the height of wind speed calculation, z_r is the reference wind speed height (10 meters in meteorological measurements), and α is the power law exponent.

It has been found, that the power law exponent varies with such parameters as elevation, time of day, season, nature of the terrain, wind speed, temperature, and various thermal and mechanical mixing parameters, and many researchers have developed methods using the log law for calculations (*Manwell et al*., 2006). A decisively influencing factor during the determination of the pedestrian wind comfort is the wind speed. In this study, the MGM values have been degraded from 10 meters to 1.5 meters using the wind logarithmic profile (or log law). The study area is a university campus that makes a dilemma for the selection of wind speed data time period. Working hours during daytime are the highest pedestrian density time period for the university, so the maximum value of wind speeds based on hourly measurement periods has been sorted. Based on this criterion, the maximum wind speed was found as 24 m/s with direction of SSW. This speed has been measured at 10 meters above the surface level, so by using this value in the wind power law equation it was transformed into the 1.5-meter height level as 9.87 m/s. Air flow in the atmosphere has both speed and direction, and this is represented mathematically by a vector. A south-southwest wind means that the wind comes from the SSW, so the wind barb (flag) would be pointed SSW, but the wind arrow would be pointed to north-northeast (*Doty*, 2015). Meteorological wind directions were converted into CFD suitable directions as input data to the software.

2.3. Turbulence models

Osborne Reynolds investigated the motion of fluids in contact with solid surfaces and found, that the relation between them depends on the relation between a physical constant of the fluid and the product of the linear dimensions of the space occupied by the fluid and the velocity (*Reynolds*, 1883). While the laminar flow determines low speeds and parallel and smoothly moving fluid flow patterns, turbulent flow patterns are irregular and the streamlines intersect each other. It is

crucial to model the turbulence with high reliability, because speed variations could be revealed by numerical investigations made behind CFD modeling software. There are many turbulence models found in literature, but it should be considered that all models have advantages and constraints when compared with each other. So, it is important for engineers to find the suitable model for every project. The most widely used turbulence models and their applications are given in *Table 2 (Bakker* and *Marshall*, 2004).

Table 2. Comparision of turbulence models

Turbulence model	Application area of the model
Standard K-epsilon	The most widely used model, it is robust, economical, and time-tested. The Reynolds stresses are not calculated directly, but are modeled in a simplified way by adding a so-called turbulent viscosity to the molecular viscosity. Its main advantages are a rapid, stable calculation, and reasonable results for many flows, especially those with a high Reynolds number. It is not recommended for highly swirling flows, round jets, or for flows with strong flow separation.
RNG K-epsilon	A modified version of the K-epsilon model, this model yields improved results for swirling flows and flow separation. It is not well suited for round jets, and is not as stable as the standard K-epsilon model.
Realizable K-epsilon	Another modified version of the K-epsilon model, the realizable K-epsilon model correctly predicts the flow in round jets, and is also well suited for swirling flows and flows involving separation.
Spalart-Allmaras	The Spalart-Allmaras model was developed for external flows in aerospace applications. It provides good answers for attached flows and flows with mild flow separation. It is not commonly used for process industry applications.
RSM	The full Reynolds stress model provides good predictions for all types of flows, including swirl, separation, and round and planar jets. Because it solves transport equations for the Reynolds stresses directly, longer calculation times are required than for the K-epsilon models.
LES	Large eddy simulation is a transient formulation that provides excellent results for all flow systems. It solves the Navier-Stokes equations for large scale turbulent fluctuations and models only the small-scale fluctuations (smaller than a computational cell). Because it is a transient formulation, the required computational resources are considerably larger than those required for the RSM and K-epsilon family of models. In addition, a finer grid is needed to gain the maximum benefit from the model and to accurately capture the turbulence in the smallest, sub-grid scale eddies. Analysis of LES data usually requires some degree of planning in advance of building the model.

Turbulence models are still in development, and many studies investigate new formulas to define the secret procedure in turbulence. One of the newest k-omega model-based turbulence model is the shear stress transport (SST) model. This model has the ability to account for the transport of the principal shear stress

in adverse pressure gradient boundary-layers. In this study, k-omega SST model is used to model the turbulence effects on wind flow around the study area. The mathematical representation of k-omega SST Model expressed by the following equations.

The turbulent energy κ is given by:

$$\kappa = \frac{3}{2}(UI)^2 \quad , \tag{2}$$

where U is the mean flow velocity and I is the turbulence intensity.

The turbulence intensity gives the level of turbulence and can be defined as follows:

$$I = \frac{u'}{U} \quad , \tag{3}$$

where u' is the root mean square of the turbulent velocity fluctuations that could be found with the following equation:

$$u' = \sqrt{\frac{1}{3}(u'^2_x + u'^2_y + u'^2_z)} = \sqrt{\frac{2}{3}k} \quad . \tag{4}$$

The mean velocity U can be calculated as follows:

$$U = \sqrt{U_x^2 + U_y^2 + U_z^2} \quad . \tag{5}$$

The specific turbulent dissipation rate can be calculated using the following formula:

$$\omega = C_\mu^{\frac{3}{4}} \frac{\kappa^{\frac{1}{2}}}{l} \quad , \tag{6}$$

where C_μ is the turbulence model constant which usually takes the value 0.09, κ is the turbulent energy, l is the turbulent length scale. The turbulence length scale describes the size of large energy-containing eddies in a turbulent flow. The turbulent viscosity ν_t is, thus, calculated as:

$$\nu_t = \frac{\kappa}{\omega} \quad . \tag{7}$$

2.4. CFD Software

Computational fluid dynamics softwares or any kind of special softwares are programmed only to analyze wind flow work based on computational methods used for flow modeling in fluid dynamics. In this study, the Simscale software was used for CFD analysis. Simscale is a web-based computer-aided engineering (CAE) program that runs on the basis of sophisticated graphical interface to analyze designs and solve complex engineering problems such as finite element analysis (FEA), computational fluid dynamics (CFD), thermal analysis, multibody dynamics, and optimization (*Simscale,* 2021).

A CFD analysis generally includes following steps which are similar in all CFD software:

a) CAD preparation (pre-processing): CAD programs used to draw 2- or 3-dimensional forms of objects.

b) Simulation setup: CFD models such as turbulence models, time periods selected and operated.

c) Post-processing: results taken in graphic, tabular, or visual forms.

d) Visualization: Examination of visual outputs of CFD analysis.

e) Error estimation (re-run simulation if needed): if there are errors so simulation steps could be restarted from any step depending on user's experience.

2.5. NNY Campus CFD Analysis

The university campus is modeled with CAD software at the selected level of scale, which has enough detail to show the perspective of buildings but does not include every tiny details of buildings, especially the ones without any possible effect on wind. This procedure was used for each building in the campus area and *Fig. 8* shows computational grid.

The mesh of the campus based on CAD model has been created by using the Simscale mesh operation. There are 5 detail levels in the software, but higher detail levels need more simulation time. Grid detail level selected as 3 (moderate level) to gain enough quality without sacrificing the simulation performance. The mesh of the Engineering Faculty building as an example part of the whole grid is given in *Fig. 9*.

Fig. 8. Campus geometry.

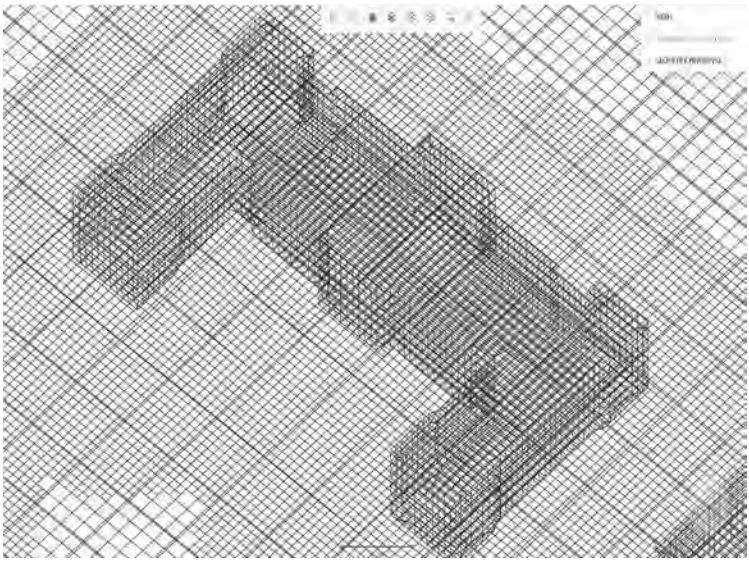

Fig. 9. Computational grid of the NNY Engineering Faculty building.

Boundary conditions include the surfaces of awind tunnel, because wind comfort studies simulate wind tunnel experiments. This kind of modeling could be affected by roughness of walls for both experimental and numerical solutions.

According to the recommendations on the use of CFD in predicting pedestrian wind environment publication, dimensions of the wind tunnel must be selected by using the height of the tallest building (H_{max}) in the domain (*Franke et al*., 2004). Dimensions for the ideal analysis are suggested as: height of tunnel is 6 H_{max}, distance from buildings (left, right, and front) is 5 H_{max}, and distance of rear tunnel wall from the last building is 15 H_{max}. In this study the wind tunnel dimensions were selected based on these criteria, and suitable values according to suggestions were given as input tunnel size parameters to the software.

3. Results

High speed winds cause many effects in the surroundings. These effects can change due to obstacles in the front of the wind flow, and possible consequences of wind damage should be separated as sea and land based on the flow environment. Outcomes of wind speeds have been defined with speed intervals to clarify the possible consequences and this is called Beaufort scale which is widely used in wind researches as given in *Table 3* (US Department of Commerce, 2021).

Table 3. Beaufort Scale

Force **Speed (m/s)** **Speed (knots)** **Description**	**Specifications for use at sea (First row)** **Specifications for use on land (Second row)**
0 0-0.3	Sea like a mirror.
0-1 Calm	Calm; smoke rises vertically.
1 0.4-1.7	Ripples with the appearance of scales are formed, but without foam crests.
1-3 Light air	Direction of wind shown by smoke drift, but not by wind vanes.
2 1.8-3.1	Small wavelets, still short, but more pronounced. Crests have a glassy appearance and do not break.
4-6 Light breeze	Wind felt on face; leaves rustle; ordinary vanes moved by wind.
3 3.2-5.3	Large wavelets. Crests begin to break. Foam of glassy appearance. Perhaps scattered white horses.
7-10 Gentle breeze	Leaves and small twigs in constant motion; wind extends light flag.
4 5.4-8.1	Small waves, becoming larger; fairly frequent white horses.
11-16 Moderate breeze	Raises dust and loose paper; small branches are moved.
5 8.2-10.9	Moderate waves, taking a more pronounced long form; many white horses are formed.
17-21 Fresh breeze	Small trees in leaf begin to sway; crested wavelets form on inland waters.

Table 3. Continue

Force Speed (m/s) Speed (knots) Description	Specifications for use at sea (First row) Specifications for use on land (Second row)
6 11.0-13.3 22-27 Strong breeze	Large waves begin to form; the white foam crests are more extensive everywhere. Large branches in motion; whistling heard in telegraph wires; umbrellas used with difficulty.
7 13.4-16.9 28-33 Near gale	Sea heaps up and white foam from breaking waves begins to be blown in streaks along the direction of the wind. Whole trees in motion; inconvenience felt when walking against the wind.
8 17.0-20.0 34-40 Gale	Moderately high waves of greater length; edges of crests begin to break into spindrift. The foam is blown in well-marked streaks along the direction of the wind. Breaks twigs off trees; generally, impedes progress.
9 20.1-23.7 41-47 Severe gale	High waves. Dense streaks of foam along the direction of the wind. Crests of waves begin to topple, tumble and roll over. Spray may affect visibility Slight structural damage occurs (chimney-pots and slates removed)
10 23.8-27.9 48-55 Storm	Very high waves with long overhanging crests. The resulting foam, in great patches, is blown in dense white streaks along the direction of the wind. On the whole the surface of the sea takes on a white appearance. The tumbling of the sea becomes heavy and shock-like. Visibility affected. Seldom experienced inland; trees uprooted; considerable structural damage occurs.
11 28.0-31.9 56-63 Violent storm	Exceptionally high waves (small and medium-size ships might be for a time lost to view behind the waves). The sea is completely covered with long white patches of foam lying along the direction of the wind. Everywhere the edges of the wave crests are blown into froth. Visibility affected. Very rarely experienced; accompanied by wide-spread damage.
12 32.0-33.3 64-71 Hurricane	The air is filled with foam and spray. Sea completely white with driving spray; visibility very seriously affected.

Results of the CFD analysis conducted on the Nuh Naci Yazgan University campus are given in *Fig. 10*.

The CFD analysis results showed that the shape as well as spatial settlement building are important parameters for the directional deflection of the wind flow. Sharp edges at all sides force wind speed to increase, meanwhile points positioned behind buildings are under the influence of variable wind speeds. Highest wind speeds were found around buildings located in the south of the university campus.

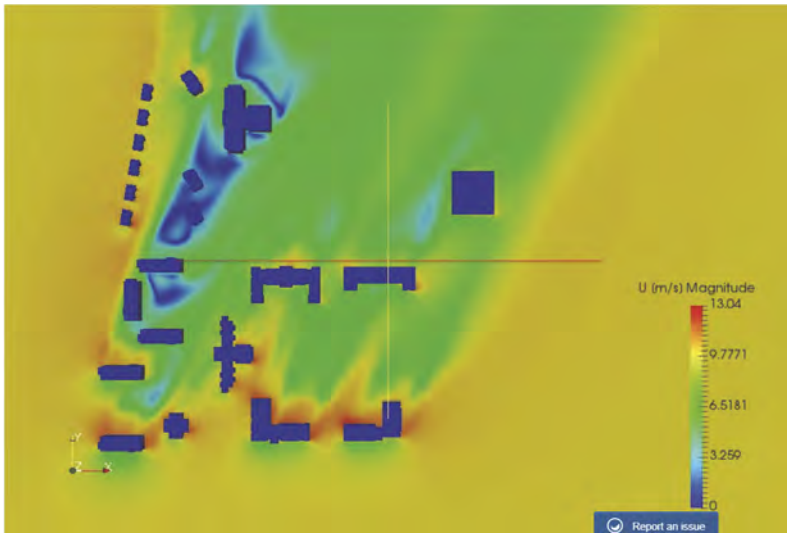

Fig. 10. Results of the CFD wind comfort analysis

4. Conclusion

In this study, a university campus pedestrian level wind comfort analysis has been conducted by using the CFD software. For this purpose, wind speed data were used during the analysis, and results showed that the position of buildings caused the increase in wind speeds, and if we consider possible changes in the campus area such as new buildings, this process would lead to higher damages in different areas. Results of the analysis indicated that, planning of a city or even more smaller regions such as a university campus should be designed with the CFD wind analysis tools in order to evaluate wind comfort analysis. Also, it could be concluded, that the intensity of pedestrian traffic should be under consideration during the planning stages. Meanwhile, pedestrian wind comfort guidelines including region specifications could guide designers about design criterias, and this would help to find the optimum solutions against undesirable wind effects. The wind speed increased to 13.04 m/s in some places, and according to the Beaufort scale this amount of wind speed creates these spesifications on land: “Large branches in motion; whistling heard in telegraph wires; umbrellas used with difficulty”. This result was obtained with CFD, and input wind speed data was found by statistical investigation of historical data measured around the research area. This means, that climate change effects that would create a change for wind data in future or relatively small obstacles (such as lamppost, bus stop, etc.) around buildings were not taken into account in the calculations, and so the

wind flow could more dramatically change if the effects of these parameters are considered. However, for rural pedestrian wind comfort studies, this kind of possible changes could be taken into account to determine possible consquences of wind speed variationsduring CFD calculations, and could be used in wind comfort evaluations in accordance with comfort criterias as well as safety regulations.

Acknowledgements: This study has been supported by TUBITAK (The Scientific and Technological Research Council of Turkey) within the scope of 2209-A Research Project Support Programme for Undergraduate Students (project number 1919B011703788). In this context, the authors would like to thank to TUBITAK.

References

Bakker, A. and *Marshall, E.M.*, 2004: Computational Fluid Dynamics. In (Ed. Lee, S.), Encyclopedia of Chemical Processing. New York: Marcel Dekker Inc. 1–23.

B*ehrouzi, F., Azwadi, N.O.R., Che, B.I.N., Nakisa, M.,* and *Witri, A.*, 2013: Numerical prediction of wind flow around the high-rise buildings by two equations turbulence models for urban street canyon. *Comput. Method. Sci. Engineer 13*,152–156.

Blocken, B., Janssen, W.D.D., and *van Hooff, T.*, 2012: CFD simulation for pedestrian wind comfort and wind safety in urban areas: General decision framework and case study for the Eindhoven University campus. *Environ. Model. Software 30*, 15–34. https://doi.org/10.1016/j.envsoft.2011.11.009

Blocken, B. and *Persoon, J.*, 2009*:* Pedestrian wind comfort around a large football stadium in an urban environment: CFD simulation, validation and application of the new Dutch wind nuisance standard. *J. Wind Engineer. Indust. Aerodynam. 97*, 255–270. https://doi.org/10.1016/j.jweia.2009.06.007

Blocken, B., Carmeliet, J., Stathopoulos, T., Carmeliet, J., and *Stathopoulos, T.*, 2007*:* CFD evaluation of wind speed conditions in passages between parallel buildings—effect of wall-function roughness modifications for the atmospheric boundary layer flow. *J. Wind Engineer. Indust. Aerodynam. 95*, 941–962. https://doi.org/10.1016/j.jweia.2007.01.013

Blocken, B., Roels, S., and *Carmeliet, J.*, 2004: Modification of pedestrian wind comfort in the Silvertop Tower passages by an automatic control system. *J. Wind Engineer. Indust. Aerodynam. 92*, 849–873. https://doi.org/10.1016/j.jweia.2004.04.004

Blocken, B., van der Hout, A., Dekker, J., and *Weiler, O.*, 2015: CFD simulation of wind flow over natural complex terrain: Case study with validation by field measurements for Ria de Ferrol, Galicia, Spain. *J. Wind Engineer. Indust. Aerodynam. 147*, 43–57. https://doi.org/10.1016/j.jweia.2015.09.007

Cui, D., Hu, G., Ai, Z., Du, Y., Mak, C. M., and *Kwok, K.*, 2019*:* Particle image velocimetry measurement and CFD simulation of pedestrian level wind environment around U-type street canyon. *Build. Environ. 154*, 239–251. https://doi.org/10.1016/j.buildenv.2019.03.025

Cui, D.J.J., Mak, C.M.M., Kwok, K.C.S., and *Ai, Z.T.T.*, 2016*:* CFD simulation of the effect of an upstream building on the inter-unit dispersion in a multi-story building in two wind directions. *J. Wind Engineer. Indust. Aerodynam. 150*, 31–41. https://doi.org/10.1016/j.jweia.2016.01.007

Doty, M.B., 2015: Wind: u and v Components. Access date: 20.07.2022 Retrieved from http://colaweb.gmu.edu/dev/clim301/lectures/wind/wind-uv

Du, Y. and *Mak, C.M.* 2017: Effect of lift-up design on pedestrian level wind comfort around isolated building under different wind directions. *Procedia Engineer. 205*, 296–301. https://doi.org/10.1016/j.proeng.2017.09.979

Enviroware, 2018: Enviroware-tools wind data tool. Access Date: 12.08.2018. Retrieved from https://www.enviroware.com/tools/

F*ranke, J., Hirsch, C., Jensen, A. G., Krus, H.W., Schatzmann, M., Miles, P.S.W.* and *S. D., Wright, N. G., 2004:* Recommendations on the Use of CFD in Wind Engineering. Cost Action C14, (May), 1–11. https://doi.org/10.1007/BF02800469

Houda, S., Zemmouri, N., Hasseine, A., Athmani, R., Belarbi, R., and Flow, U., 2012: A Cfd Model for Simulating Urban Flow in Complex, *2*(1), 1–10.

Hu, C.H. and *Wang, F.,* 2005: Using a CFD approach for the study of street-level winds in a built-up area. *Build. Environ. 40*, 617–631. https://doi.org/10.1016/j.buildenv.2004.08.016

Kang, G., Kim, J.J., Kim, D.J., Choi, W., and Park, S.J., 2017*:* Development of a computational fluid dynamics model with tree drag parameterizations: Application to pedestrian wind comfort in an urban area. *Build. Environ. 124*, 209–218. https://doi.org/10.1016/j.buildenv.2017.08.008

Mamou, M., Benmeddour, A., Khalid, M., Fitzsimmons, J., Sengupta, R., Cooper, K. R., and *Sengupta, R.,* 2008: Correlation of CFD predictions and wind tunnel measurements of mean and unsteady wind loads on a large optical telescope. *J. Wind Engineer. Indust. Aerodynam. 96*, 793–806. https://doi.org/10.1016/j.jweia.2007.06.050

Manwell, J., Mcgowan, J., and *Rogers, A.* 2006: Wind Energy Explained: Theory, Design and Application, Second Edition. 10.1260/030952406778055054.

Meroney, R.N. and *Neff, D.E.,* 2010: Wind Effects on Roof-Mounted Solar Photovoltaic Arrays: CFD and Wind-Tunnel Evaluation. *T*he Fifth International Symposium on Computational Wind Engineering, (May), 1–8.

Mochida, A., Tabata, Y., Iwata, T., and *Yoshino, H.,* 2008: Examining tree canopy models for CFD prediction of wind environment at pedestrian level. *J. Wind Engineer. Indust. Aerodynam. 96*, 1667–1677. https://doi.org/10.1016/j.jweia.2008.02.055

MGM, Turkish State Meteorological Service, 2021: Meteoroloji Sözlüğü. Access date: 07.07.2021, Retrieved from https://www.mgm.gov.tr/genel/meteorolojisozlugu.aspx? (In Turkish)

NNY, Nuh Naci Yazgan University, 2021: NNY University. Retrieved July 20, 2021, from https://www.nny.edu.tr/?p=contact

Qi, Y. and *Ishihara, T.,* 2018: Numerical study of turbulent flow fields around of a row of trees and an isolated building by using modified k-ε model and LES model. *J. Wind Engineer. Indust. Aerodynam. 177*, 293–305. https://doi.org/10.1016/j.jweia.2018.04.007

Reynolds, O., 1883: An experimental investigation of the circumstances which determine whether the motion of water shall be direct or sinuous, and of the law of resistance in parallel channels. *Philosoph. Transact. Roy. Soc. London, 174*, 935–982. https://doi.org/10.1098/rstl.1883.0029

Simscale, 2021*:* SimScale Documentation | Online Simulation Software | SimScale. Retrieved February 26, 2021, from https://www.simscale.com/docs/

US Department of Commerce, 2021: N. N. W. S. Beaufort Wind Scale. NOAA's National Weather Service, Access Date: February 20, 2021, Retrieved from https://www.weather.gov/mfl/beaufort

Van Druenen, T., van Hooff, T., Montazeri, H., and *Blocken, B.,* 2019: CFD evaluation of building geometry modifications to reduce pedestrian-level wind speed. *Build. Environ. 163*, 106293. https://doi.org/10.1016/j.buildenv.2019.106293

Willemsen, E., and *Wisse, J.A.,* 2007: Design for wind comfort in The Netherlands: Procedures, criteria and open research issues. *J. Wind Engineer. Indust. Aerodynam. 95*, 1541–1550. https://doi.org/10.1016/j.jweia.2007.02.006

Yoshie, R., Mochida, A., Tominaga, Y., Kataoka, H., Harimoto, K., Nozu, T., and *Shirasawa, T.,* 2007: Cooperative project for CFD prediction of pedestrian wind environment in the Architectural Institute of Japan. *J. Wind Engineer. Indust. Aerodynam. 95*, 1551–1578. https://doi.org/10.1016/j.jweia.2007.02.023

Yoshie, R., Mochida, A., Tominaga, Y., Kataoka, H., and *Yoshikawa, M.,* 2006: CFD Prediction of Wind Environment around a High-rise Building Located in an Urban Area. *Jwe, 1*(108), 129–132.

IDŐJÁRÁS

Quarterly Journal of the Hungarian Meteorological Service

Editorial Office: Kitaibel P.u. 1, H-1024 Budapest, Hungary
P.O. Box 38, H-1525 Budapest, Hungary
E-mail: journal.idojaras@met.hu

Indexed and abstracted in Science Citation Index Expanded™ and Journal Citation Reports/Science Edition
Covered in the abstract and citation database SCOPUS®
Included in EBSCO's database

Subscription by mail:
IDŐJÁRÁS, P.O. Box 38, H-1525 Budapest, Hungary
E-mail: journal.idojaras@met.hu

INSTRUCTIONS TO AUTHORS OF *IDŐJÁRÁS*

The purpose of the journal is to publish papers in any field of meteorology and atmosphere related scientific areas. These may be

- research papers on new results of scientific investigations,
- critical review articles summarizing the current state of art of a certain topic,
- short contributions dealing with a particular question.

Some issues contain "News" and "Book review", therefore, such contributions are also welcome. The papers must be in American English and should be checked by a native speaker if necessary.

Authors are requested to send their manuscripts to

Editor-in Chief of IDŐJÁRÁS
P.O. Box 38, H-1525 Budapest, Hungary
E-mail: journal.idojaras@met.hu

including all illustrations. MS Word format is preferred in electronic submission. Papers will then be reviewed normally by two independent referees, who remain unidentified for the author(s). The Editor-in-Chief will inform the author(s) whether or not the paper is acceptable for publication, and what modifications, if any, are necessary.

Please, follow the order given below when typing manuscripts.

Title page should consist of the title, the name(s) of the author(s), their affiliation(s) including full postal and e-mail address(es). In case of more than one author, the corresponding author must be identified.

Abstract: should contain the purpose, the applied data and methods as well as the basic conclusion(s) of the paper.

Key-words: must be included (from 5 to 10) to help to classify the topic.

Text: has to be typed in single spacing on an A4 size paper using 14 pt Times New Roman font if possible. Use of S.I. units are expected, and the use of negative exponent is preferred to fractional sign. Mathematical formulae are expected to be as simple as possible and numbered in parentheses at the right margin.

All publications cited in the text should be presented in the *list of references*, arranged in alphabetical order. For an article: name(s) of author(s) in Italics, year, title of article, name of journal, volume, number (the latter two in Italics) and pages. E.g., *Nathan, K.K.,* 1986: A note on the relationship between photosynthetically active radiation and cloud amount. *Időjárás 90,* 10–13. For a book: name(s) of author(s), year, title of the book (all in Italics except the year), publisher and place of publication. E.g., *Junge, C.E.,* 1963: *Air Chemistry and Radioactivity.* Academic Press, New York and London. Reference in the text should contain the name(s) of the author(s) in Italics and year of publication. E.g., in the case of one author: *Miller* (1989); in the case of two authors: *Gamov* and *Cleveland* (1973); and if there are more than two authors: *Smith et al.* (1990). If the name of the author cannot be fitted into the text: *(Miller,* 1989); etc. When referring papers published in the same year by the same author, letters a, b, c, etc. should follow the year of publication. DOI numbers of references should be provided if applicable.

Tables should be marked by Arabic numbers and printed in separate sheets with their numbers and legends given below them. Avoid too lengthy or complicated tables, or tables duplicating results given in other form in the manuscript (e.g., graphs). *Figures* should also be marked with Arabic numbers and printed in black and white or color (under special arrangement) in separate sheets with their numbers and captions given below them. JPG, TIF, GIF, BMP or PNG formats should be used for electronic artwork submission.

More information for authors is available: journal.idojaras@met.hu

Published by the Hungarian Meteorological Service

Budapest, Hungary

ISSN 0324-6329 (Print)

ISSN 2677-187X (Online)